HOLLOW CORE PHOTONIC BANDGAP FIBERS FOR MEDICAL APPLICATIONS

A THESIS

SUBMITTED TO THE DEPARTMENT OF MATERIALS SCIENCE AND NANOTECHNOLOGY

AND THE INSTITUTE OF ENGINEERING AND SCIENCES

OF BILKENT UNIVERSITY

IN PARTIAL FULFILLMENT OF THE REQUIREMENTS

FOR THE DEGREE OF

MASTER OF SCIENCE

By

Mert Vural

August 2009

I certify that I have read this thesis and that in my opinion it is fully adequate, in scope and in quality, as a thesis for the degree of Master of Science.

Assist. Prof. Dr. Mehmet Bayındır (Supervisor)

I certify that I have read this thesis and that in my opinion it is fully adequate, in scope and in quality, as a thesis for the degree of Master of Science.

Assist. Prof. Dr. Alper Kiraz

I certify that I have read this thesis and that in my opinion it is fully adequate, in scope and in quality, as a thesis for the degree of Master of Science.

Assist. Prof. Dr. Selçuk Aktürk

I certify that I have read this thesis and that in my opinion it is fully adequate, in scope and in quality, as a thesis for the degree of Master of Science.

Ress. Assist. Prof. Dr. Tamer Uyar

Approved for the Institute of Engineering and Sciences:

Prof. Dr. Mehmet Baray
Director of Institute of Engineering and Sciences

ABSTRACT

HOLLOW CORE PHOTONIC BANDGAP FIBERS FOR MEDICAL APPLICATIONS

Mert Vural
M.S. in Materials Science and Nanotechnology
Supervisor: Assist. Prof. Dr. Mehmet Bayındır
August 2009

The design, fabrication and characterization of photonic band gap (PBG) based optical polymer fibers is discussed. Unlike conventional total internal reflection (TIR) fibers, used primarily in telecommunications, PBG fibers can be made hollow core and can be used to guide infrared radiation of any wavelength, a property known as wavelength scalability. Since the electromagnetic radiation is transmitted in the hollow core of the fiber, the intrinsic absorption of the fiber core as well as the insertion Fresnel losses at front and end faces are avoided, giving rise to extraordinarily high power densities to be delivered.

The fiber production line includes material characterization, and the design of nanoscale quarter wavestacks using common thermoplastic polymers (poly ether sulphone and poly ether imide) and chalcogenide glasses (As_2S_3, As_2Se_3, $Ge_{15}As_{25}Se_{15}Te_{45}$). The fiber preform is fabricated using rolling mechanism of thermally evaporated chalcogenide glasses on large area polymers. Subsequently, the fiber preforms are thermally drawn to obtain nano-structured PBG fibers.

Two different fibers are designed and produced, signifying wavelength scalability of the overall process, for the widely used holmium (Ho:YAG) and carbon dioxide (CO_2) medical lasers. The transmission characteristics of the fibers proved that they can be used to safely deliver 15 W laser power, along a 3 meter fiber with external diameter of 1.5 mm and hollow core diameter of 0.5 mm, corresponding to a laser power density of 1kW/cm^2 with a loss of -10dB/m.

The PBG fibers are expected to be widely used in high precision surgical laser for incision, photoablation and coagulation where infrared radiation is the radiation of choice for its superior laser-tissue interaction properties.

Keywords: Photonic Band Gap, Photonic Crystal, Fiber Optics, Optical Waveguides, Medical Lasers, Chalcogenides, Engineering Thermoplastics

ÖZET

MEDİKAL UYGULAMALAR İÇİN FOTONİK BANT YAPILI İÇİ BOŞ FİBERLER

Mert Vural
Malzeme Bilimi ve Nanoteknoloji Yüksek Lisans
Tez Yöneticisi: Yar. Doç. Dr. Mehmet Bayındır
Ağustos 2009

Fotonik bant yapısına sahip polimerik optik fiberlerin tasarımı, üretimi ve karakterizasyonu bu tez boyunca tartışılmıştır. Telekomunikasyon amaçlı konvansiyonel optik fiberlerden farklı olarak fotonik bant yapılı fiberler içleri boş olarak tasarlanabilir, kızılötesi dalgaboylarının tamamını taşıyabilir, malzeme soğurmasından ve ışığın fiber içerisine girerken ve çıkarkan maruz kaldığı Fresnel kayıplarından etkilenmez, bu sayede yüksek güç yoğunluklarında kolaylıkla çalışabilir.

Fiber üretim hattı malzeme karakterizasyonu, nano boyutlarda çeyrek dalga katmanlarının sıradan termoplastik polimerleri ve kalkojen camları kullanarak tasarımını içerir. Fiber önformu ise termal buharlaştırma ile kalkojen kaplanmış yüksek alanlı polimerik filmlerin bir kalıp etrafına sarılması ile oluşturulur. Bu işlemin ardından fiber preformunun termal olarak çekilmesi ile nano yapılı fotonik bant fiberlerinin fabrikasyon işlemi son bulur.

Bütün sistemin dalgaboyuna göre oranlanabilir olduğunu göstererek holmium (HO:YAG), CO_2 gibi iki önemli medikal lazer için iki farklı fiber yapısı tasarlanmış ve üretilmiştir. Bu fiberlerin iletim karakteristikleri 3 metre boyunda, 1.5

mm dış ve 0.5 mm iç çapa sahip bir fiber yapısının 15 W lazer gücünü 1kW/cm^2 değerine tekabül eden bir güç yoğunluğu ve -10dB/m kayıp değeri ile sorunsuz olarak taşıdığını göstermiştir.

Fotonik bant fiberlerinin yüksek hassasiyet gerektiren cerrahi operasyonlarda kızılötesi dalgaboyunun en iyi doku etkileşimini sağladığı işlemler olan kesme, yakma ve koagülasyon işlemlerinde yaygın olarak kullanımı öngörülmektedir.

Anahtar Kelimeler: Fotonik Bant Aralığı, Fotonik Kristal, Fiber Optik, Optik Dalga Klavuzları, Medikal Lazerler, Kalkojenler, Mühendislik Termoplastikleri

ACKNOWLEDGMENTS

First, I would like to thank to my thesis advisor Prof. Mehmet Bayındır, Dr. Mecit Yaman who give me inspiration with his knowledge, my tutors who furnished my mind, dearest workers of Nanotechnology Research Center (UNAM) who are willing to sacrifice so much for science and Prof. Salim Çıracı who accepted me to work as a scientist at the most prestigious Materials Science Institution of my country.

I would also like to thank to my dearest friends at Bayındır research group: Kemal Gürel, Murat Celal Kılınç, Adem Yildirim, Özlem Şenlik, Yavuz Nuri Ertaş, H. Esat Kondakçı, Duygu Akbulut, Özlem Köylü, Hülya Budunoğlu, Erol Özgür, Ekin ,Özgür, Dr. Abdullah Tülek, Dr. Hakan Deniz who have became the brightest star inside a dreadful storm called science and my dearest colleagues at UNAM Can Koral, Mehmet Kanık and Ahmet Ünal who sacrificed so many hours of their youth to assist my work.

I wish to express my gratitude to my parents who encouraged me, teach me, helped me and love me with their immaculate heart. I am happy, proud and grateful to be their beloved son.

The financial support from TUBİTAK, Ministry of Health of Turkey and State Planning Organization is also gratefully acknowledged.

Contents

List of Figures

List of Tables

Dedicated to my beloved family and Ms. Bronte who owns the *Evening Solace*:

The human heart has hidden treasures,

In secret kept, in silence sealed;

The thoughts, the hopes, the dreams, the pleasures,

Whose charms were broken if revealed. . .

Charlotte Bronte (Evening Solace)

Chapter 1

INTRODUCTION

This thesis concerns the design, fabrication and characterization of photonic band gap (PBG) fibers for high power laser delivery. Unlike the conventional optical fiber, PBG fibers can operate at whole infrared spectrum with extraordinary power densities. Specifically, the fibers are designed for the delivery of infrared medical lasers, e.g. holmium (2.1 μm) and carbon dioxide (10.6 μm) radiation. The fibers provide a conduit for the delivery of high power electromagnetic radiation to the surgical site in medical operations.

PBG fibers are also known as one dimensional photonic crystal fibers (1-D PCF) due to the origin of their photonic band gap. 1-D PCF is a hybrid structure consisting of dielectric mirrors to guide light inside the fibers. A dielectric mirror is basically simultaneous layers of quarter wavestacks (QWS) however a perfect dielectric mirror requires a set of materials with high refractive index difference [1]. In order to use the dielectric mirrors in fibers, they need to be thermo-mechanically compatible to prevent structural deformation during optical fiber drawing process [2].

The dielectric mirror layers are generally designed as thin film structures, however it is possible to place these layers at the inner surface of a hollow fiber [3].

This modification allows this fiber to guide a certain spectrum of light through air efficiently. It is possible to engineer the spectrum of guiding by changing the dimensions of mirror layers. Guiding light through air has certain advantages over guiding light through dense media, especially for applications such as high-energy laser transmission, fiber lasers, fiber based sensors [4, 5]. The realization of such fibers is succeeded in recent years. However, use of these fibers for medical purposes is examined slightly. Only a transmission fiber is designed to deliver high power CO_2 laser [4]. Additional to high power laser delivery, sensing applications and use of cavity structures inside these fibers are barely investigated [6, 7, 8]. This work includes materials and processing principles employed in the development of 1-D PCFs, as well as the optical characterization and performance analysis of the resultant fibers. Along this thesis we will heavily focus on transmission fibers for various wavelengths then we will define a transmission fiber for CO_2 sensing and explain the design and fabrication of external reflector fibers. External reflector fibers are the basis of cavity applications of such structures. We will present a detailed explanation at Chapter 6.

As we mentioned above the sole purpose of this thesis is dedicated to design and fabrication of 1-D PCFs that could guide high-energy holmium and CO_2 lasers with least possible loss. These lasers are mainly used for certain medical applications. The holmium laser used at refractive surgery procedure called laser thermal keratoplasty. This procedure is used to correct mild to moderate cases of farsightedness and some case of astigmatism. Moreover, there are some other medical procedures which possess holmium laser treatment, namely soft tissue procedures, laser lithotripsy, incision of urethral strictures [9, 10]. The use of CO_2 laser for medical procedures is a newly developing field at clinical sciences. However, there are many publications incident about use of CO_2 lasers at clinical applications, mostly surgical purposes [11, 12, 13, 14]. So, it is possible to claim that in a short amount of time a great need will show up for a delivery system of such lasers. After briefly mentioning our motivations, we will begin

this work with providing related information about dielectric mirrors, fiber optics and design concerns at Chapter 2. We will continue with investigation of certain material properties as the first step for the design of 1-D PCFs at Chapter 3. The material characterization will help us to design and plan the fabrication procedure of 1-D PCFs at Chapter 4. After the fabrication procedure these fibers optical performance is characterized with respect to their working purpose at Chapter 5. As we shall see, additional to the marvelous performance of 1-D PCFs for guiding purposes, sensing ability of these fibers is also noteworthy. Another 1-D PCF design for reflecting the incident radiation from the outer surface of the fiber is also investigated during this thesis [15]. These fibers optical performance encourages us to use these fibers as optical barcodes, filters and switches [15]. This thesis will conclude with declaration of a brief outline and broad future research options.

Chapter 2

THEORETICAL BACKGROUND

2.1 Dielectric Mirrors

The idea to use a multilayer media as a reflector is a well known concept since Lord Rayleigh has published one of the first analyses about optical properties of multilayer films in 1887 [16]. He tried to explain reflection mechanisms through a predecessor of Bloch's Theorem. However later on at 1917 Lord Rayleigh has diverged from this aspect and he tried to explain the reflection phenomena for multilayer media as the sum of multiple reflections and refractions that can occur at each surface [17]. In 1914, C.G. Darwin has suggested that each ordinary crystal has a band gap for X-ray waves [18]. In the light of this information Eli Yablanovitch claimed that it is possible to produce an optical band gap for any frequency of electromagnetic spectrum through manipulating the crystal structure [19]. In order to create an optical band gap the crystal structure can be periodic along several dimensions as for multilayer media the periodicity is incident for only one dimension. Including the idea of band gap, general

theory of reflection from multilayer dielectric media is summarized briefly by Pochi Yeh [20]. But the theory is completed by J.D. Joannopoulos and his colleagues. Joannopoulos and his colleagues contributed this field by introducing the significance of coupling light from atmosphere to reflector which explained the reflector works independent from angle of incidence engendering a complete photonic band gap [1].

As for theory, the fundamental reflection mechanism for dielectric layered media is based on QWS structures [21]. QWS mechanisms can inherit a photonic band gap for certain frequencies depending on thickness and refractive indices of layers. The relation between the thickness ($\mathbf{d}$), refractive indices of the layers ($\mathbf{n}$) and the central frequency of the band gap (ω) is described as :

$$\mathbf{d} = \frac{\mathbf{c}}{\mathbf{4n}\omega} \tag{2.1}$$

It is possible to verify whether if the hypothesis is true or not by inspecting the propagation of light through this dielectric periodic structure. The general way to observe the behavior of light in a media is to solve Maxwell's Equations. These equations are a set of differential equations which demands accurate boundary conditions. The system that the light is propagating through must be well defined in terms of boundary conditions. This solution will lead to a translation matrix which defines the structure by using plane wave solutions of the Maxwell's Equations and continuity of boundary conditions at individual layer surface. Resulting matrix completes the relation between the incident (E_i) and reflected (E_r) electric field components of an electromagnetic wave are presented at Eq. 2.2.

$$\begin{pmatrix} A & B \\ C & D \end{pmatrix} \begin{pmatrix} E_r \\ E_i \end{pmatrix} = e^{-iKa} \begin{pmatrix} E_r \\ E_i \end{pmatrix} \tag{2.2}$$

The expression e^{-iKa} corresponds to the phase shift of the electromagnetic wave while propagating along a path which can be expressed as lattice translation length. The value K is simply known as bloch wave number. In light of these informations it is possible to claim that the phase shift of the layers corresponds to the eigenvalues of the translation matrix [20]. So as it can be inferred from the phase value it is possible to obtain whether real or imaginary solutions for Bloch wave numbers which determines whether the light can propagate through this structure. The imaginary solutions of Bloch wave numbers result the electromagnetic wave to be forbidden for propagation, but in case of real solutions of K the electromagnetic can propagate through the system. In order to clarify the situation the solutions of the Bloch wave numbers are expressed in means of frequency(ω), incident light wave vector($k_{//}$) and polarizations. The simplified expression for a periodic structure which is demonstrated at Figure 2.1 is given at the following expression Eq. 2.1.

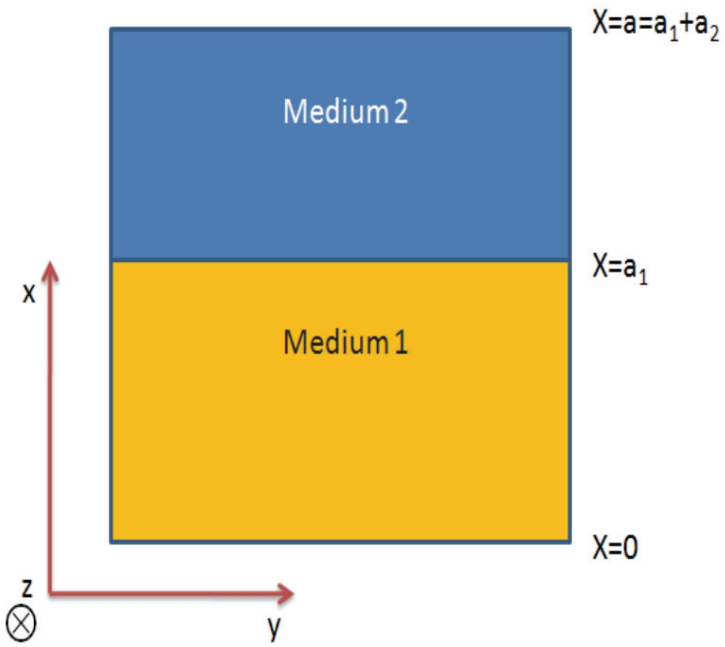

Figure 2.1: A periodic layered media.

$$\cos\left(k_{//}a\right) = \cos\left(\frac{n_2 a_2 \omega}{\mathbf{c}}\right)\cos\left(\frac{n_1 a_1 \omega}{\mathbf{c}}\right) - \left(\frac{n_1^2 + n_2^2}{2n_1 n_2}\right)\sin\left(\frac{n_2 a_2 \omega}{\mathbf{c}}\right)\sin\left(\frac{n_2 a_2 \omega}{\mathbf{c}}\right) \tag{2.3}$$

where

$$k_{//} = \sqrt{(k_x^2 + k_y^2)}$$

If the wave vector of the propagating electromagnetic wave is defined by its components along x and y axes, the expression can illustrate whether a wave vector is incident for a certain frequency, yet the influence of coupling the light from air to system must be considered. The expression is clarified through expressing the components of the wave vector as a function of frequency. The final expression is named as *Projected Band Diagram* which is demonstrated at Figure 2.2 for a mirror which is designed to reflect a spectrum between the wavelengths of 1.8 μm and 2.5 μm.

The light line is the expression of a band structure or dispersion relation defines the relation between the frequency ω and the wave vector $k_{//}$ for plane wave solution of the Maxwell's Equation at air. The dispersion relation is defined as :

$$\omega = \mathbf{c}k_{//} \tag{2.4}$$

The entity of the *Light Line* completes the band gap effect to all incident wave vectors. Because propagation of light is not allowed outside of the light cone which is determined by *Light Line*. In conclusion the band gap is valid for all angle of incidence leading to an omnidirectional reflection.

As it can be confirmed through the expression of the band structure, higher index contrast between periodic pairs of dielectric layers lead to shorter evanescent

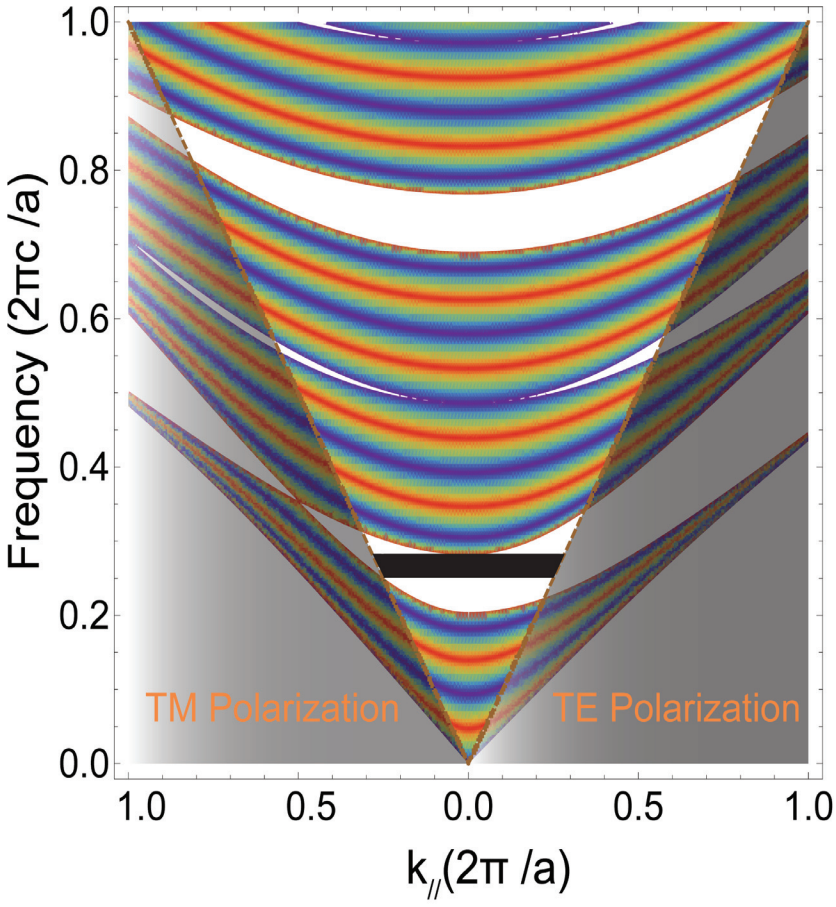

Figure 2.2: Projected band diagram of an infinite layered periodic media with refractive indices of layers alternating from 2.74 to 1.65 is presented for transverse electric (TE) and transverse magnetic (TM) polarizations. The white regions represent the forbidden regime and the allowed regime is shown at various colors. The area under *Light Line* is also forbidden to light propagation in case of coupling the light from air to system. The black trapezoid implies the forbidden band which is caused by periodic media rather than *Light Line*.

decay lengths and smaller electric field power densities of reflected electromagnetic waves in reflecting layers. This will help the structure to reflect the incident light efficiently with fewer periodic layers which leads to a reduced material light interaction. In addition to low absorption values due to reduced light material interaction, higher index contrast give rises to an expansion at the spectrum of the photonic band gap.

The expressions that define the propagation of light through dielectric mirror layers indicate that it is possible to tune the central frequency of the band gap by

changing the thickness of dielectric layers. Moreover theoretically the dielectric mirror layers are capable to reflect with efficiencies near %100 due to low absorption losses. Unlike dielectric mirrors highly reflective metallic mirrors tend to absorb significant amount of light and they fail to reflect efficiently at higher frequencies [22]. The consecutive layers of dielectric media form a periodic structure which can be referred as a macro crystalline lattice. It is a known fact that impurities can diffuse through the crystalline structure to instigate a change in properties of the material. The effect of an impurity layer between dielectric layers has an identical influence on dielectric mirror structures. The impurity layer thickness and position can be determined in order to filter a certain frequency inside the band gap [23]. These structures with unique optical properties has found application as gain flatteners in optical communication, add drop channel filters in dense wavelength division multiplexing systems, laser resonator components, or simple high efficiency reflectors.

2.2 Optical Waveguides and Fibers

Waveguides and optical fibers are considered as the spine of the telecommunication industry. Waveguides can interconnect several networks by guiding light which can carry serious amount of information. There are two major systems that allow waveguides to route a defined frequency of light, namely metallic [22, 24, 25, 26] and dielectric [4, 26, 27, 28]. Including dielectric and metallic waveguides, most of the electromagnetic wave guiding mechanisms work with reflection of light from a smooth surface. The only difference between a mirror and a waveguide is the geometry of the system. Optical fibers can be generally named as dielectric waveguides because they tend to operate at optical frequencies unlike metallic waveguides which tend to work at lower frequencies. Nowadays, major information transfer is acquired through dielectric fibers rather than coaxial metallic waveguides [29]. Metallic waveguides has lost its importance

on industry since their performance has been proved to be inferior to dielectric waveguides. They tend to be highly absorbing, they are hard to shape, they work efficiently at very low frequencies which limit their performance as an information carrier. However, they offer the greatest prospect at radio frequencies. The optical performance of a metallic waveguide can be characterized similar to its layered predecessor. It can be seen through *The Projected Band Diagram* of a metal (Aluminum) layered structure at Figure 2.3 that reflected wave vectors decrease with increasing frequency leading to an angular dependence for reflection. This is the reason why metallic mirrors and waveguides tend to operate better at lower frequencies.

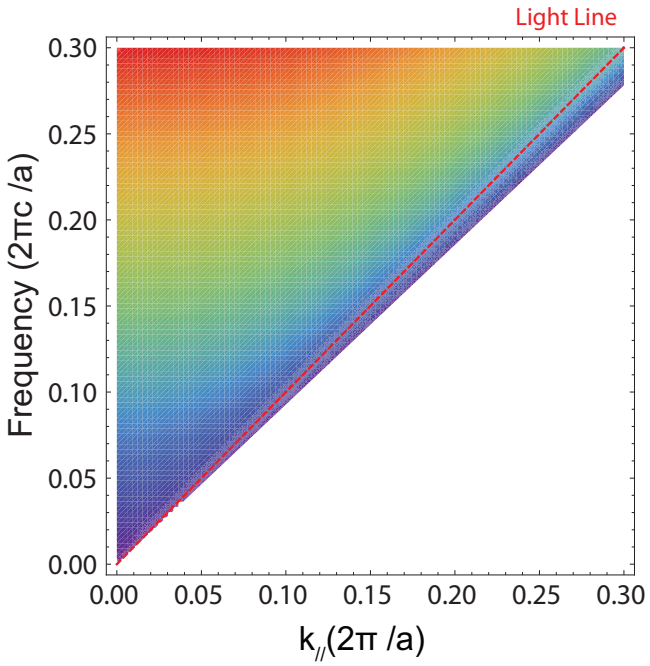

Figure 2.3: Projected band diagram of a metallic mirror which only has a 50 μm thick Aluminum layer is presented for TE polarizations. The white regions represent the forbidden regime and the allowed regime is shown at various colors.

Dielectric waveguides are considered to be the most efficient way to transfer information. They found to be indispensable for optoelectronics and telecommunication industries due to their unique properties. Such that, they can guide higher frequencies of light and they exhibit low absorption levels. Dielectric

waveguides can guide electromagnetic waves by using two different mechanism of reflection. The most famous one is referred as traditional index guiding or total internal reflection (TIR) mechanism [30]. Conventional silica fibers and chalcogenide guiding fibers are waveguides that use this mechanism to guide light [31, 32]. Another mechanism is described previously as the reflection mechanism for dielectric mirrors. This mechanism which is originated from a photonic band gap is named as *photonic band gap reflection*. One dimensional and two dimensional PCFs are general examples of waveguides that guides light by photonic band gap [4, 33].

2.2.1 Index Guiding Waveguides and Fibers

Index guiding waveguides and fibers are found to be the best possible solution for information transfer. Traditional infrastructure of telecommunications is based on silica fibers which use index guiding for reflecting light [27]. These mechanisms exhibit very low loss levels and works efficiently for various frequencies depending on structure and material selection. Propagation of light in such structures is best characterized by remembering that when light with free-space propagation constant K encounters an interface between two materials with refractive indices n_1 and n_2, the component of the wave vector parallel to the interface between two materials remains unchanged. So the system works basically depending on index contrast between two materials (n_1 and n_2). The theoretical explanation of system can be done simply through Eq. 2.5 which is known as Snell's Law.

$$n_2 \sin(\theta_2) = n_1 \sin(\theta_1) \tag{2.5}$$

The relation express θ_2 (the angle of refraction) in terms of θ_1 (angle of incidence) and refractive index contrast. The critical angle (θ_c) corresponds to a

refraction angle of 90 ° which leads the expression $\sin(\theta_2)$ to 1. The critical angle can be defined by Eq. 2.6 .

$$\theta_c = \arcsin\left(\frac{n_2}{n_1}\right) \tag{2.6}$$

The angle of incidences which are greater than (θ_c) leads to complete reflection of incident light. This phenomenon is generally known as *Total Internal Reflection* (TIR). It can be inferred from the theoretical explanation that this system is bound to several parameters. The material selection for index contrast determines the critical angle of incidence which determines the least coupling angle of the system. The TIR mechanism itself restricts the light to be guided at air because the mechanism requires the media of propagation to have a higher refractive index than the cladding media. The only exception is done by using sapphire as cladding media [34]. The dispersion relation of the media of propagation is also crucial in terms of loss output of the fiber which is known as the most limiting case for TIR mechanism. The optical performance limitations have a serious influence on mechanical properties of the materials. Most of the materials that are optically transparent are rigid materials, so the fibers that are made of these materials have a limited flexibility. Even though numerous limitations are set to bound TIR mechanism, there are plenty of TIR fibers which are unrivalled at certain frequencies. Silica fibers are the most famous of all because of their undisputed guiding performance at wavelength of 1.55 μm. This wavelength is the conventional operation spectrum of the telecommunications systems. The projected band diagram of a conventional silica fiber is presented at Figure 2.4.

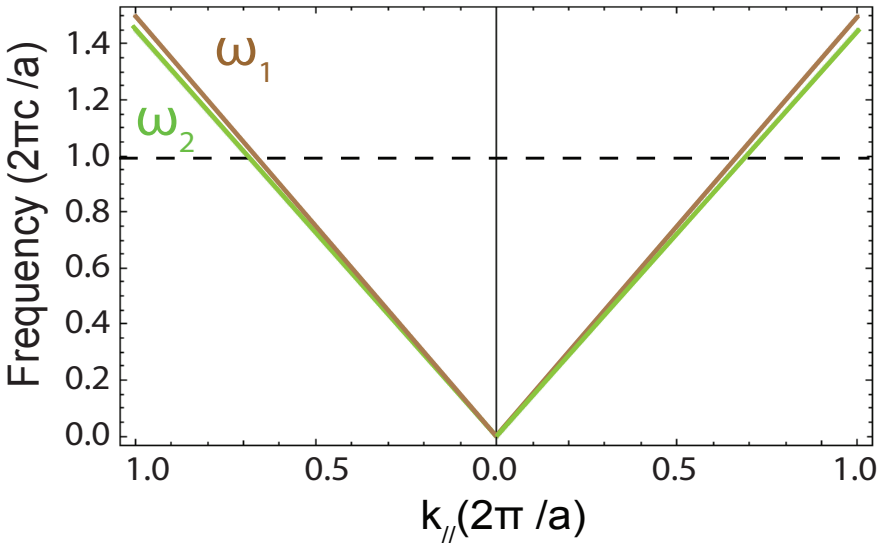

Figure 2.4: Projected band diagram of a conventional silica fiber which has a core material with refractive index of 1.5 (ω_1) and a cladding material with refractive index of 1.45 (ω_1) is presented for both polarizations. The orange colored regions which reside between two light lines that is described for core and cladding materials represent the guiding regime. The dotted line represents the frequency corresponds to working wavelength (1.55 μm) of conventional silica fibers.

The fibers which use TIR as guiding mechanism generally made of two main parts namely core and cladding. Core is the media of propagation for these fibers. Cladding is the media covering the denser core region which leads to index guiding of incident light.

Each pulse of light is composed of different rays with varying angles of incidence on the core-cladding boundary. Thus, one pulse of light will have several rays bouncing around in the core at different incident angles, or different *modes*. A fiber that allows this is called a multimode fiber [35].On the other hand, when the fiber's core diameter is really small, on the order of a few wavelengths of light, there is not much room for the rays to bounce around and the light pulse travels straight in the fiber. The incident modes of 1-D PCFs will discussed briefly at further sections.

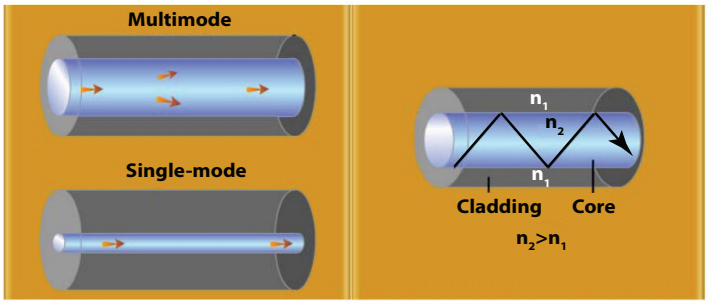

Figure 2.5: Schematic structure of the conventional index guiding fibers. Adopted from [35].

2.2.2 Photonic Band Gap Waveguides and Fibers

As the name refers photonic band gap waveguides and fibers use the photonic band gap mechanism for reflecting light which is explained in detail at Dielectric Mirrors section. However instead of planar geometry most of the waveguides and fibers form a cylindrical geometry so the periodic structure which provides the band gap could be formed in different geometries other than periodic dielectric layers. These structures will help the reflecting mechanisms to guide light through waveguides and fibers. In order to clarify the guiding mechanisms the photonic band gap waveguides and fibers will be discussed separately.

Optical waveguides are becoming increasingly important in communications and for integrated optical circuits. However, bends in waveguides introduce special problems: TIR mechanism and metallic reflectors introduce certain loss mechanisms. The waveguides that use TIR mechanism have a critical radius of curvature for guiding beam through waveguide and metallic mirrors introduces absorption losses. Due to these problems photonic band gap waveguides have received enormous interest. Photonic band gap waveguides can be classified due to their periodicity in dimensions. The periodic structure which provides the optical band gap could be defined as a crystal. A crystal structure could be periodic in all dimensions. In case of waveguides it is possible to define photonic crystals

for every dimension. The periodic structure in one dimensional photonic crystal waveguides built to be periodic only for one dimension the structure is homogeneous at other dimensions. One of the reported structures includes two one dimensional photonic crystal layers with different periodicity and a specialized one dimensional photonic crystal waveguide structure [36]. Waveguide structures that guide the light without loss and even around sharp corners is demonstrated with the help of two dimensional photonic crystal waveguides [37, 38]. The photonic crystal waveguides have been created inside a lattice of sufficient size as a line defect by removal of one or several rows of atoms. Waveguides are designed as line defects in two dimensional photonic crystals which the defect will lead to propagation of a certain frequency along the waveguide. These structures are found to be useful at planar light-wave circuits.

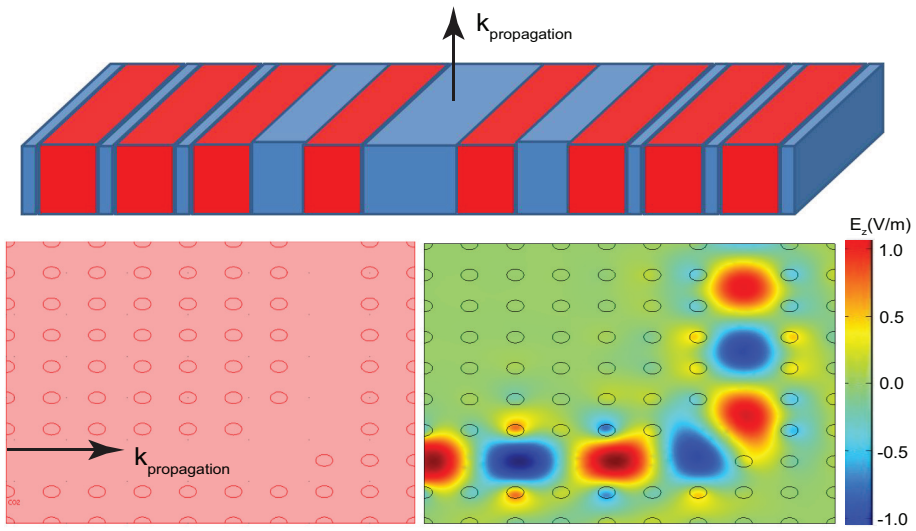

Figure 2.6: (A) One dimensional photonic crystal with varying periodicity, (B) The Finite element analysis of a two dimensional photonic crystal waveguide that helps the light with a wavelength of 1 μm to turn a sharp corner are presented [37]. The finite element analysis is made with commercially available Comsol Multiphysics software.

The first three dimensional photonic crystal with a complete band gap is fabricated by Yablonovitch [39]. The structure which Yablonovitch had suggested is designed to work at microwave regime however it has been demonstrated by

Scherer [40] that these structures can be fabricated to reflect incident radiation with a wavelength of 1.5 μm. A structure which is quite different from Yablonovite has been realized by Fan [41] as a three dimensional photonic crystal reflector. Although many three dimensional photonic crystal structures with different geometries have been introduced a waveguide design from these structures is a different story. Several options have been demonstrated by Chutinan and Noda [42]. This model is quite similar to the waveguide designs at conventional one and two dimensional photonic crystal waveguide designs which involve a defect at crystal in order to allow the propagation of a certain wavelength along the waveguide.

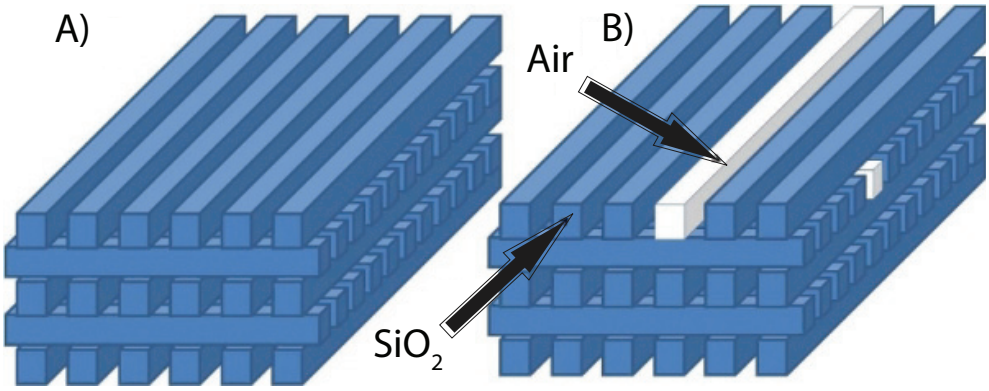

Figure 2.7: (A) Three dimensional photonic crystal without any waveguide structure, (B) Three dimensional photonic crystal with a defect rod introduced for waveguiding are presented

Optical fibers can be referred as a subsection of optical waveguides, however due to their unique geometry fiber structures are considered as a separate research field. Optical fibers can be expressed as an excellent approximation of two dimensional structures because they are infinite in the third dimension. Due to their structure they are invariant along their length, with all interfaces are parallel to the fiber axis. It could be possible to guide an electromagnetic wave with such ease by using fiber structures. Moreover different from waveguides, optical fibers can be used in applications other than guiding of electromagnetic waves including supercontinuum generation [43] and focusing of light into subwavelength dimensions [44]. The main concern of this thesis is related to guiding

of an electromagnetic wave at a certain frequency range so the focus in the case for optical fibers will be propagation of light through photonic band gap fiber structures. It is possible to characterize photonic band gap fiber structures as it has done for photonic band gap waveguides. But it is important to state that there are optical fibers which include photonic crystal structures that guide light through TIR mechanism [45]. So here the fibers that are presented as PCFs only refer to the ones that guide light by a photonic band gap. Additionally because of three dimensional PCF are yet to be presented only one and two dimensional PCFs will be explained briefly.

PCF confine light using an optical band gap like dielectric reflectors rather than TIR mechanism which can be exemplified with conventional optical telecommunication fibers. The main motivation behind the development of Photonic crystal fibers is to guide the electromagnetic wave inside air rather than a dense media as it is the case for TIR fibers. As a result of this property of band gap guiding, effects of losses are decreased and unwanted non-linear effects are avoided [33]. The lowest loss value reported for hollow core fibers is 13dB/km [46].

The concept of 2-D PCF is first introduced by Birks and his colleagues [47]. The most common design can be described as a hollow core fiber in which the cross section is a periodic array of air holes placed along the length of the fiber [33]. The origin of the band gap for 2-D PCFs is similar to the two-dimensional band gaps that are being investigated for planar light-wave circuits [38]. The most common geometry for 2-D PCFs is presented at Figure 2.8.

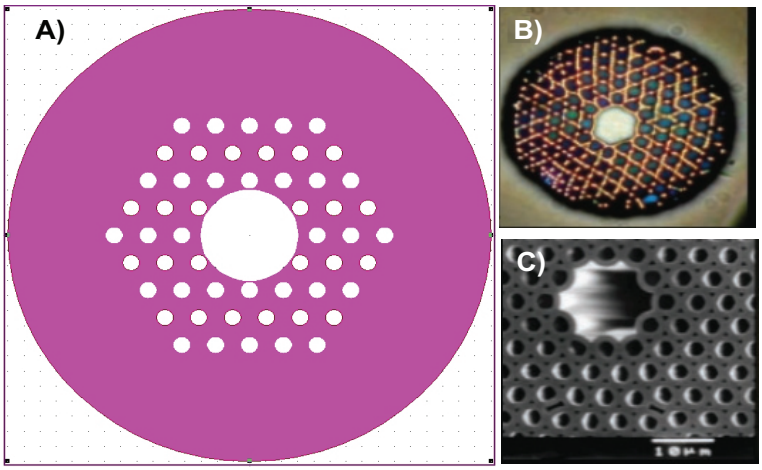

Figure 2.8: (A) Most common geometry for 2-D PCFs, (B) Optical micrograph of a different shaped(honeycomb) 2-D PCF, (C) Scanning electron microscope (SEM) image of the conventional 2-D PCF with a hollow core are presented. Adopted from Russel [28].

In order to realize such structures a preform of the resulting fiber must be fabricated. The preform is a macroscopic scale version of the PCF which will be scaled down to fiber dimensions during drawing procedure. This procedure will be explained in detail at fiber design and fabrication section of this thesis for 1-D PCFs. In case of 2-D PCF's the preform is made from capillaries which are stacked around a mold which will be released in order to form the hollow core of the fiber [2]. The resulting fibers are presented at the Figure 2.9. In order to bond the capillaries to each other for the formation of a rigid structure the preform is baked inside a high temperature oven. Another inferior method for fabrication of PCF's is known as extrusion of such preforms [48].

The resulting fibers are generally used for guiding applications as it was stated before, however it is possible to use these structures as optical sensors for several materials [49]. Moreover these fibers are used to make fiber lasers because of their capability to guide electromagnetic waves through air [50]. Although 2-D PCFs are reported to be useful for several applications their performance is limited for the case of guiding. 2-D PCFs are generally used at higher frequencies. They

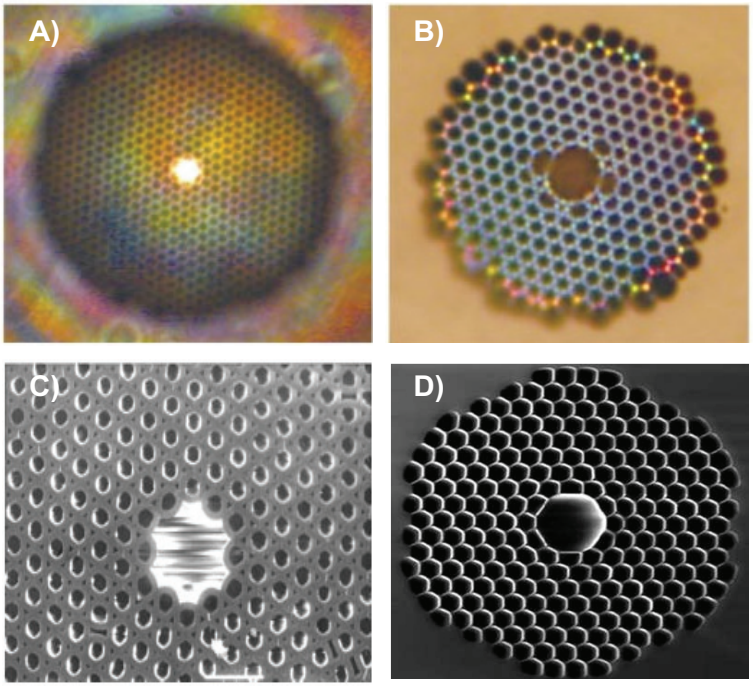

Figure 2.9: (A) Optical micrograph of an index guiding PCF , (B) Optical micrograph of a band gap guiding PCF, (C) SEM image of a band gap guiding PCF made from capillaries, (D) SEM image of a band gap guiding PCF with honeycomb structure are presented. Adopted from Knight [3].

are not feasible to work at lower frequencies because of their structure, their dimensions and material dispersion problems.

Instead of using two dimensional periodicity to make a band gap fiber, it is possible to use a one dimensional periodicity as it is made for dielectric mirrors for planar surface. Different from planar surface, this periodic structure is placed inside a cylindrical geometry in order to use one dimensional periodicity to make a band gap fiber. Such structure is first proposed by Yeh et al. [20] who is named with the most important figures behind the theory of dielectric mirror structures. Fink et al. [3] has realized such structures experimentally. The 1-D PCFs are made with layers of low index polymeric material and high index glassy material which can be observed from Figure 2.10. These layers act as a dielectric mirror and help these fibers to confine a certain frequency of light inside a hollow core. Due to their unique way of guiding light they are highly excelled at high power laser delivery which makes them quite useful for medical applications

[4, 51]. The frequency dependency of reflectance can be compensated through proposing a frequency scalable production method. The appropriate method of fabrication will help produce 1-D PCFs with varying working frequency with respect to their dimensions. The only disturbance left to introduce to this system is absorption behavior of dielectric material couple which can be eliminated with an appropriate material couple.

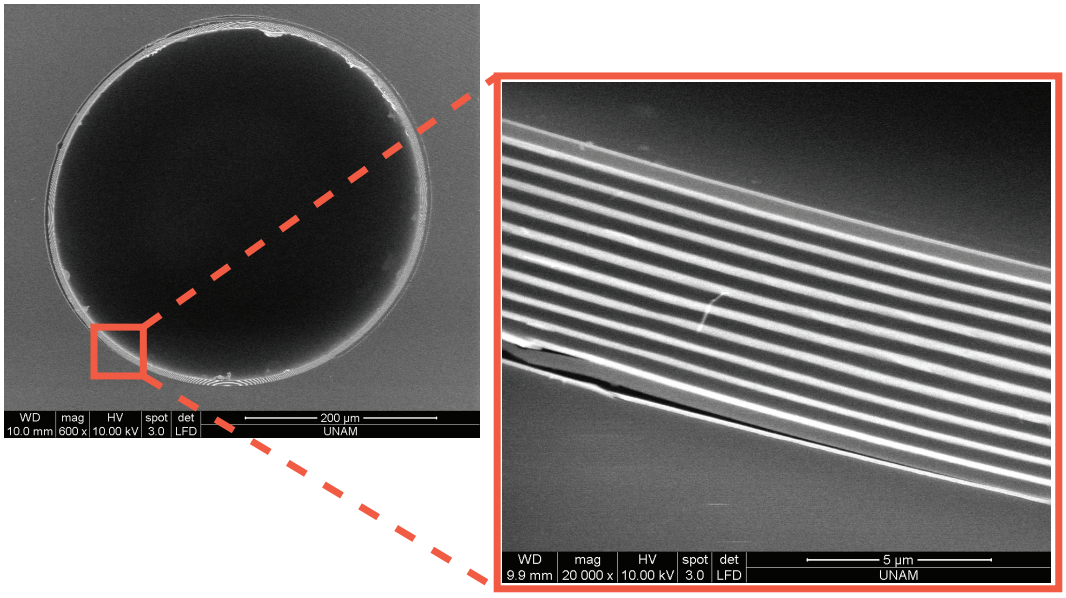

Figure 2.10: Scanning electron microscope (SEM) image of a 1-D PCF for HO:YAG laser guiding are presented.

Theoretical explanation of spectral response of such fibers is made similar to dielectric mirrors. Projected band diagram is the fundamental presentation method of photonic crystal structures, so naturally the spectral response of 1-D PCFs are expressed through projected band diagram. Other than projected band diagram which represents the band structure with respect to frequency, intensity density plots can be used to visualize omnidirectional reflection mechanism inside these fibers. The both visualization methods will be used to express the structures related to this thesis. A projected band diagram and an intensity density plot of reflective layers inside a CO_2 laser guiding fiber is presented at Figure 2.11.

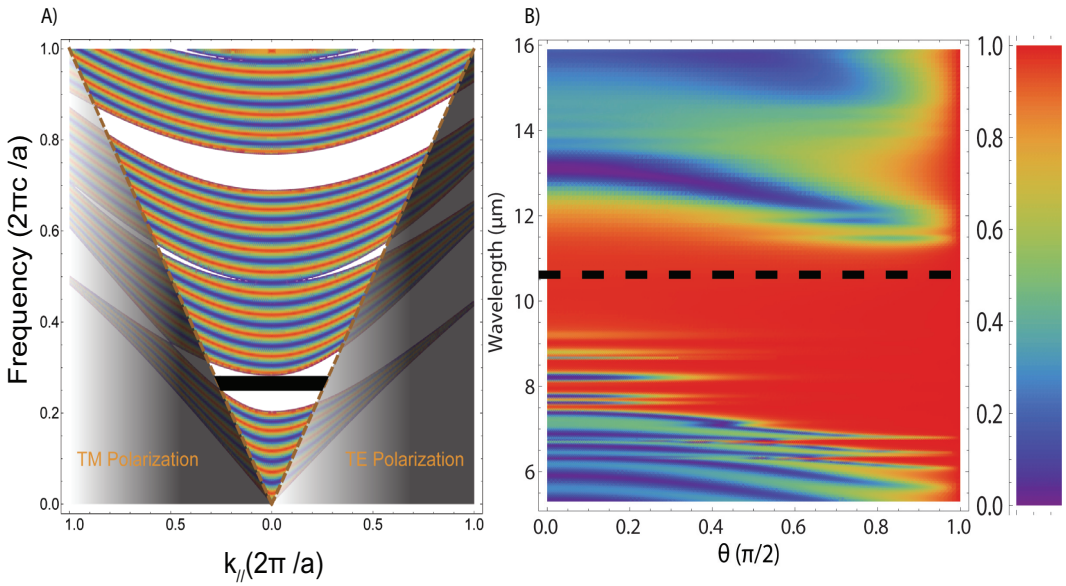

Figure 2.11: (A) Projected band diagram and (B) Intensity density plot of reflective layers of a CO_2 laser guiding fiber are presented.

In recent years the performance analysis of such fiber structures are investigated with respect to guided modes and losses incident inside these fibers [52, 53, 54]. It is demonstrated on one of these publications that 1-D PCFs can guide light inside a huge hollow core with just a single propagation mode [52]. Additionally, Ibanescu et al. points out the similarity between the modal behavior of a metallic waveguide and 1-D PCFs. This paper claims that the modal behavior of a metallic waveguide and 1-D PCF has a single phase difference [53]. The lowest loss mode of 1-D PCFs are reported to be TE_{01} which is interestingly the case for hollow metallic waveguides. The losses of such fibers can be identified with two main subjects namely cladding losses and inter-modal coupling. Cladding losses include material absorption, radiation leakage due to finite sized crystal and scattering from disorder. Cladding losses seem to decrease with increasing core diameter however it is useful to state that increasing core diameter has a negative effect on inter-modal coupling losses. Inter-modal coupling incident can be summarized as the transfer of energy from one mode to another with the same frequency but different momentum. The increase in inter-modal coupling losses with increasing diameter is related to two main problems.

First, the number of modes guided inside the core increases with increasing core diameter, so the mode spacing decreases which allows for the energy transfer between modes. Second, even for stable mode spacing, the inter-modal coupling due to fiber bends will increase with increasing core diameter [55]. The modal and loss behavior of one dimensional photonic crystal will be used during design of these fibers at Chapter 4 and optical characterization at Chapter 5.

In summary, along this chapter we have mentioned relevant background information about dielectric mirrors, photonic crystal phenomena, waveguide and fiber structures. Most of this information is based on theoretical explanations originating from solutions of electromagnetic equations under given boundary conditions. This theoretical information will direct the course of this thesis and it will provide the fundamentals which support the architecture of 1-D PCF structures for medical applications. Moreover, these basics will be used to build fiber based devices such as sensors and external band reflectors. The issues on design, fabrication of 1-D PCFs and fiber devices along with optical measurement results will be presented at upcoming chapters. Next chapter is related with optical and mechanical characterization of candidate material properties which is acknowledged as the first step to build a 1-D PCF.

Chapter 3

MATERIALS CHARACTERIZATION

3.1 Introduction

The field of optical fibers demands several qualities from materials which constitute the body of the fiber. The materials are required to be non-absorbent along the spectrum of guiding. Moreover the fabrication procedure requires these materials to be drawn in a viscous state without disturbing each other in a controlled manner [27, 56]. This thesis particularly interested in the fabrication of 1-D PCFs which are known as a new subsection of optical fibers. These structures which are also known as *Bragg Fibers* have a composite structure different than conventional optical fibers which mainly consist of a core and a cladding layer.

As it was mentioned before the fabrication procedure of such structures requires viscous drawing of composite materials. In order to acquire optically transparent materials in a viscous regime the materials are heated in order to decrease their viscosity. In case of fiber geometry, a solid macro model of the fiber

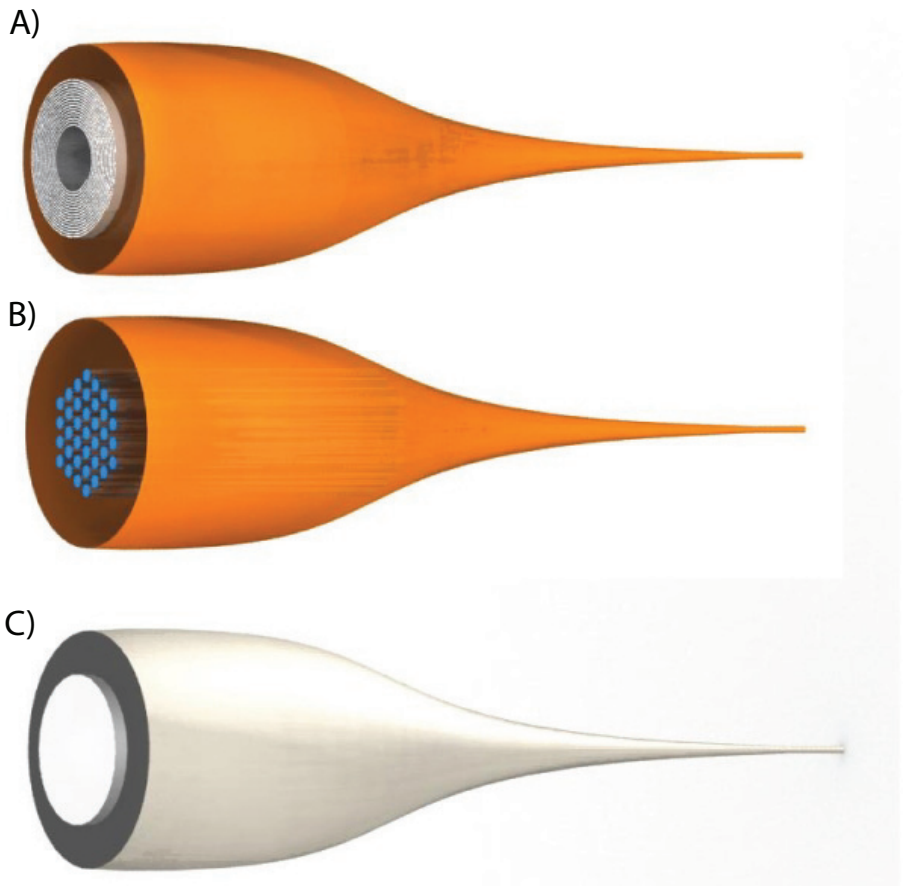

Figure 3.1: Thermo-mechanical drawing of (A) Bragg Fiber, (B) 2-D PCF for TIR waveguiding, (C) Conventional silica fibers is presented

(preform) which is made from these materials is heated and thermo-mechanically reshaped to fiber dimensions. This is the case for conventional optical fiber drawing mechanism [27]. But it is crucial to state that the structure we plan to fabricate is composite material which consists of many submicron layers which requires precise material matching both optically and thermo-mechanically [7]. The main focus in this chapter is to clarify the options of material couples which have compatible optical and thermo-mechanical properties. The structure of a Bragg Fiber consists of many submicron dielectric layers and a dielectric cladding for mechanical support. The reflection mechanism of these fibers requires a high index contrast between two candidate materials. In light of this information

supporting layers are chosen from polymeric material candidates with low refractive indices and the coupling reflective layers are chosen from glassy materials which have a higher refractive index. The characterization of optical and thermo-mechanical properties of candidate materials is reported through this section.

3.2 Thermo-mechanical Characterization

Non-crystalline solids lack a systematic and regular arrangement of atoms over relatively large atomic distances. Sometimes such materials are called *amorphous materials*. In atomic structures of the amorphous materials there is no repeating unit or crystal structure, due to this formation the viscosity of an amorphous material varies with temperature continuously between liquid and solid state of the material. This viscosity behavior allows these materials to be drawn with the help of the heat which manipulates viscosity [57, 58]. Amorphous materials especially inorganic glasses and thermoplastic polymers are known to be the best possible choice for fabricating optical fiber designs.

The different viscosity behavior of crystalline and amorphous materials can be explained through the phase transition relation of such materials. Crystalline materials experience a first-order phase transition at the melting temperature of the material which leads to a discontinuous change in volume and viscosity with varying heat at melting temperature [59]. Unlike crystalline materials, temperature modulations lead to quasi-continuous changes in volume and viscosity at amorphous (glassy) materials [60]. The following Figure 3.2 indicates the temperature dependence of a glassy material's and a crystalline material's volume. This figure is adopted from Debenedetti et al. [61].

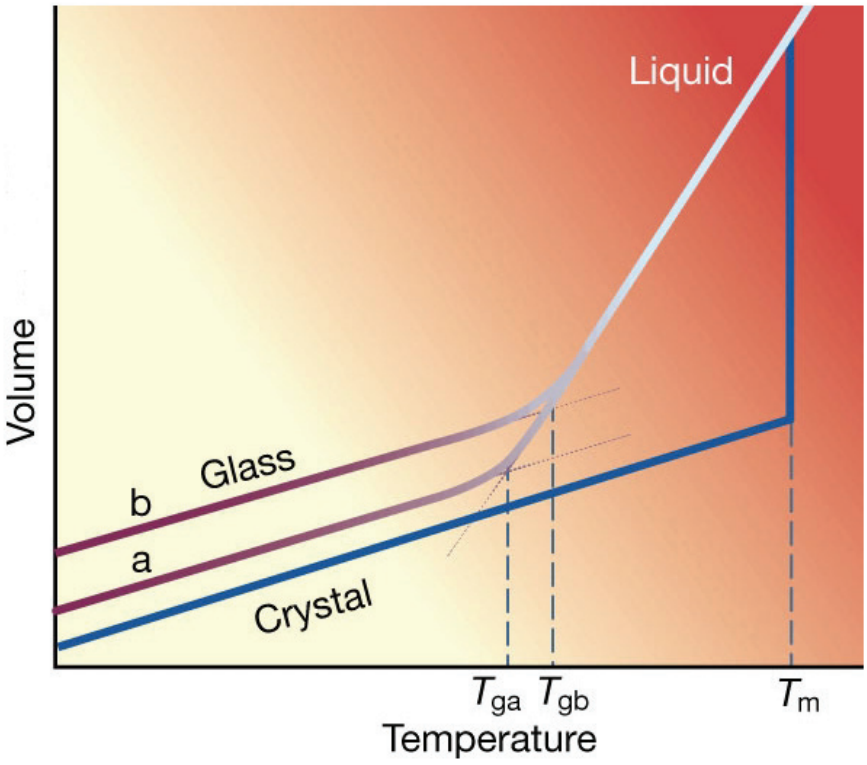

Figure 3.2: The temperature dependence of a liquid's volume is presented. T_m indicates the equilibrium melting temperature, T_{ga} and T_{gb} represents the glass transition temperature of two glassy materials. Adopted from Debenedetti et al. [61].

There are several polymeric and glass materials which satisfy the optical parameters, however due to incompatibility of thermo-mechanical properties, very few of them are found to be useful for Bragg Fiber fabrication. The investigation of properties of candidate materials through literature leads to the conclusion that the use of chalcogenide glass as higher index media and engineering thermoplastics as low index media is the best possible choice for fabrication of Bragg Fibers [7, 62, 63, 64]. However there are many materials available along both for chalcogenide glasses and engineering thermoplastics which indicate the need of a thorough examination of candidate materials in order to clarify the appropriate material couples. The thermo-mechanical properties of candidate materials are examined through their glass transition temperatures in order to confirm whether they are amorphous or not, their viscosity-temperature dependence under extensional strain, their stress and strain values during drawing procedure.

The glass transition temperature (T_g) represents the temperature point when the material viscosity and volume begins to change drastically with respect to temperature. In case of organic polymers like engineering thermoplastics secondary, non-covalent bonds between the polymer chains become weak above T_g [65]. In inorganic glasses, joining bonds are broken through thermal fluctuations as a result of increased temperature so that broken bonds begin to form clusters. The temperatures above T_g lead to an increase in the size of these clusters which helps material to flow easily [59]. As a result of such mechanisms, material temperatures higher than T_g result in very low viscosity values for materials which allows materials to be reshaped through force namely plastic deformation [66]. As for most of the glassy materials the glass transition temperature gives the first intuition about whether two materials can be used together in a thermo-mechanical process without disturbing each other. The candidate glassy materials are chosen from infrared transparent chalcogenide glasses in order to limit absorption values. The candidate materials are reported as As_2Se_3, As_2S_3 which are commercially obtained from Amorphous Materials and commercially known as Amtir-2 and Amtir-6 respectively. Another glass which consist of Ge, As, Se, Te molecules is synthesized through using recipes from literature [67, 68, 69]. Glassy materials used in this thesis are obtained from the methods presented above. The polymeric materials used along this thesis are acquired from Ajedium films and their commercial names are Ultem (PEI) and Ultrason E (PES).

It is a known fact that low atomic interconnectivity leads to low softening points for glass materials. As the case for chalcogenide glasses *8-N Rule* [70] is used to determine the coordination of an atom [60, 71]. However if we consider the reported chalcogenide glasses at Figure 3.3 it can be seen that most of them have near atomic interconnectivity. The atomic interconnectivity is known as the strongest effect on T_g but it is also crucial to state the influence of atomic weight on T_g. If the atomic weight of the material gets high due to addition

of heavy elements the glass transition tends to decrease while increasing the refractive index of the glass [59]. This phenomenon can be explained by lower binding energy of atoms at heavier elements and enhanced polarizability of outer electrons at heavier and bigger molecules. This effect can be clearly seen on the measurement acquired from TA Instruments Q2000 Differential Scanning Calorimetry System (DSC) at Figure 3.3.

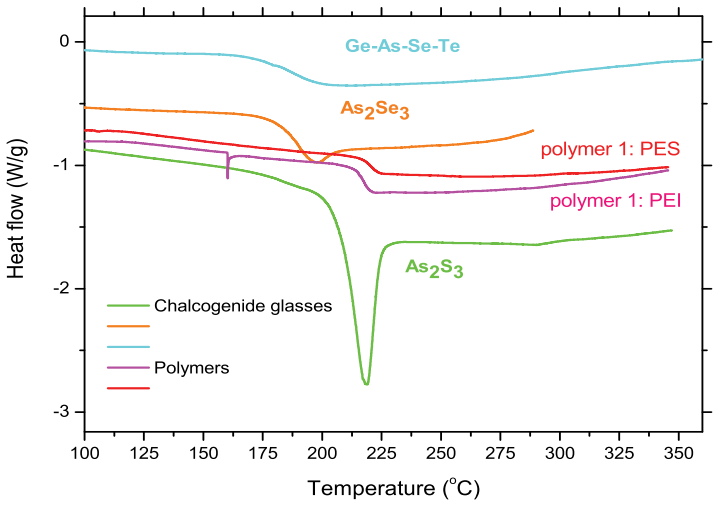

Figure 3.3: The DSC data of several candidate materials are presented. The most appropriate glasses are reported as As_2Se_3, As_2S_3, $Ge_{15}As_{25}Se_{15}Te_{45}$(a type of GAST material) and the compatible polymeric materials are reported as Polyetherimide (PEI), Polyethersulfone (PES).

The T_g and atomic weight of candidate materials have been presented at Table 3.1.

Table 3.1: Atomic weight and glass transition temperatures of candidate glass and polymeric materials. Blank entries are left empty due to variance in atomic weight of polymeric materials.

Materials	Atomic weight (g/mol)	Glass Transition Temperature (°C)
As_2Se_3	387	196
As_2S_3	246	212
$Ge_{15}As_{25}Se_{15}Te_{45}$	9885	190
PES		223
PEI		221

One of the most crucial thermo-mechanical properties in production of nano-structured Bragg Fibers can be cited as viscosity-temperature dependence of the material couples. Especially this behavior is quite important when an amorphous structure is reshaped under high temperature and considerable stress. If we consider that Bragg Fibers are made from two amorphous materials like a composite structure, the first condition for appropriate fabrication of these fibers will be the harmony of these amorphous materials viscosity-temperature dependence. A theoretical explanation will be provided for behavior of viscosity-temperature dependence of candidate materials. The very basic relation for viscosity is the relation between proportionality constant (η) of viscosity and constant stress (σ) applied to material which will result in a strain rate ($d\epsilon/dt$):

$$\sigma \propto \eta \frac{d\epsilon}{dt} \tag{3.1}$$

The relation presented here can be applied to all viscous materials. However for some materials viscosity remains constant independent from variations in stress or strain rate. These materials are referred as *Newtonian Fluids*. The viscosity model for material candidates of Bragg Fiber is done assuming that these materials behave as a newtonian fluid although they generally tend to behave as non-newtonian fluids in reality. In case of glass materials there is a consistent model defined to explain the temperature viscosity dependence of materials [72]. However the situation is different for polymeric materials in which there are plenty of model incident. There is a certain model which excels to describe temperature dependence of viscosity for thermoplastic polymer liquids namely William-Landel-Ferry Model [73]. The theoretical explanation of viscosity behavior with respect to temperature for polymeric candidates will be done through using this model. Glass melts can be characterized due to viscosity behavior. The glasses which behave with respect to Arrhenius model are named as *strong*

liquids and glasses with more abrupt viscosity changes are named as *fragile liquids*. The Arrhenius model is presented at Eq. 3.2 in which E_η corresponds to activation energy, R corresponds to universal gas constant and η_0 corresponds to a material dependent viscosity constant.

$$\eta = \eta_0 \exp\left(\frac{E_\eta}{RT}\right) \tag{3.2}$$

Arrhenius model is a general model which is used for all glass with strong liquid behavior. However in recent years a specific model for chalcogenide glasses has been published [72]. The general relation for chalcogenide glasses is presented at Eq. 3.3.

$$log(\eta) = log(\eta_0) + \left(\frac{C\exp(D/T)}{2.3RT}\right) \tag{3.3}$$

Here C and D are material constants which are determined through empirical techniques [72]. In light of this model the temperature dependence of viscosity for As_2Se_3 can be described through following expression:

$$log(\eta) = -3.09 + \left(\frac{(18878)\exp(876/T)}{2.3RT}\right) \tag{3.4}$$

Additional to As_2Se_3 the temperature dependence of viscosity for As_2S_3 can also be described through this model:

$$log(\eta) = -3.62 + \left(\frac{(33744.1)\exp(650.83/T)}{2.3RT}\right) \tag{3.5}$$

The custom made GAST materials temperature dependence of viscosity is yet to be modeled so the viscosity compatibility of this material will be acquired from experiments. However the T_g of GAST materials is so close to the crystallization

temperature of these materials which will cause crystallization of GAST materials during drawing procedure. So it is hard for a GAST material to be drawn efficiently with other amorphous materials.

The temperature dependence of viscosity of polymeric materials will be expressed by William-Landel-Ferry Model. The main expression of this model is reported at Eq. 3.6.

$$log(\eta) = log(\eta_0) + \left(\frac{-C_1(T - T_r)}{C_2 + T - T_r}\right) \tag{3.6}$$

In this relation C_1, C_2 and T_r are fitting parameters. Because this model describes the behavior of polymeric liquids by using several measurement data, these parameters are specifically assigned to a certain sample. The data required to determine the relation is acquired from real time drawing data in which the stress, the strain rate and the temperature are recorded. The viscosity can be acquired through Trouton relation (Eq. 3.7) which is derived from Eq. 3.1 [74].

$$\sigma = 3\eta\frac{d\epsilon}{dt} \tag{3.7}$$

The viscosity of PES and PEI is calculated from real time drawing data. The viscosity of PES is found to be $9.5x10^4 Pa * s$ at 536 Kelvin and the viscosity of PEI is found to be $6.68x10^4 Pa*s$ at 555 Kelvin. According to this viscosity values a modified version of Van Krevelen methodology is used at William-Landel-Ferry Model which defines fit parameters as $C_1 = 8.86$, $C_2 = 52.86$, $T_r = T_g + 43K$ and set η_0 value from a given measurement data of a certain material [75]. In which it is found to be $5.0685x10^4 Pa * s$ for PES and $6.52x10^5 Pa * s$ for PEI. The temperature viscosity dependence of candidate materials except GAST has been presented on Figure 3.4.

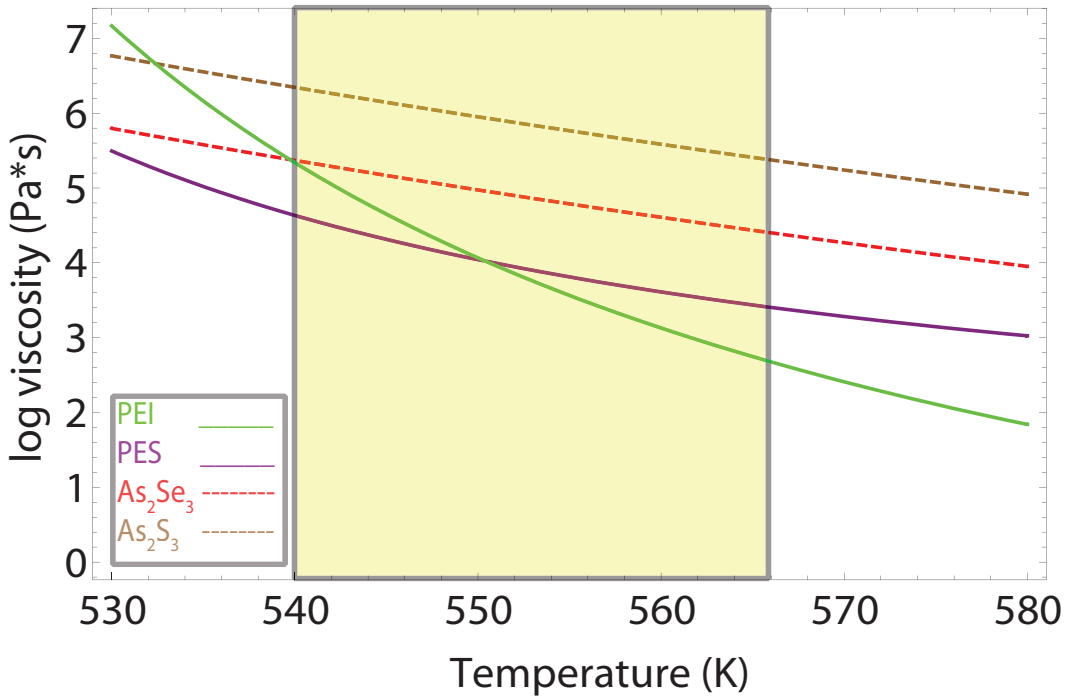

Figure 3.4: The temperature viscosity dependence of several candidate materials are presented. Shaded region corresponds to drawing temperature regime where the glasses and polymers viscosity values are in harmony.

The remaining parameters for thermo-mechanical characterization of candidate materials are stress and strain during drawing which will be addressed as dynamic analysis of drawing procedure at Chapter 4. These parameters can be acquired experimentally but also we can find those values by using Trouton approximation. The viscosity temperature dependence of all candidate glass and polymeric materials has been presented at this section. So according to Trouton approximation only parameter needed to obtain the stress temperature dependence of candidate materials is strain rate of these materials. It is useful to state that strain rate can be described through dimension change in fiber structures during drawing procedure (Eq. 3.8).

$$\frac{d\epsilon}{dt} = \frac{(\nu - V)}{V} \tag{3.8}$$

The relation between the feed speed (V) and drawing speed (ν) will be explained at Chapter 4. But it is possible to illustrate the stress behavior of candidate materials by using one of the sample fiber geometry. The temperature dependent stress values of candidate materials for a sample fiber geometry which is drawn with V=0.465 mm/min, ν=364 mm/min can be observed from Figure 3.5. This fiber geometry has an inner diameter of 421 μm and an outer diameter of 1.14 mm.

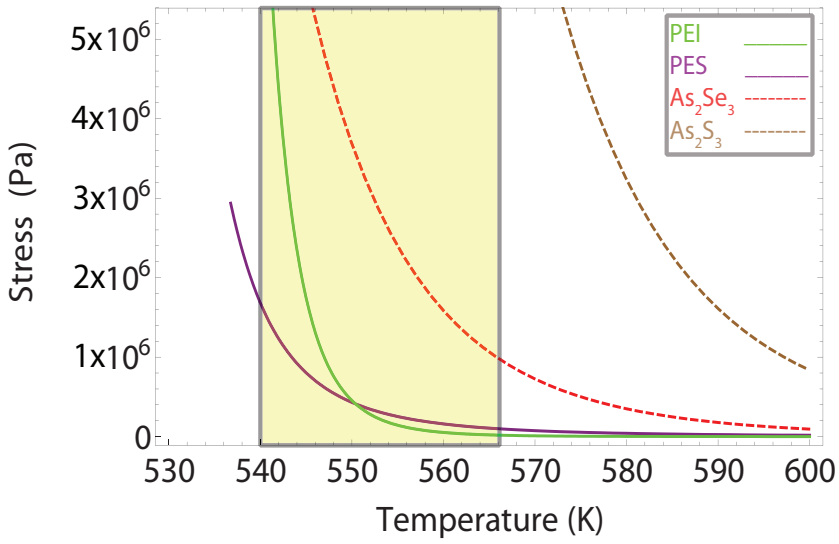

Figure 3.5: The temperature stress dependence of several candidate materials are presented. Shaded region corresponds to drawing temperature regime where the glasses and polymers stress values are comparable.

The stress temperature dependence for the sample geometry helps us to obtain the tension values incident on materials during drawing procedure which will be deterministic in order to decide the appropriate material couples for Bragg Fiber production through drawing. The tension values of candidate materials for same fiber geometry are presented at Figure 3.6.

Tension is an important parameter to determine because it is possible to measure tension of a fiber during drawing procedure which will help to confirm the given approximation for temperature dependency of stress and viscosity. The

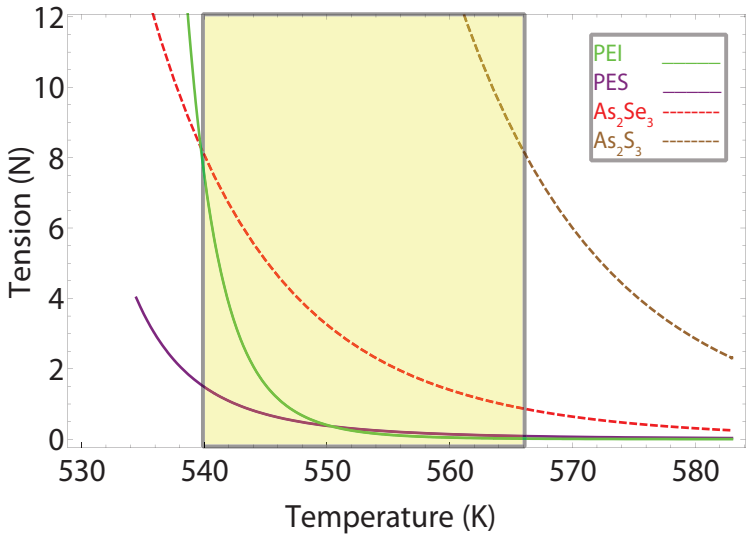

Figure 3.6: The temperature tension dependence of several candidate materials are presented. Shaded region corresponds to drawing temperature regime where the glasses and polymers stress values are comparable.

numerous experimental data are found to satisfy the presented model as we further develop fiber drawing procedure.

During the thermo-mechanical characterization, some of the materials are assumed to be in bulk form. However we need to consider a thin film geometry especially for chalcogenide glasses which are modeled without using experimental data. The GAST materials are omitted as a candidate material as they fail to be drawn homogeneously with polymeric materials. So As_2Se_3 which is decided to be the most appropriate chalcogenide glass for candidate polymeric materials is examined through X-Ray diffraction methods. X-Ray diffraction method will help us to determine whether the amorphous behavior of the glassy material is conserved or not. The results of a powder sample and a thin film sample measured with Pananalytical X'pert Pro Materials Research Diffractometer(MRD) is presented at Figure 3.7.

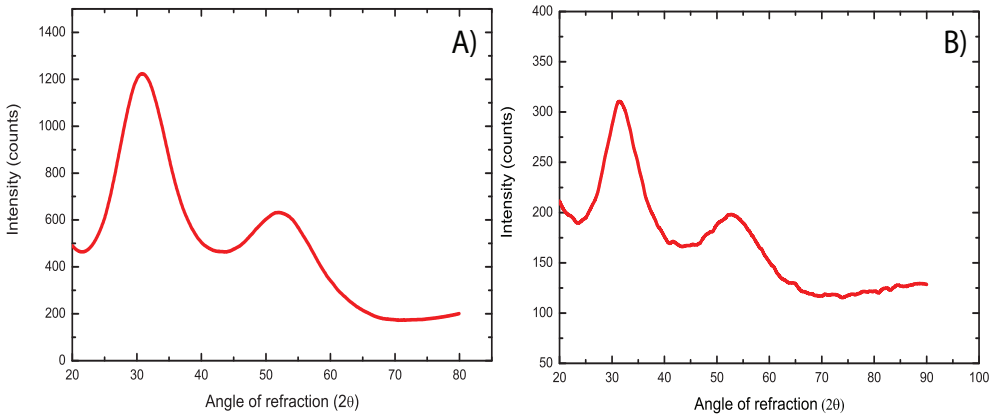

Figure 3.7: X-Ray Diffraction results of (A) thin film formed As_2Se_3 and (B) powder formed As_2Se_3 is presented. The amorphous behavior of material is observed to be conserved at both formation.

In conclusion several chalcogenide glasses are matched with their proper polymeric pairs by identification of several important properties of candidate materials. Important parameters such as glass transition temperature, temperature dependence of viscosity, stress and tension are identified throughout this section. The amorphous behavior of As_2Se_3 seems to be conserved in thin film formation which supports the accuracy of the information about chalcogenide glasses presented in this section. In light of acquired information several candidates of glasses and polymers are found to be convenient for Bragg Fiber manufacturing namely As_2Se_3, As_2S_3, $Ge_{15}As_{25}Se_{15}Te_{45}$ for glass materials and PES, PEI for polymeric materials. The optical performance of thermo-mechanically selected candidates will be carried out at next section.

3.3 Optical Characterization

Optical characterization of materials is vitally important during the design of the fiber. The information acquired from optical characterization of candidate materials will present whether they are appropriate for the purpose of the optical

fiber or not. The working wavelength of the optical fiber is the most detrimental parameter during the analysis of candidate materials. In order to be labeled as adequate candidate materials are required to have a convenient index and low loss values at operating wavelength of the fiber. As we consider the case for Bragg Fibers in which the operating wavelength varies with application field it is possible to address several wavelengths for medical applications. The operating wavelengths of several important medical lasers can be stated as 2.1 μm for Holmium:YAG(yttrium aluminum garnet) lasers, 10.6 μm for CO_2 lasers, 2.94 μm for Er:YAG, 2.6 to 3 μm for Hyrdogen Flouride lasers and 5 to 6 μm for CO lasers. This thesis only interest in developing fibers for Holmium:YAG and CO_2 lasers. So the wavelengths to focus on can be reduced to 10.6 μm and 2.1 μm.

In order to understand the behavior of candidate materials at a certain wavelength an ellipsometric investigation of candidate materials is essential. Every candidate glass material is deposited on a glass substrate as a few μm thick layers. The resulting samples are then optically characterized at J.A. Woollam IR-Vase Ellipsometer for infrared regime and V-Vase Ellipsometer for visible regime. In order to reach the dispersion relation for each material the acquired results are fit into a related function. The Cauchy function [76] can describe dispersion for a material that is essentially non-absorbing over the measured wavelength range. Similar to Sellmeier and Pole oscillators, the Cauchy function is most effective when the data curve is fit to normal dispersion. It is important to state that the dispersion relation which is given at Table 3.3 is described in terms of refractive index n ($Re[\sqrt{\epsilon}]$).

Table 3.2: Cauchy Equations and fitting parameters are reported.

Equations	Parameters	Variables
$N_n = A_n + \frac{B_n}{\lambda^2} + \frac{C_n}{\lambda^4}$	A_{nn}=A_n (dimensionless)	N_n (refractive index)
$K_n = \alpha.e^{\beta(E-\gamma)}$	$B_{nn} = B_n$ (μm^2)	K_n (absorption coefficient)
$\epsilon_n = (N_n + iK_n)^2$	$C_{nn} = C_n$ (μm^4)	ϵ_n (complex index of refraction)
	λ (μm)	
	A_{kn}=α (dimensionless)	
	B_{kn}=β (eV^{-1})	
	C_{kn}=γ (eV)	

In Cauchy equation the term A_n represents the asymptotic behavior at longer wavelengths while B_n and C_n are the dispersion terms that add upward slope to the dispersion relation at shorter wavelengths. The Cauchy dispersion is designed to represent the normal dispersion which is generally incident on transparent materials like glasses. The measured and fit data will lead to a dispersion relation which is presented from Figure 3.8 to Figure 3.10 for candidate glasses.

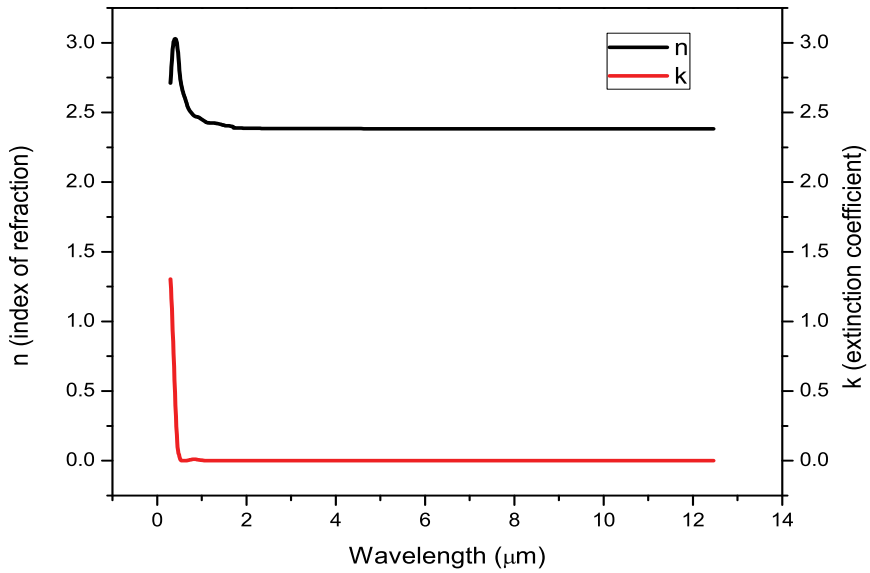

Figure 3.8: The optical properties of As_2S_3 is presented.

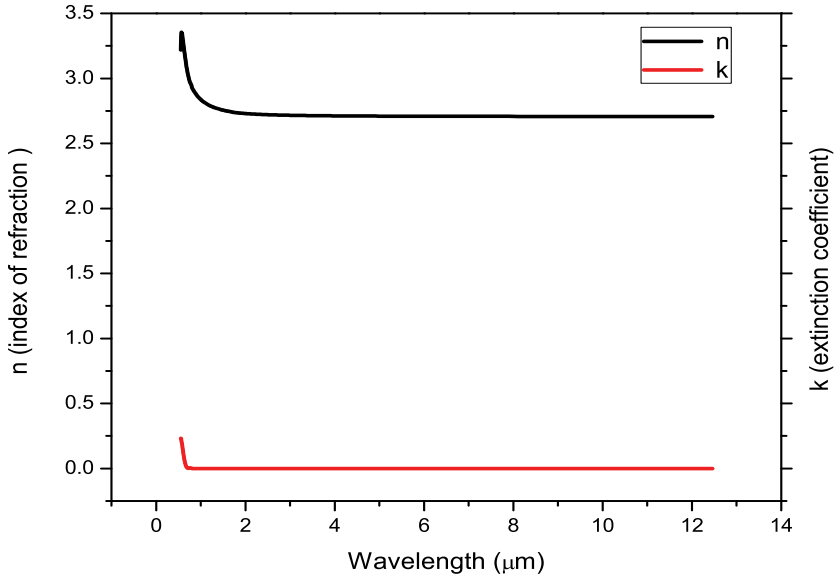

Figure 3.9: The optical properties of As_2Se_3 is presented.

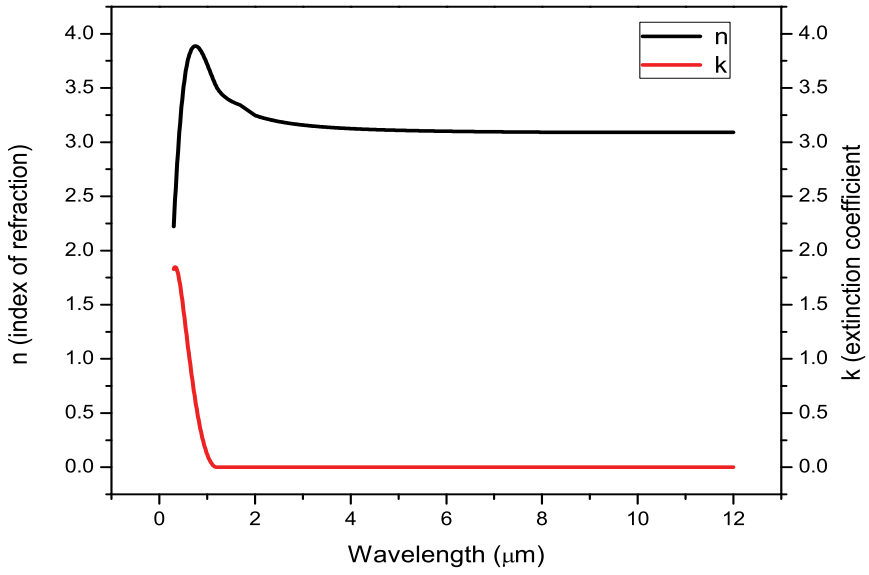

Figure 3.10: The optical properties of $Ge_{15}As_{25}Se_{15}Te_{45}$ is presented.

Unlike glasses the polymeric materials tend to absorb heavily at various wavelength values which makes their dispersion relation quite different from Cauchy equation. Many absorption lines incident on polymeric material data can only be fit through using several oscillator models. The fit data for polymeric materials is presented at Figure 3.11 and Figure 3.12.

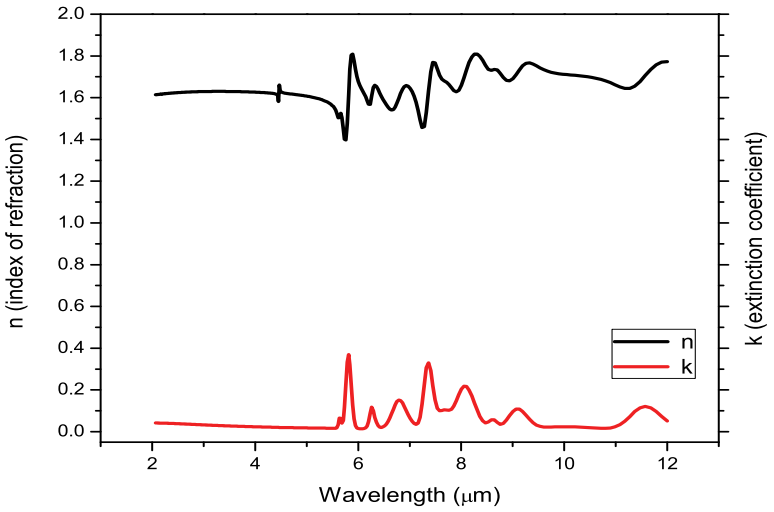

Figure 3.11: The optical properties of PEI is presented.

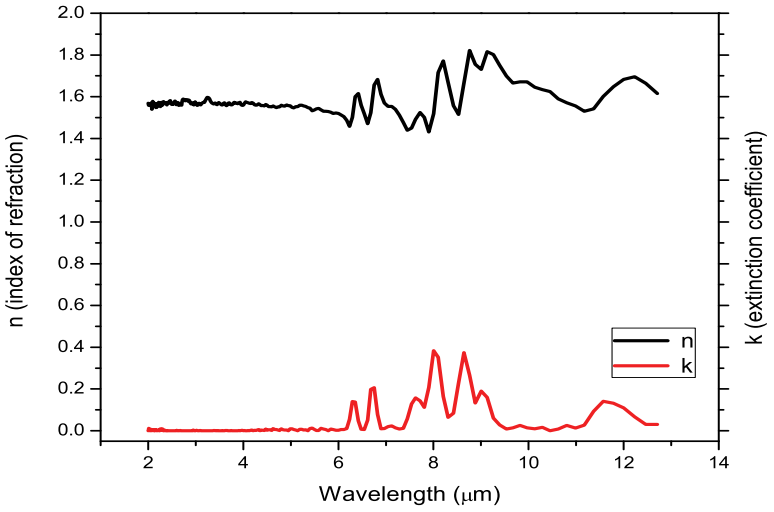

Figure 3.12: The optical properties of PES is presented.

In conclusion it is possible to claim that PEI and PES will both work fine as polymeric material for dielectric bragg fibers which are used to guide Ho:YAG laser. However PEI tend to absorb more intense than PES around 10.6 μm so the use of PES as polymeric material for dielectric bragg fibers which are used to guide $C0_2$ laser guiding is more appropriate. Most of the glass candidates are found to be suitable for fabrication of dielectric bragg fiber for guiding incident light at infrared region of the spectrum. If we sum up the information that is built on thermo-mechanical characterization section with optical characterization section, we can decide the appropriate material couple for bragg fiber fabrication for guiding incident light at wavelength of 2.1 μm and 10.6 μm. The appropriate material couple for guiding incident light at 2.1 μm regime can be reported as PEI, As_2Se_3 and the most convenient material couple for 10.6 μm regime is reported as PES and As_2Se_3. The bragg fibers which are used as an external reflector can be built with each material couple because of the external reflector fibers large reflection spectrum. The design and fabrication based evaluations of materials will be explained on the Chapter 4.

Chapter 4

FIBER DESIGN AND FABRICATION

4.1 Dielectric Bragg Fiber Designs

In this section, we will present the fiber designs that include photonic band gap structures. The optical scheme of photonic band gap structure design is already covered along with material issues at preceding chapters. So this section will focus on specific fiber designs for special optical applications. However, it is important to state that these fibers will be designed in light of the information from preceding chapters about photonic band gap structures and candidate dielectric material properties. It is possible to assort the designs by using the purpose of the fibers. The optical fibers are generally used as an electromagnetic waveguide for a certain frequency range which is one of the main motivations behind this thesis. Additional to fiber designs related to guiding of an electromagnetic wave, it is possible to design fibers which are used to reflect or filter a certain frequency of light. These fibers are generally referred as *External Reflector Fibers*.

Along this section the design of guiding fibers and external reflector fibers will be explained separately.

4.1.1 Design of Dielectric Bragg Fibers for Waveguiding

The conventional silica fibers which are named as the backbone of telecommunications industry uses index guiding mechanism to guide an electromagnetic wave at certain frequency. However the interest of this thesis lies in guiding of light at certain frequency by using photonic band gap effect. A photonic band gap can exist at two fundamentally different fiber system namely 1-D and 2-D PCFs. The design proposals will be built mainly on 1-D PCFs. The structure of one dimensional photonic crystal mirror is mainly formed by consecutive dielectric layers for planar geometry. The situation is quite similar in the case of fiber geometry. Bragg fibers geometry is a well known fact for many years however the realization of such fibers is accomplished in recent years [4]. The fabrication method of such fibers is somewhat similar to the conventional silica fibers fabrication method which requires the macro form of the fiber to be drawn with heat. The main design parameters are originated from purpose of the fiber, selected materials and demands of the fabrication method. The one dimensional photonic crystal mirrors requires a certain ratio between consecutive layer thicknesses which is determined through the ratio of refractive indices of layer materials. If this ratio is preserved a photonic band gap is incident on a frequency which is determined through the thickness values of consecutive layers. So it is possible to tune the frequency of the band gap by rescaling the structure without changing the thickness ratio related to refractive indices of layer materials. In light of this information it is possible to claim that the very first step at design of a Bragg Fiber is the material selection. The selection of appropriate materials leads us to determine the golden ratio required for a photonic band gap. If we know the ratio then we can build a one dimensional photonic band

gap for a certain frequency which is the case for planar geometries. The main advantage of the fiber geometry resides at this problem. The fiber geometry has the option to elongate along fiber axis and result in a rescale at the fiber cross section due to conservation of mass. This utility of fiber geometry allows us to rescale the frequency of the band gap. But it is important to state the physics of elongation. The thermo-mechanical analysis of candidate materials which is presented at Chapter 3 will help us to clarify this issue. As it is mentioned before drawing or rescaling of fiber is done through heating and pulling the macro sized fiber geometry. This will lead us to use of amorphous materials which has a second order phase transformation. After the material couple which will be used to build the fiber structure is determined the macro form of the fiber is ready to be fabricated. In the case of a bragg fiber the reflecting layers should be placed to the inner surface of a hollow fiber. After placing the fiber a polymer cover needs to be placed on top of the layers in order to provide mechanical support and protection for the reflecting layers. The dimensions of the macro sized fiber model are determined through the thermo-mechanical capabilities of the material couples. Because the excessive rescaling will lead the reflecting layers to be disrupted or destroyed during drawing procedure. The fabrication of the anticipated design will be discussed at fabrication section.

The purpose of the fiber is also important because it determines the working frequency of the bragg fiber. This thesis will mainly focus on guiding electromagnetic waves with wavelengths at 2.1 μm and 10.6 μm for medical applications. These wavelengths demand several qualities from materials as we discussed at Chapter 3. The appropriate materials for fibers which will work at 2.1 μm are determined as As_2Se_3 for glass layer and PEI for polymeric layer due to low absorption values and consistent thermo-mechanical properties of these materials. The bragg fibers which are designed to guide 10.6 μm is decided to be fabricated from As_2Se_3 and PES. The layer thickness ratios for both fibers are presented at Table 4.1.

The optical reflectivity performance of designs is simulated through a custom built code by using commercially available *Mathematica* software. The results are presented for bragg fiber designs at Figure 4.1.

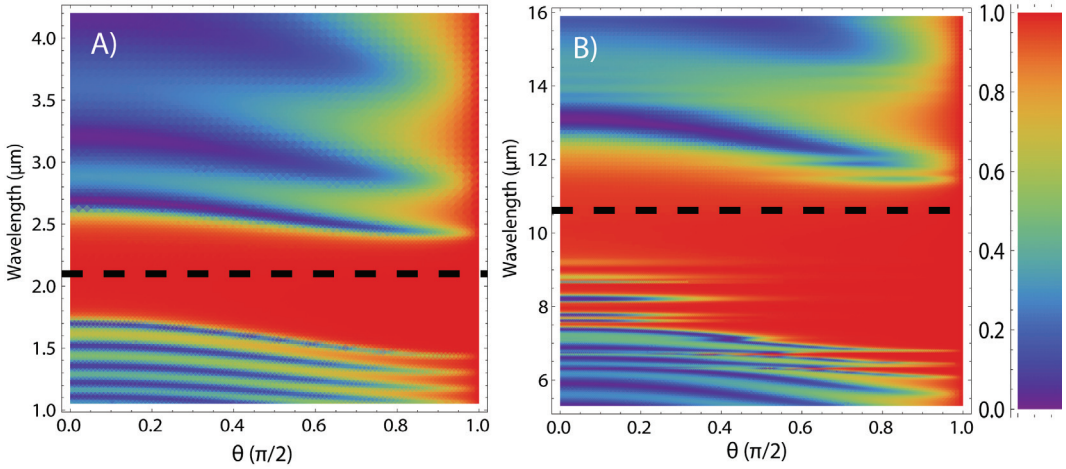

Figure 4.1: The simulated reflectance performance of transmission bragg fiber designs are represented with intensity density plots for (A) $C0_2$ laser guiding and (B) Hol:YAG laser guiding purposes.

According to simulations the designs are found to be guiding the incident light with high efficiency. Every parameter acquired from this section will be used at fabrication section so it is important to verify the performance of the designed waveguide structures.

Table 4.1: The design parameters for bragg fibers for specific wavelength guiding.

Fiber Type	Material Set	Refractive Index	Thickness Ratio	Layer Thickness
CO_2 (10.6 μm)	As_2Se_3	2.58@(10.6 μm)	1.56/2.54 = 0.6	1 μm
	PES	1.56@(10.6 μm)		1.7 μm
$Hol:YAG$ (2.1 μm)	As_2Se_3	2.73@(2.1 μm)	1.65/2.73 = 0.6	190 nm
	PEI	1.65@(2.1 μm)		317 nm

4.1.2 Design of Dielectric Bragg Fibers as External Reflectors

The bragg fibers are designed as a waveguide however it is possible to transform these fibers into external reflectors or filters [5]. The use of an appropriate fiber design it is possible to obtain a reflector which can reflect light from ultraviolet (UV) to Mid-IR from a single continuous fiber. It has been showed that external reflector fibers can be used as radiation barriers, filters and optical barcodes [15]. Along this section we will try to cover the design of external reflector fibers which can reflect light from ultraviolet to Mid-IR regime of the spectrum. The structure of the external reflector fibers is designed similar to the bragg fibers for wave guiding with one important difference; the reflecting layers are placed external surface of the fiber rather than inner surface. So if we consider we want to sweep the spectrum of reflection from UV to Mid-IR we need to obtain several different fiber diameter values along the fiber. This requires the layer thicknesses of dielectric layers placed on the macro sized preform of fiber to be quite thin due to damage incident on dielectric layers at high rescaling ratios. However even with thin layered preforms it is hard to sweep the spectrum from UV to Mid-IR by a photonic band gap. The answer resides in the projected band diagram which is presented at dielectric mirrors section. It is possible to observe there is a second order band gap incident on higher frequencies which corresponds to lower wavelengths. These band gaps help these systems to sweep the spectrum of reflection from UV to Mid-IR without any problem. Several photonic band gap options along desired frequency interval are presented with their central wavelength, required layer thicknesses and central wavelength of their second order band gap at Table 4.2.

This table indicates the design parameters for a single fiber thread according to desired reflectance spectrum. If a fiber can change the thickness of reflecting layers along its length it is possible for this fiber to reflect a frequency range

Table 4.2: The design parameters for external reflector fibers for reflecting a certain frequency.

Center of band gap	Material Set	n	S.O. band gap	Layer Thickness
4.5 μm	As_2Se_3	2.71@(4.5 μm)	1.5 μm	415 nm
	PEI	1.595@(4.5 μm)		705 nm
3 μm	As_2Se_3	2.715@(3 μm)	1 μm	276 nm
	PEI	1.638@(3 μm)		458 nm
2.1 μm	As_2Se_3	2.73@(2.1 μm)	600 nm	190 nm
	PEI	1.65@(2.1 μm)		317 nm
1.7 μm	As_2Se_3	2.742@(1.7 μm)	550 nm	115 nm
	PEI	1.655@(1.7 μm)		257 nm
1 μm	As_2Se_3	2.742@(1.7 μm)	210 nm	88 nm
	PEI	1.655@(1.7 μm)		150 nm

that is varying along its length. So if this fiber can change the reflecting layer thicknesses according to Table 4.2. It is possible for this fiber to reflect light from UV to Mid-IR along its length. This could be achieved through manipulating the fiber diameter along the fibers length. Every different diameter will correspond to a different frequency of reflection. The fabrication of external reflector fibers and the diameter manipulation of a single fiber thread will be explained at next section.

The performance of the fiber is going to be explained in detail with experimental results at Chapter 5. But the optical performance of such structures can be simulated easily by using *Transfer Matrix Method* (TMM) as it is done for guiding fibers at previous section. The dispersion relation of materials will be included into simulation which will be problematic for As_2Se_3 because of it is highly absorptive behavior at visible regime. However, according to simulation results which is presented at Figure 4.2 it is possible to talk about an omnidirectional reflection for a small frequency range. So it is not trivial to claim that second order band gaps are quite useful for reflecting light at lower wavelengths.

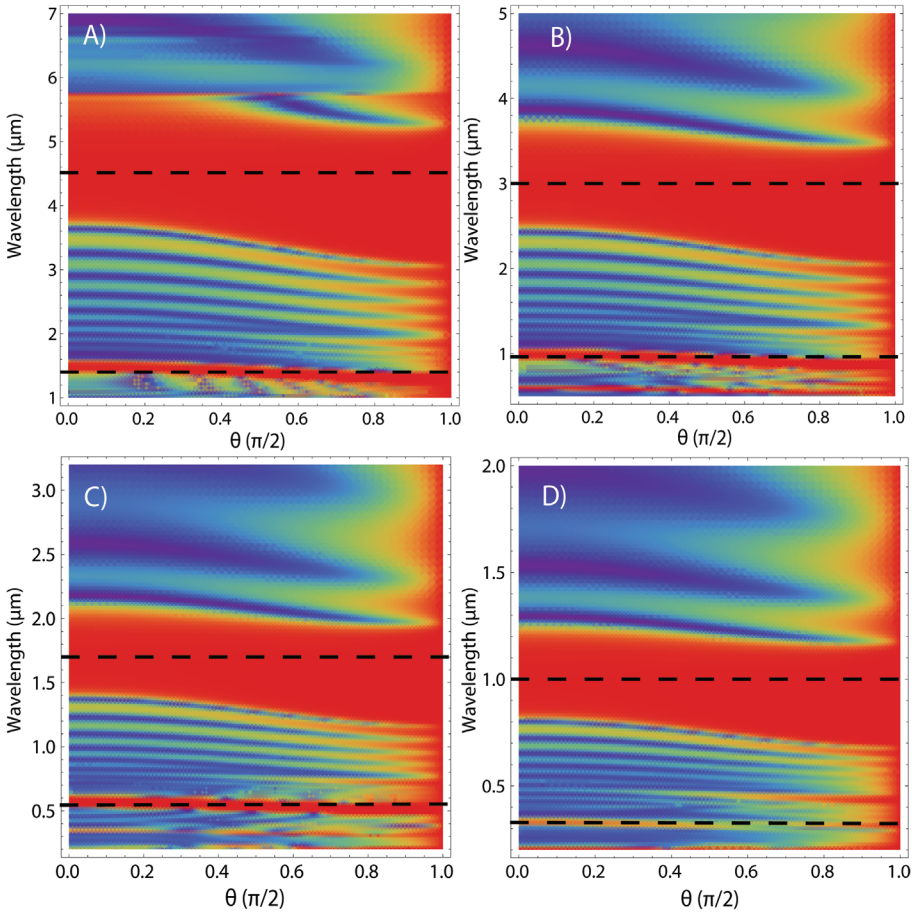

Figure 4.2: The simulated reflectance performance of an external reflector fiber design for various band structures are represented with their first and second order band gaps. The graphs are organized according to central wavelength of the band gap as A) represents 4.5 μm, B) represents 3 μm, C) represents 1.7 μm and D) represents 1 μm.

In conclusion it is theoretically possible to build a fiber which can reflect from UV to Mid-IR without having any problem. The designed structure and its structural parameters are presented along with performance simulations during this section. In light of the simulations the fiber design is found to be working efficiently as an omnidirectional reflector at a huge frequency range.

4.2 Dielectric Bragg Fiber Fabrication

The fiber designs which are presented at previous section describe the structure of the fiber and the parameters related to reflecting layers. The realization of proposed structures demands not only design information but also material characteristics. So this section will use most of the information presented at previous chapters and sections. The main framework of fabrication method covers three major steps including *Preparation of Reflective Bilayers*, *Formation of Hollow Core Preform* and *Drawing of Preform*. Along this section these major steps will be explained for proposed fiber designs separately with use of information from previous chapters.

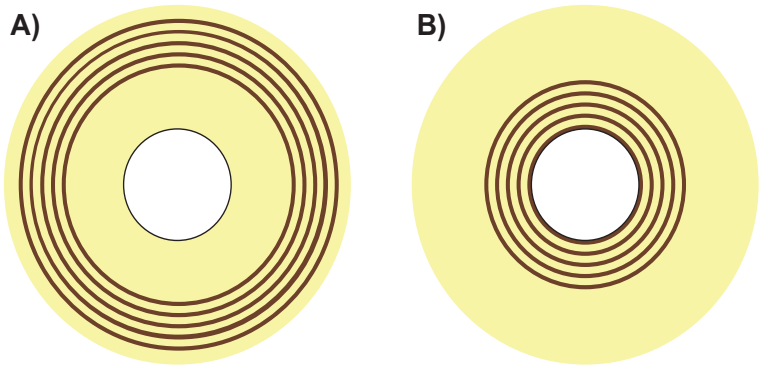

Figure 4.3: The schematic cross section of the proposed fiber designs for (A) external reflector bragg fiber and (B) waveguide bragg fiber is presented.

4.2.1 Fabrication of Dielectric Bragg Fibers for Waveguiding

The bragg fiber structures are known to guide light inside air through photonic band gap structures such as one dimensional photonic crystals. In light of this information it is possible to state that a conventional bragg fiber is a hollow core fiber. So the photonic band gap structure must be placed the inner surface of the hollow core fiber structure.

Preparation of Reflective Layers

The fabrication procedure of such structures will begin with production of reflective layers which will form the photonic band gap structure at the inner surface of the fiber. The first step to build the reflective layers of the bragg fiber is to determine the material set. The material set has two dependences which are optical transparency and thermo-mechanical consistency. The optical transparency of materials must be examined near the working frequency of the bragg fiber. So in order to determine the appropriate material couple, first the purpose of the fiber must be determined. As it is stated at preceding chapters the interest of this thesis only covers the wavelengths of 10.6 μm and 2.1 μm which are known as the working wavelengths of important medical lasers. The appropriate material set of these wavelenghts are presented at previous section as PES and As_2Se_3 for 10.6 μm, PEI and As_2Se_3 for 2.1 μm.The thermo-mechanical consistency of this material sets are confirmed with the information that is presented at Chapter 3.

The second step relating to fabrication of reflective layers is to determine how to build the chosen material set. The fabrication method requires these layers to be formed as thin film coatings. So in order to place these materials back to back in a thin film formation we need to determine a deposition method which is appropriate for given material sets. The polymers are materials which are likely to be coated on substrates with chemical methods, however the matching glass materials are generally deposited on a substrate with physical deposition methods. This dilemma will lead us to the conclusion that one of these materials is needed to be used as substrate. The form of substrate is needed to be a large area thin film with precise thickness uniformity. The candidate polymeric materials are commercially available in thin film form with relatively small thickness values, but glass materials are generally known to be brittle at bulk form and cannot be processed easily into thin film formation. So, in order to obtain reflective layers in thin film formation candidate polymeric materials are coated with

glassy materials through *Thermal Evaporation*. The conventional evaporation system of Vaksis Corp. is presented at Figure 4.4.

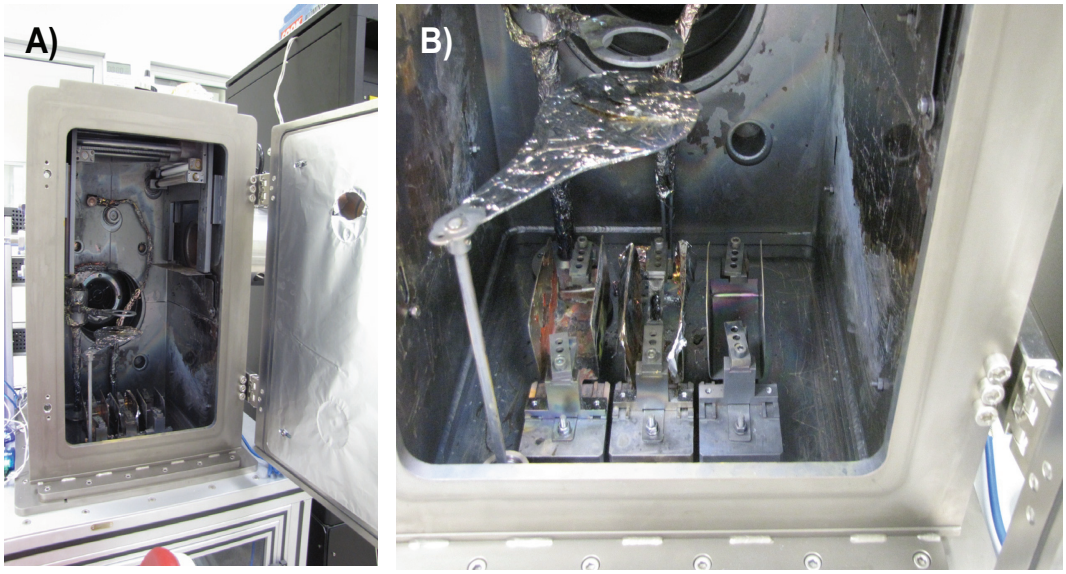

Figure 4.4: Thermal evaporator ELIF of the Vaksis Corp. is presented with (A) general view of the evaporator and (B) evaporation boats, substrate holder, shutter.

Thermal evaporation method can coat appropriate substrates at relatively small dimensions with high uniformity. But it is hard for a thermal evaporator to coat a large area film with high uniformity. A custom built thermal evaporation system can compensate this uniformity problem through scanning the large area film with small intervals. So the conventional evaporation system ELIF has been modified to coat large area polymer films without disturbing the uniformity of glass layers. The modification proposes a rotating cylinder mechanism which the substrate film is wrapped around. The rotating cylinder helps the coating to be made in small area intervals rather than exposing the whole large area film into deposition. It has been experimentally shown that it is possible to coat a 22 cm to 75 cm polymeric thin film with a 13 μm thick glass layer with conformity lower than 5 percent. The modification designs and assembled version of the thermal evaporator is presented at Figure 4.5.

The adhesion between material sets are found to be an important parameters to be examined however both materials are amorphous materials which have close

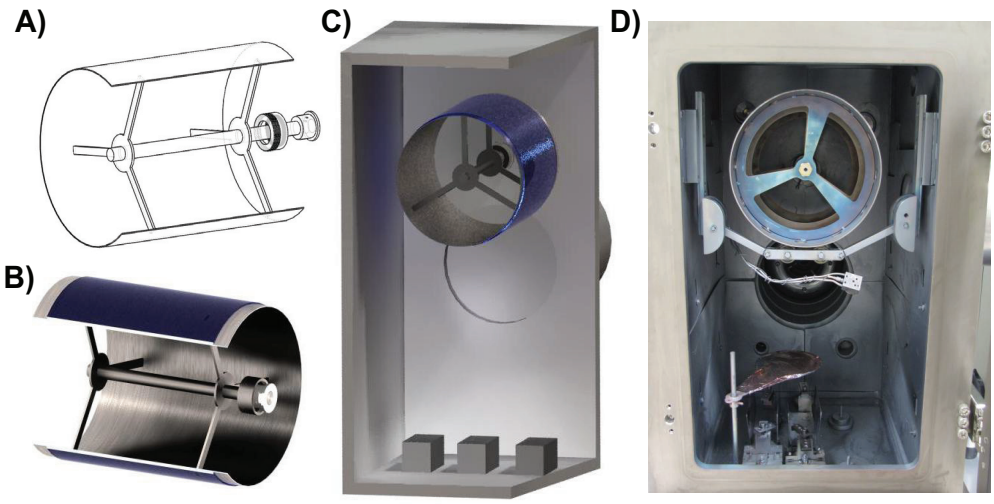

Figure 4.5: The computer aided drawings (CAD) are presented for the final design of the drum (A,B) with assembled version of the thermal evaporator ELIF of the Vaksis Corp. (C,D).(Courtesy of Can Koral)

glass transition temperatures. The use of a contact angle measurement which is the most detrimental method for adhesion is nearly impossible to be performed to determine adhesion between these materials. So the adhesion between material sets are observed after deposition and the glass material As_2Se_3 found to form a coherent structure with both polymeric materials. In order to improve the interest of two materials, the argon plasma which modifies the surface of the polymeric film and cleans all of the unwanted organic compounds placed on the surface of the film is performed before each deposition. The plasma treatment is performed with a microwave source operating at 2.4 Ghz and the argon gas is supplied to system with a rate of 50 sccm which corresponds to a stable pressure of 2.10^{-1} Torr. The microwave source is ignited with 100Watt for 5 minutes. The resulting surface modification is presented with surface topography measurements acquired from PSIA XE100E Atomic Force Microscope and contact angle measurements acquired from Dataphysics OCA 30 contact angle measurement system at Figure 4.6.

The AFM images indicate the plasma treatment has increased the roughness on the surface of the polymer film. This will result in a hydrophilic polymer

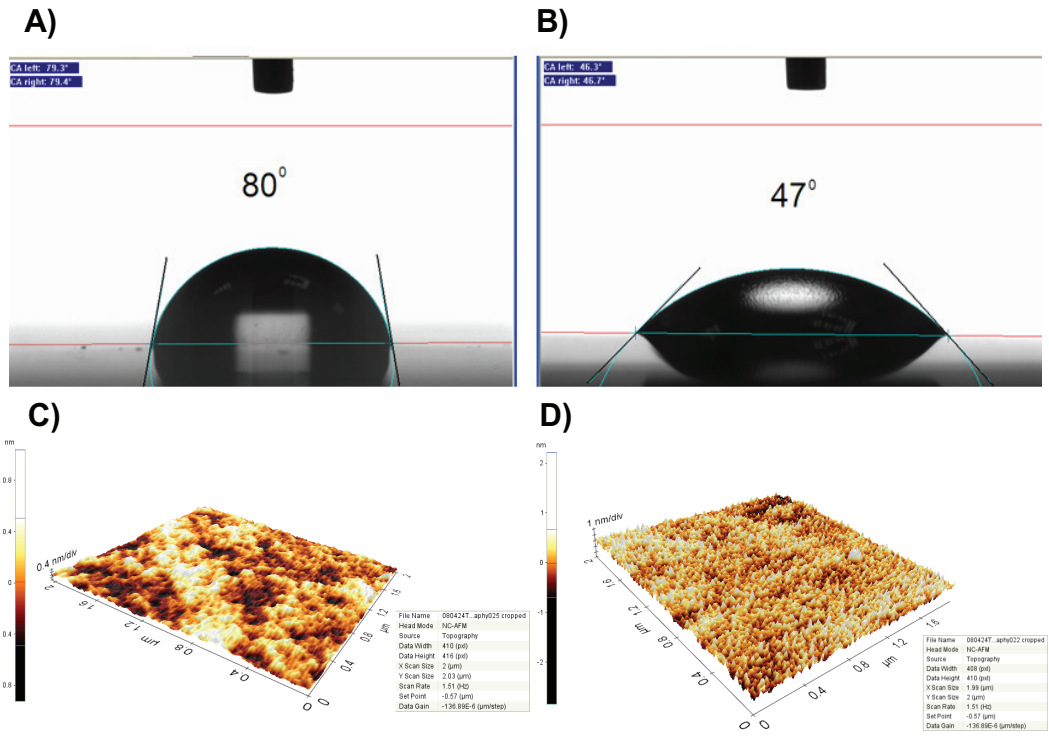

Figure 4.6: The plasma treated and untreated polymeric films are characterized through contact angle measurement and Atomic force microscope (AFM) images. A) presents the contact angle of the untreated polymeric film, B) presents the plasma treated polymeric film, C) presents the AFM image of the untreated polymeric film and D) presents the plasma treated polymeric film.

surface which can be observed from the contact angle measurement results. The contact angle between a water drop and an untreated polymer surface is found as 80 °, after plasma treatment the contact angle between the water drop and the polymer surface is reported as 47 °. It can be observed from the Figure 4.6 that plasma treatment will cause the water droplet to disperse into a larger area on the polymer film surface. In light of this information it is possible to state that the plasma treatment of the polymeric film will lead to an increase in interaction between viscous coating material and the substrate polymeric film. The increase in interaction will result in more uniform and stable deposition of coating material into substrate polymeric film.

The coating of each waveguide fiber is different due to their working frequency. If we consider wave guiding 10.6 μm we can use a thicker substrate polymer film which provides us more mechanical stability for coated film. However thicker polymeric film requires thicker glass coating which will lead glass material to behave more brittle. The optimized reflector layers for waveguide fibers at 10.6 μm is found to be a 50 μm thick polymeric film and a pair of 15 μm thick As_2Se_3 layer which is placed on both surface of the polymeric film. The dimensions of PES thin film for coating are presented as 22 cm x 75 cm x 50 μm for waveguide fibers at 10.6 μm. The dimensions of the PEI film which will be used for waveguide fibers at 2.1 μm is similar to PES film, however the thickness of the film is found to be 10 μm. The 3 μm thick As_2Se_3 layers are placed on both surface of the thin PEI film in order to form the reflective layers of the waveguide fibers at 2.1 μm. These layers are determined through the QWS mechanism parameters which are explained at Chapter 2. The visual results of the coatings are presented with optical photography and SEM images acquired from FEI Quanta 200 FEG Environmental Scanning Electron Microscope at Figure 4.7.

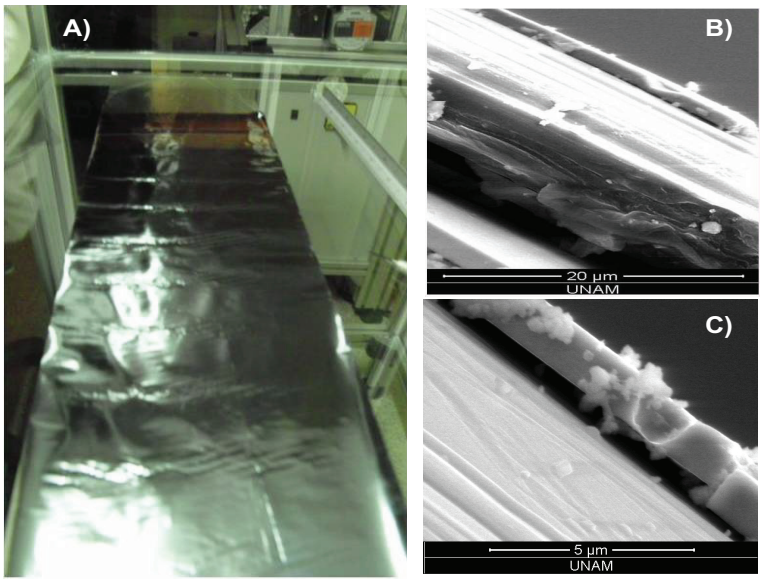

Figure 4.7: (A) The photo of the coated polymeric film, (B,C) SEM images of the cross section of the coated film for waveguide fibers at 2.1 μm is presented.

The surface characterization of coatings is important in means of scattering of light inside fibers which will lead to an excessive amount of intensity loss. The surface characterization of a bare PEI film and a PEI film coated with As_2Se_3 is presented with AFM images at Figure 4.8.

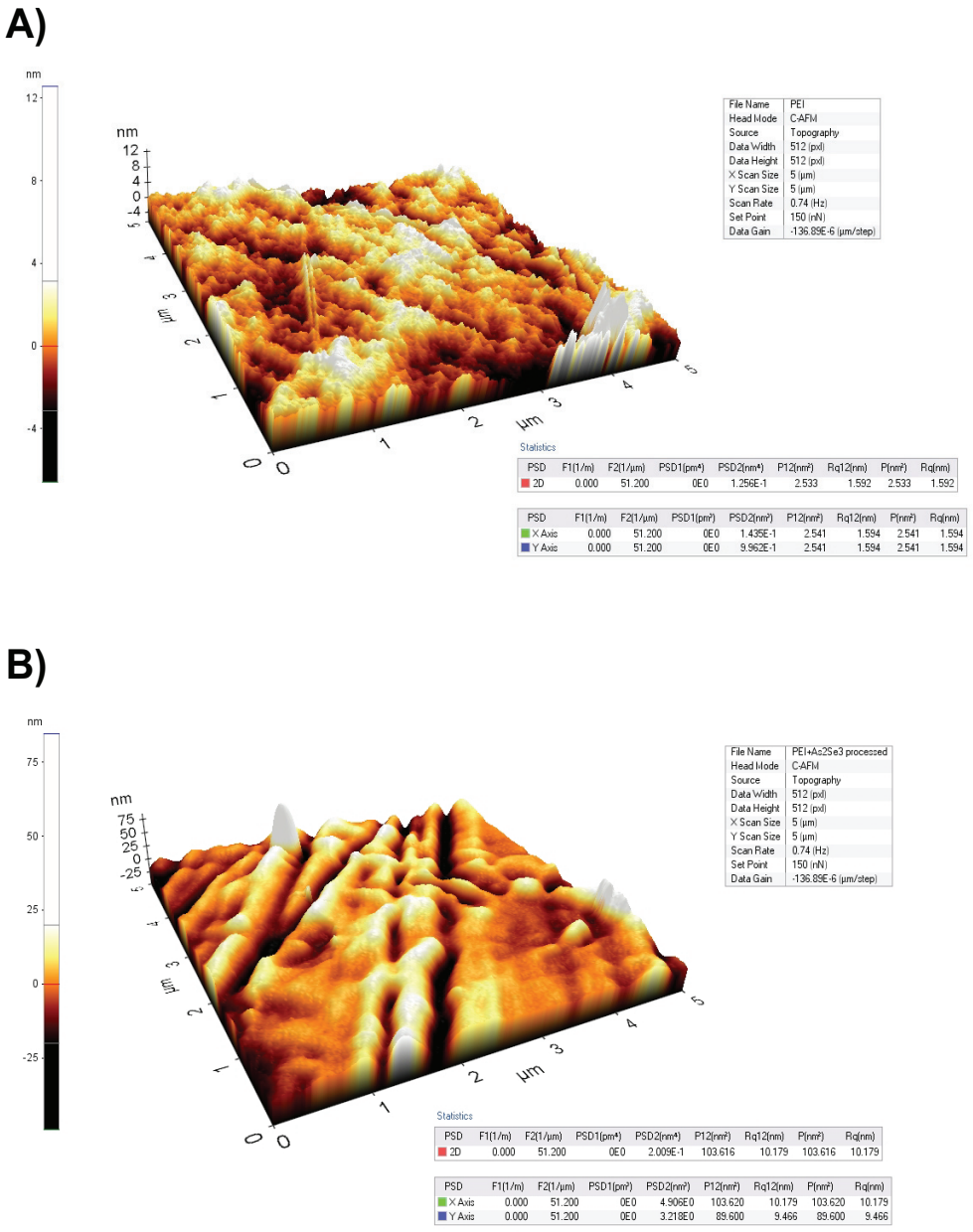

Figure 4.8: The AFM images of (A) bare and (B) coated PEI films are presented.

It is possible to state that the coatings are not rough enough to cause light scattering. The AFM images report that the Route Mean Square (RMS) of the surface roughness is 10.719 nm which is so small compared to the guiding wavelength of 2.1 μm. Additionally if we consider these layers are rescaled to smaller dimensions the roughness will be even lower than this value. So the use of these coatings as reflective layers on waveguide fibers is appropriate.

Formation of Hollow Core Preform

After preparation of reflective layers, the second main step of the fabrication procedure is mentioned as formation of hollow core preform. The preform can be briefly explained as the macro model of the fiber. The dimensions of the preform are determined through the rescaling factor of the reflective layers and the final diameter of the waveguide fiber. The formation of preform starts with wrapping the reflective layers on to a mold which will form the hollow core. The material of the mold is important due to scattering problems caused by the roughness of the mold surface which might be observed at the inner surface of the resulting fiber. A surface characterization is made through AFM measurements of two candidate mold materials namely silica glass and polytetraflouroethylene (PTFE) which is commercially known as teflon. Silica is chosen due to its low surface roughness and teflon is chosen because it can be removed easily from the preform after solidification of the structure. The roughness values for both materials are presented with AFM images at Figure 4.9.

It is possible to note that there is no significant difference in roughness values of both materials. So it is possible to claim that the use of teflon rod will be more appropriate in means of releasing problems. It is useful to state that the glass must be etched with Hydroflouric acid in order to be removed from solidified preform. This process takes time and it is quite dangerous because of the concentration level of the acid. The reflective layers are ready to be wrapped

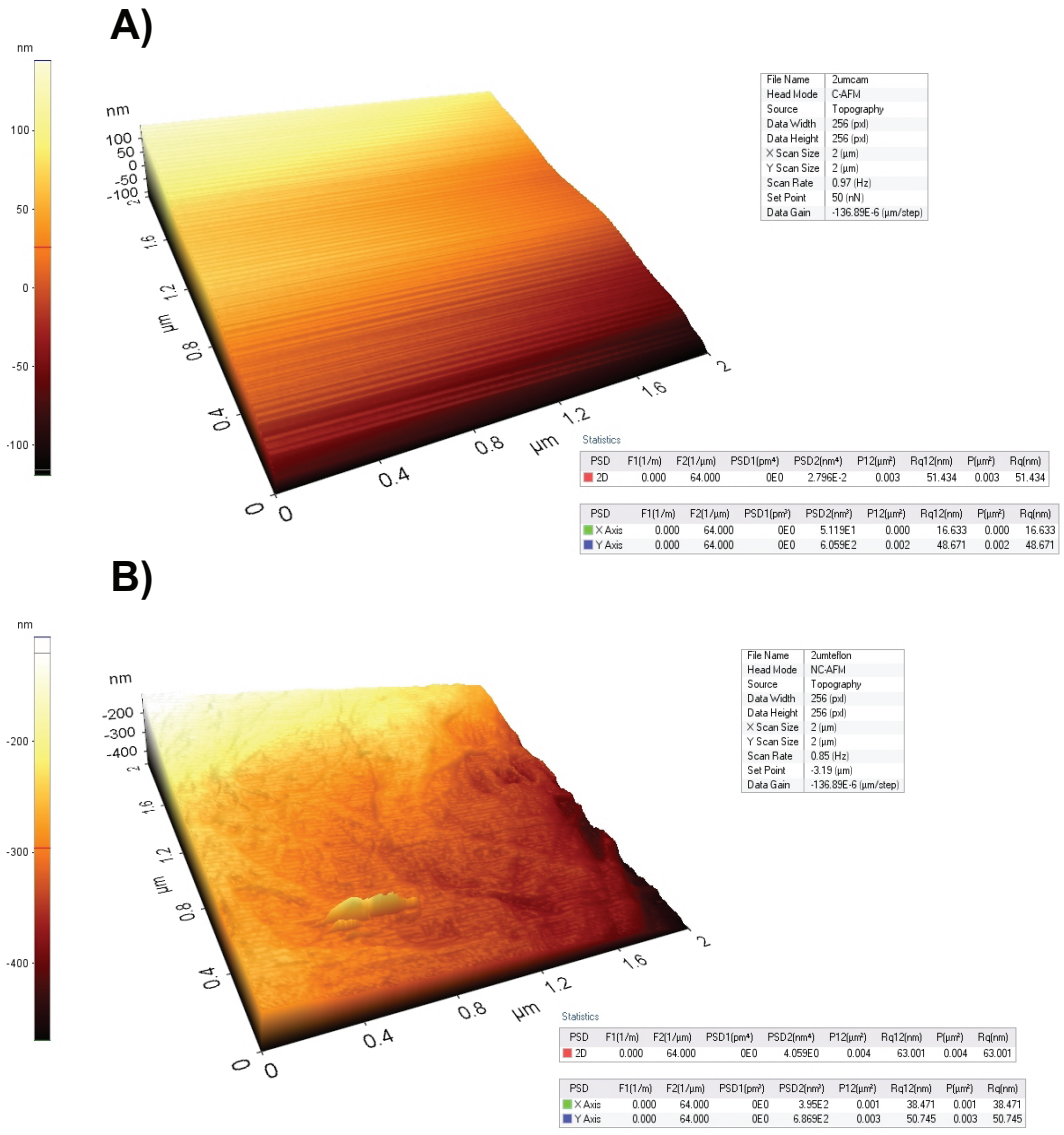

Figure 4.9: The Atomic Force Microscopy(AFM) images of (A) silica glass and (B) teflon rod pieces are presented.

around the teflon mold which is cylindrical in shape and have a diameter of 15.4 mm. The diameter of the mold will decide the final orifice diameter of the fiber. The reflective layers are wrapped to the mold with extreme care. During the wrapping of reflective layers, it is possible to observe that the coated polymeric films will form a periodic QWS structure. Every turn around the mold will correspond to a single crystal lattice and then eventually after 10 rounds the coating layers will complete the formation of a one dimensional photonic crystal structure placed around the teflon mold.

The reflective layers will provide the omnidirectional reflection, however if we consider the thickness of incident layers it is not possible for such structure to be mechanically stable. The most reliable method to enhance this mechanically weak structure is to cover this structure with a mechanically stable and flexible material without disturbing its thermo-mechanical consistence. The polymeric materials of the composite layer structure are known to be a member of engineering thermoplastics which are mechanically though and flexible. So the supporting structure is introduced through wrapping a thicker polymeric film around reflective layers. Each waveguide bragg fiber design use its proposed polymeric film for thermo-mechanical consistency. The outer diameter of the preform is set to a value which is enough to build a mechanically resilient fiber. Most of the preforms are produced with an outer diameter of 38 mm which corresponds to an appropriate fiber diameter of 1.2 mm for Ho:YAG laser guiding and 1.5 mm for $C0_2$ laser guiding. The wrapping of polymeric supporting layers continues until the desired diameter is obtained for fiber preform. The schematic presentation of wrapped preform structure is shown at Figure 4.10.

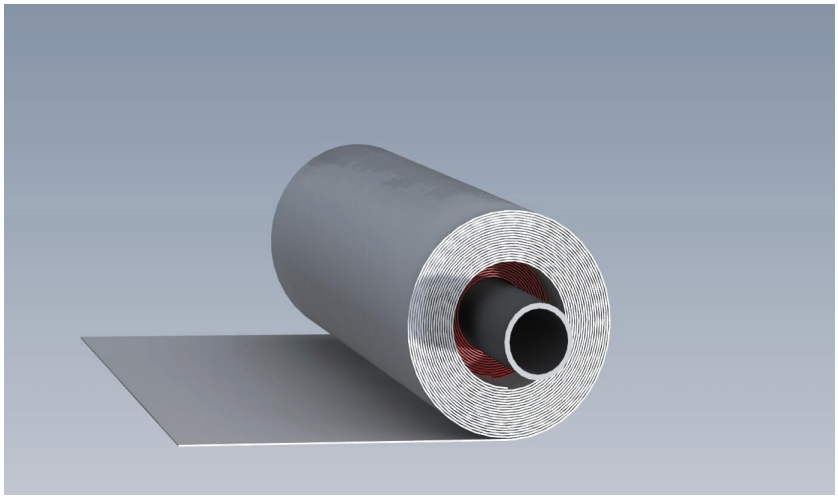

Figure 4.10: The schematic presentation of a wrapped preform for a waveguide bragg fiber.

After wrapping the polymeric supporting layer, protruding thin films are pinned to preform with the help of a vacuum tape and the laminated preform

structure is covered with a teflon band in order retain its shape during solidification process. The solidification process consists of heating the preform slightly above the glass transition temperature of preform materials inside a homogenous temperature gradient. The homogeneous temperature gradient is acquired through heating this structure inside a mid-level vacuum furnace with precise temperature control. The optimum temperature gradient is obtained through many solidification trials. The effect of the inappropriate temperature gradient can be observed from Figure 4.11.

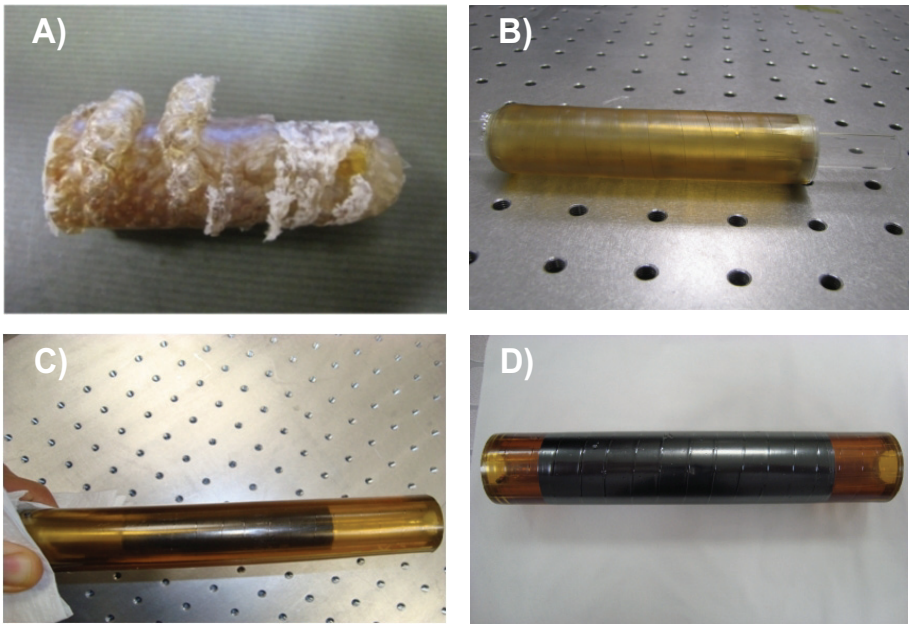

Figure 4.11: The effect of temperature gradient can be observed through (A) excessive heated preform, (B) semi-solidified preform, (C) successive transmission fiber preform and (D) successive external reflector fiber preform.

The successive preforms are acquired through consolidating the preform at a vacuum level of 9.10^{-3} Torr and using a temperature gradient described at Figure 4.12. As it can be seen from the figure the solidification procedure has two phase, namely preheating and consolidation. Preheating is performed in order to eliminate the unwanted temperature fluctuations which arise from swift heating of system. The solidification is performed with rigorous heating schedule at both phases. The temperature is heated from room temperature to 180 °C with a rate of 20 °C/min and then the structure is hold at this temperature for

45 minutes in order to confirm that the temperature gradient is stabilized along the preform. After the preheating phase the temperature is increased with a constant rate of 10 °C/min until 255 °C. The consolidation phase takes place at 255 °C which is quite important because the merging of laminated layers occurs in this phase. The temperature is kept constant at consolidation temperature for 60 minutes. The consolidated preform is immediately exposed to room temperature after purging the system. The release of the mold which forms the hollow core is the next step. The silica mold bonds to the preform surface during consolidation and it can be released only through chemical etching with the use of hydroflouric acid. But teflon mold can be removed easily just by pulling out the mold inside preform. Teflon has a significantly high thermal expansion coefficient which allows it to extend and shrink swiftly with temperature. Due to this reason and the surface properties of teflon it is possible to release the teflon mold from the system without disturbing the inner surface of the preform.

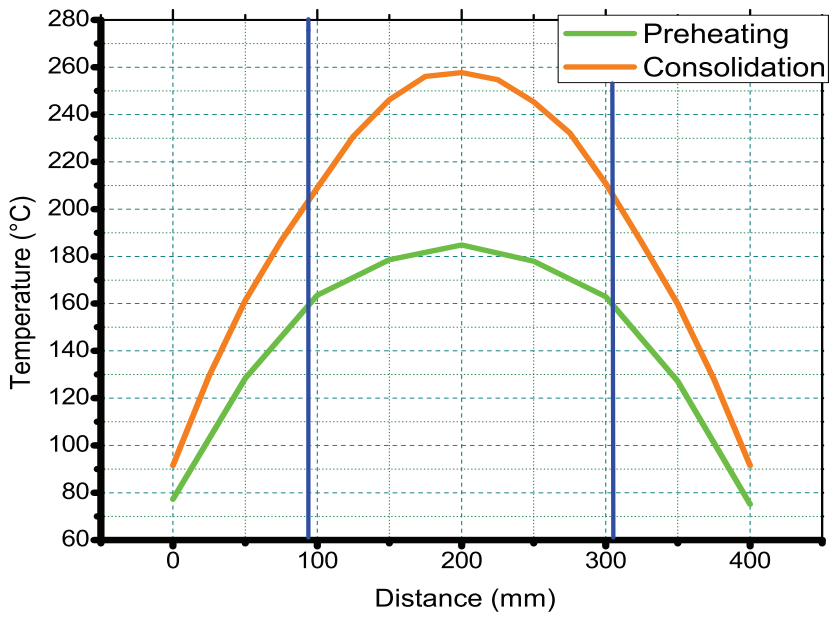

Figure 4.12: Optimum heating gradient for consolidation is presented with respect to dimensions of the furnace and the distance between blue lines corresponds to the place of the preform.

Drawing of Hollow Core Preform

Most of the optical fibers including hollow core infrared fibers are fabricated with thermal drawing of a fiber preform [77]. The drawing is performed with a fiber tower which is specifically designed for each different fiber structure. Moreover, drawing parameters also vary with different optical fibers because of the difference in shape and material of the fiber preforms. Preform materials determine the heating regime and temperature gradient of the drawing procedure. The incident temperature during drawing procedure is determined from the thermo-mechanical properties of the preform materials. The temperature regime in which both glassy and polymeric materials are seems to be in harmony is reported at thermo-mechanical characterization of preform materials. The appropriate drawing temperature regime is reported for both transmission fiber designs between 267 °C and 292 °C.

The shape of the preform influence many parameters including the heat transfer profile of the preform and mechanical setup of the fiber tower. The shape of the preform for dielectric bragg fibers are presented at previous chapters. The preform is built in shape of a hollow core cylinder. The heat transfer model for a similar structure is already described at literature [78]. In order to determine the appropriate heating regime for the furnace, the shape of the furnace and preform is considered with the required temperature values of the preform for drawing procedure. The temperature profile of the drawing furnace is calculated from a finite-element simulation program referred as Cosmos/Desingstar. The fiber tower furnace is remodeled by using a commercially available CAD program called Solidworks which is presented at Figure 4.13. This model is introduced into Cosmos/Desingstar with appropriate boundary conditions. The outer surface of the furnace is well insulated, so conduction, convection and radiation from outer surface of the furnace are neglected. However a slight convection is incident at the entrance and exit of the cylindrical shaped furnace. This convection is

introduced into system as 1 Watt/m^2K which varies from 10 to 100Watt/m^2K at open air depending on the existence of any flow. The simulated drawing temperature gradient is presented for each dielectric bragg fiber design for transmission at Figure 4.14.

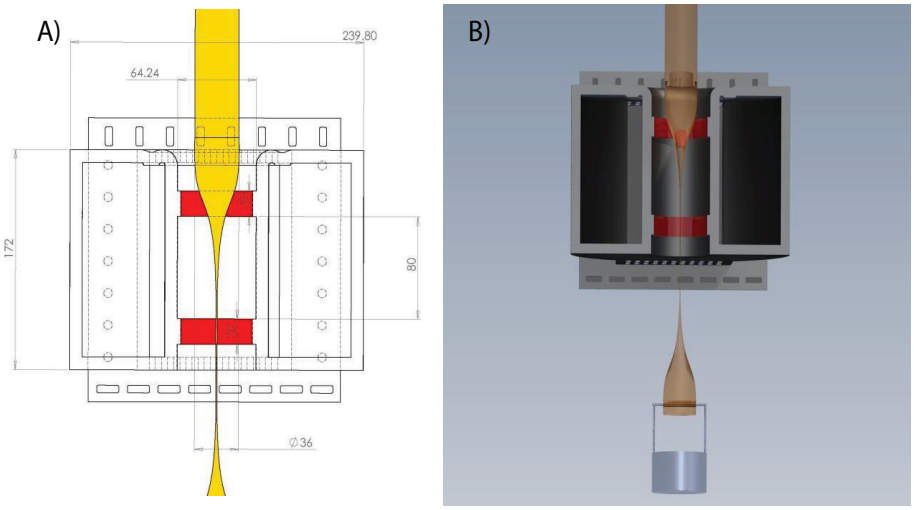

Figure 4.13: (A) The front section of the furnace model with dimensions and (B) 3D render model of the furnace during drawing is presented. (Courtesy of Can Koral)

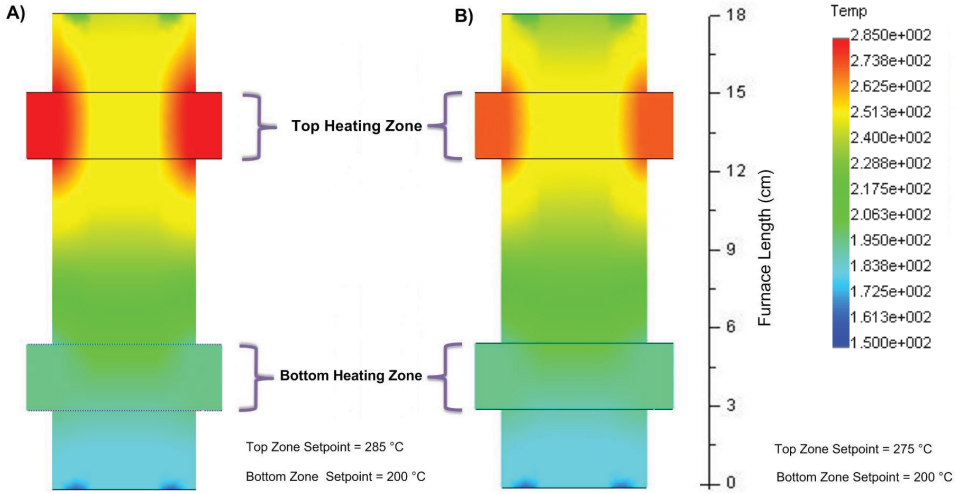

Figure 4.14: The simulated drawing temperature gradient for transmission bragg fibers at wavelengths of (A) 2.1 μm and (B) 10.6 μm is presented.

According to simulated heat profile of the furnace, appropriate heating zone set-points for drawing of transmission bragg fibers are defined as 285 °C for Ho:YAG laser guiding preform and 275 °C for CO_2 laser guiding preform. The

resulting temperatures of the preform surface is reported as 274 °C for Ho:YAG laser guiding preform and 268 °C for CO_2 laser guiding preform. The resulting viscosity values are calculated to be $3.15x10^4$ Pa.s for both structures. This values match well with the experimental results from the drawing procedure. However viscosity results at given temperatures are considered too high for drawing of such structures. Because of this reason the assigned heating zone set-points are lowered 5 °C after the preform is thinned down to fiber dimensions.

The physical explanation of drawing procedure seem to be complicated, however the rescaling procedure of preform structures into elongated fibers can be explained through using a basic concept like conservation of mass. If we consider the density of materials that are fed to the furnace will remain unchanged, conservation of mass can be referred as conservation of volume. The feed speed (V) and fiber drawing speed (ν) can be explained related to outer (R_{out}), inner (R_{in}) diameters of the preform and outer (r_{out}), inner (r_{in}) diameters of the fiber through using conservation of volume.

$$\nu = \frac{(R_{out} - R_{in})}{(r_{out} - r_{in})} V \tag{4.1}$$

The rescaling factor is reported as the ratio between R_{out} and r_{out}. The outer diameter of the preform tends to resize to fiber dimensions according to conservation of volume. But the inner fiber diameter we are going to obtain can diverge from expected dimensions due to slight collapse of the fiber during drawing procedure. The parameters relating to collapse and rescaling factor are symbolized with C and R.

$$r_{out} = R.R_{out} \tag{4.2}$$

$$r_{in} = C.R.R_{in} \tag{4.3}$$

If we redescribe the conservation of volume under consideration of collapse phenomenon, the resulting expression (Equation 4.6) can be calculated by using following statements:

$$\nu = V\gamma \tag{4.4}$$

$$\alpha = (R_{in}/R_{out})^2 \tag{4.5}$$

$$\gamma = \frac{1}{R^2}\frac{(1-\alpha)}{(1-C^2\alpha)} \tag{4.6}$$

The total length of the fiber (l) that can be obtained from a preform with length L can be calculated through Equation 4.7. The dimensional drawing parameters are presented at Figure 4.15.

$$l = \frac{1}{\gamma}L \tag{4.7}$$

The dimensional analysis of drawing procedure is concluded with previous expression and now it is possible to talk about dynamic analysis of the drawing procedure which is theoretically explained at Chapter 3. The dynamic analysis is composed of dimensional analysis which feed and draw speed parameters are introduced and viscosity analysis which explains the viscosity of the structure with respect to temperature gradient.

The viscosity analysis is made separately for both polymeric and glass material candidates at Chapter 3 along with dynamic analysis for a sample fiber geometry. It is possible to evaluate dynamic analysis of the drawing procedure for any fiber geometry through using the analogy provided at Chapter 3. The

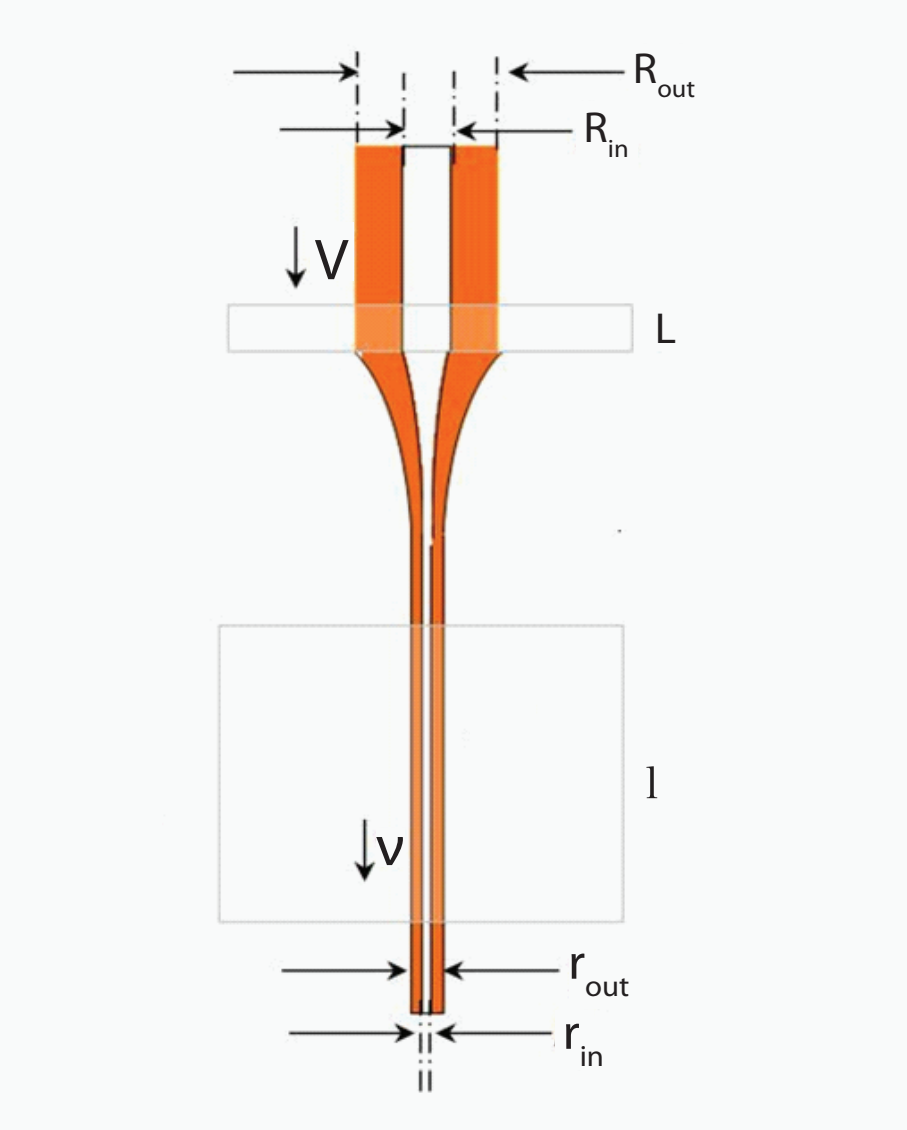

Figure 4.15: The dimensional drawing parameters are presented.

experimental dynamic analysis is done during drawing procedure through measuring tension, thickness, temperature gradient along the furnace with feed and draw speeds. All of these variables are monitored and recorded along the fiber drawing procedure. The experimental data acquired during drawing procedure proves the accuracy of the models that are used at Chapter 3. The resulting fibers visual and performance characterization will be presented at Chapter 5.

4.2.2 Fabrication of Dielectric Bragg Fibers as External Reflectors

The general outline of the dielectric bragg fiber production procedure, related simulations and calculations are presented at preceding section about fabrication of dielectric bragg fiber structures for wave guiding. This section will only include specific fabrication methods about fabricating external reflector bragg fibers. The bragg fibers which are designed to work as an external reflector is basically made through placing the reflector layers at the outer surface of the fiber. So most of the main fabrication steps are similar to the fabrication of a dielectric bragg fiber for wave guiding.

Preparation of Reflective Layers

The reflective layers are generally designed according to working frequency of the fiber as it was stated before. External reflector bragg fibers are designed to reflect a frequency range between UV to Mid-IR through changing its spectrum of reflection along its length. The required layer thicknesses for reflecting certain frequency ranges are presented at Table 4.2. Although required thickness values for Mid-IR seems convenient, the thickness values required to obtain an effective reflector at UV regime seems to be quite small, even if we consider the band gap corresponding to UV is a second order gap. The answer to fabricate such a fiber reflector is to decrease the macro sized layer dimensions to minimum level. The case is similar to the bragg fiber which is designed to guide Ho:YAG laser, so the same layer thickness and same material set is used to produce reflecting layers of external reflector fibers.

Formation of Hollow Core Preform

The hollow core preform of the external reflector bragg fiber is prepared through changing the wrapping sequence of the reflective layers with protective polymeric layers. This modification will cause the reflective layers to be placed at the outer surface of the preform and the resulting fiber. In order to provide mechanical protection for reflective layers an additional PEI thin film is wrapped around the reflective layers for several rounds. The schematic presentation of wrapped preform structure is shown at Figure 4.16. The material of the mold is chosen to be teflon because the reflective layers are placed at the outer surface of the preform. The consolidation process is made similar to the process made for waveguide bragg fibers. Heating gradient of the furnace remains unchanged because the material set is chosen same with the Ho:YAG laser transmission fiber. The resulting preform is presented at Figure 4.11.

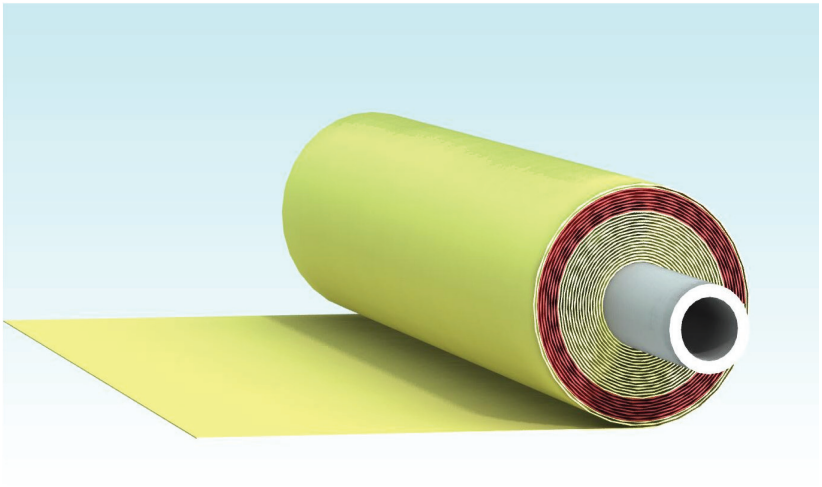

Figure 4.16: The schematic presentation of a wrapped preform for an external reflector bragg fiber.

Drawing of Hollow Core Preform

The fundamentals of drawing procedure kept constant for external reflector fibers. The distinctive point resides in the purpose of external reflector fibers which can

be summarized as long range band reflecting. The diameters of these fibers need to vary unlike transmission fibers which are required to have the same diameter along the fiber. So the drawing parameters are set to build a fiber to reflect at Mid-IR regime and after the drawing procedure begins the diameter of the fiber is decreased through increasing the temperature and fiber drawing speed. It is possible to obtain a fiber which has its first order photonic band gap placed at visible regime of the spectrum. This methodology will lead us to a reflector fiber with desired reflecting properties. The optical performance of such fibers will be discussed at next chapter of this work.

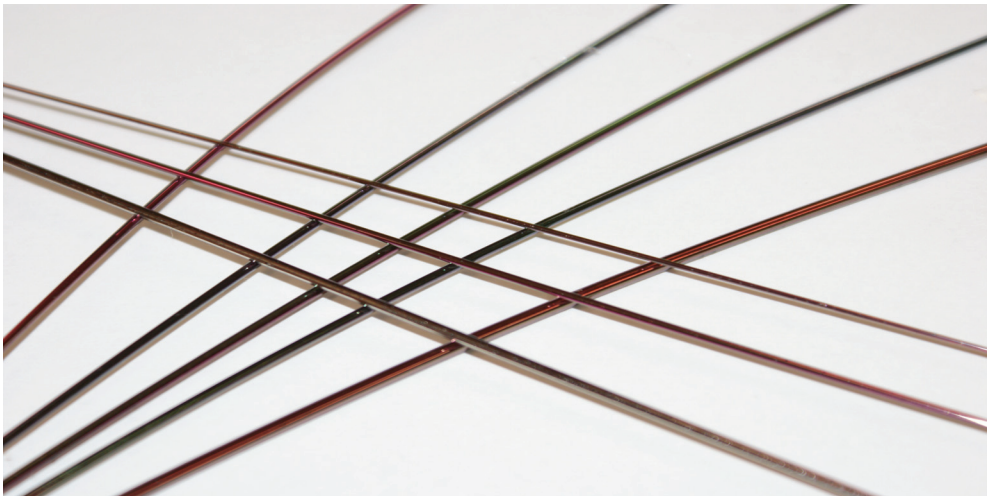

Figure 4.17: External Reflector Fibers.

Chapter 5

FIBER CHARACTERIZATION

Theoretically proposed structures are fabricated through a complex fabrication procedure. The reliance of the method and the optical performance of fabricated fibers will be examined along this chapter. The reliance of the fabrication method will be examined visually by using SEM images of the resultant fibers. The optical performance analysis will be concluded with a Fourier Transform Infrared Spectrometer (FTIR). Every fiber will be analyzed at a different section relating to their purpose and structure.

5.1 Dielectric Bragg Fibers for Waveguiding

The transmission fiber designs which are realized throughout this thesis specially focused on medical applications. As it was mentioned before the main wavelengths concern this thesis is reported as 2.1 μm and 10.6 μm which corresponds to working wavelength of HO:YAG and CO_2 lasers. These lasers are practically used for different surgical operations as a scalpel and used to scorch open wounds. The fibers that are fabricated must be characterized visually in order to identify whether the fabrication method is working as it was anticipated.

Even though it might look easy, the visual characterization of such fibers needs several sample preparation steps and extreme care. The sample preparation procedure involves resin embedding for microtomy procedure. The cross section of the fiber is flattened with a microtomy procedure at cryo conditions. Before flattening, the inner core of the fiber is filled with water under cryo conditions. The frozen water will provide an extra rigidity to fiber which maintains stability of the fiber during cutting procedure. The clean cut fiber sample is placed into a SEM. The SEM images of fabricated fibers acquired from FEI Quanta 200 FEG Environmental Scanning Electron Microscope are presented at Figure 5.1 and Figure 5.2.

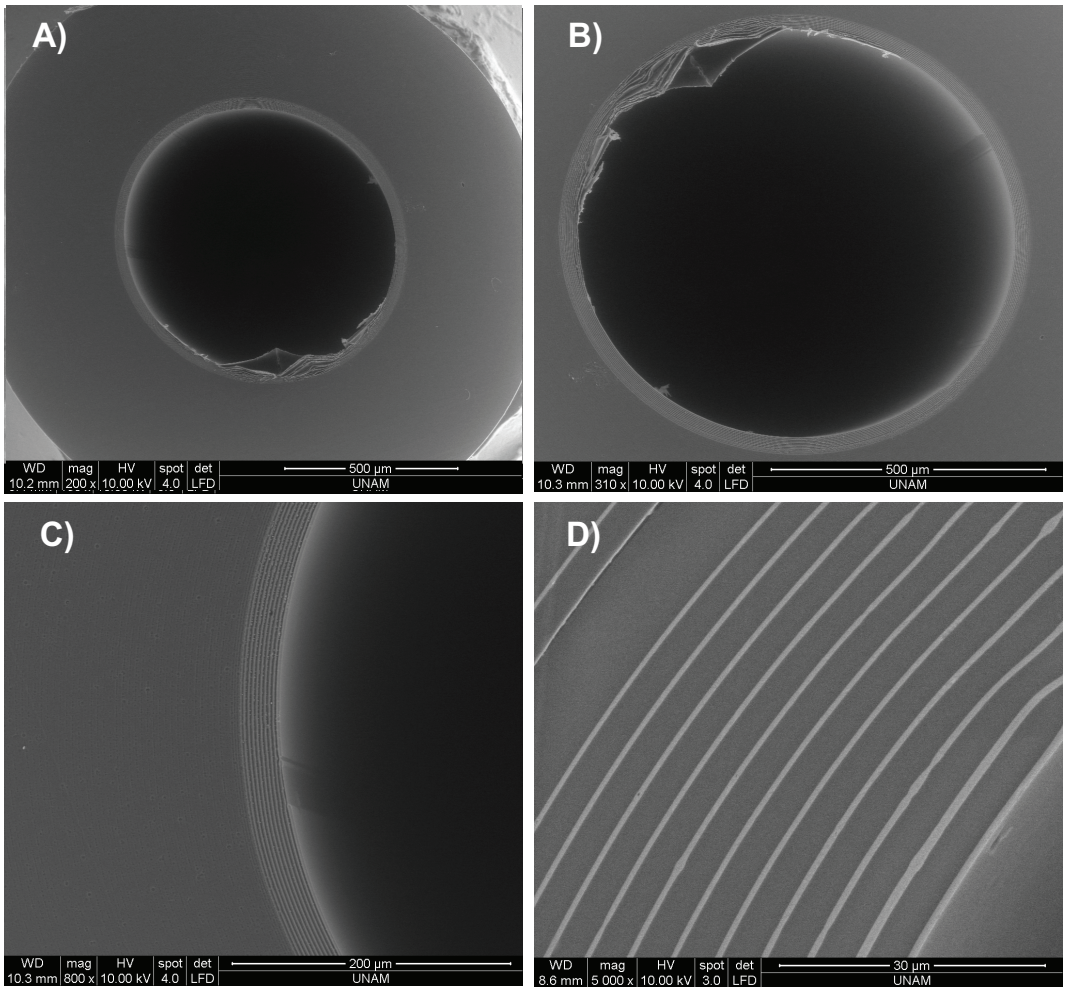

Figure 5.1: SEM images of dielectric bragg fibers for waveguiding at 10.6 μm.

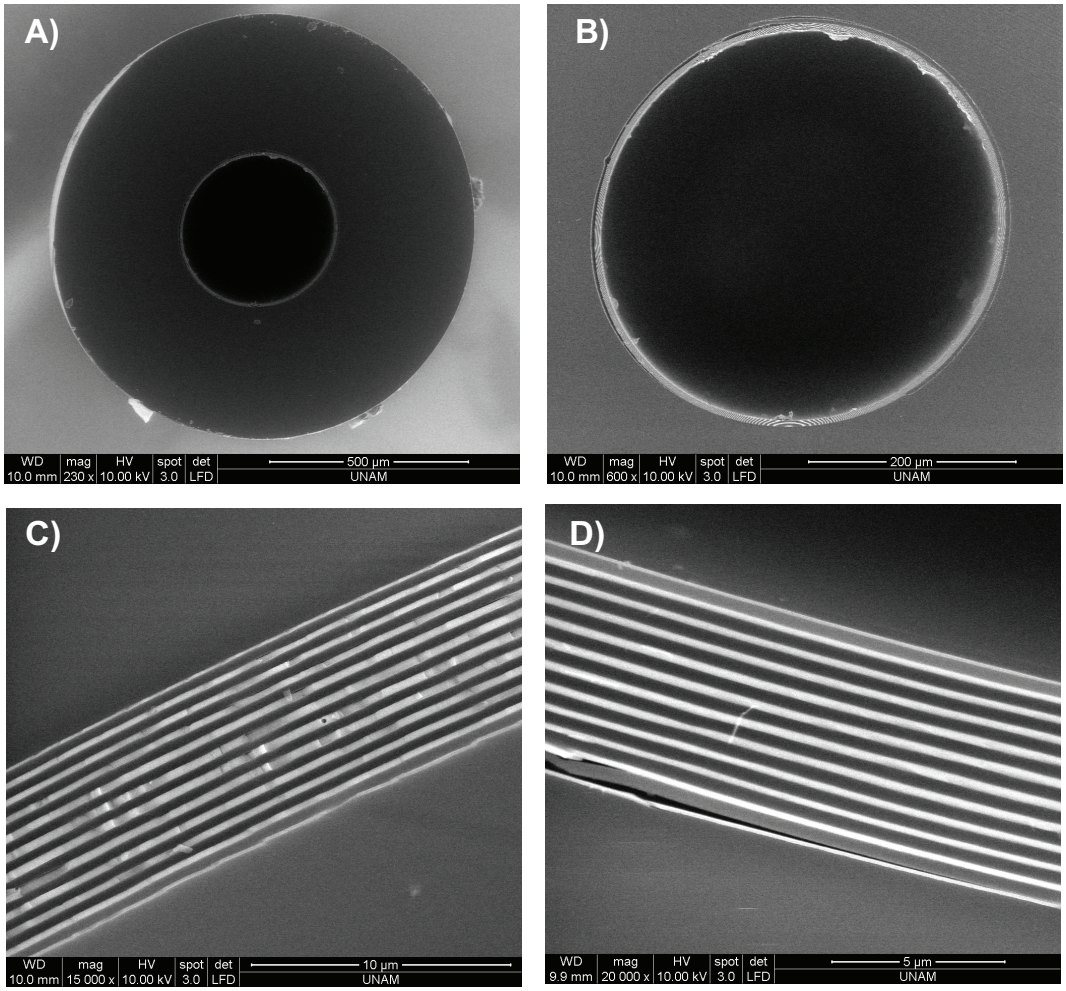

Figure 5.2: SEM images of dielectric bragg fibers for waveguiding at 2.1 μm.

It is possible to confirm from the images that fabrication method can built desired bragg fiber designs with high dimensional accuracy. However, the success of a device is dependent to its performance during its duty. In order to judge the performance of the fiber it is a must to state the theoretical expectations from this fiber. In theoretically predicting the spectral expectations of these fibers it is possible to use photonic band structure calculations including a projected band diagram, a spectral intensity diagram and an angle dependent spectral intensity diagram. Projected band diagrams of HO:YAG laser guiding fiber and CO_2 laser guiding fiber are presented at Figure 5.3.

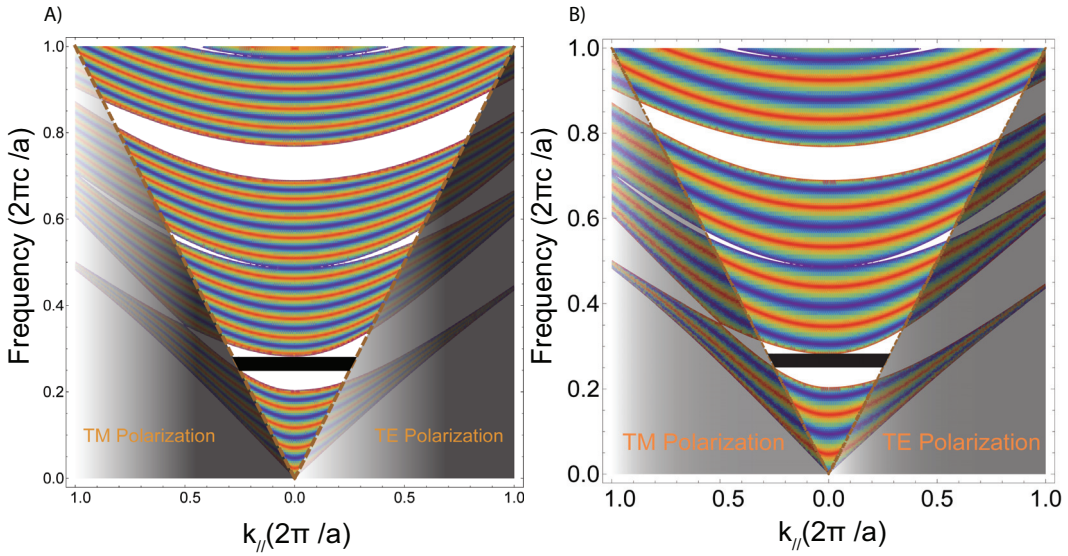

Figure 5.3: Projected band diagram of (A) CO_2 laser guiding fiber and (B) HO:YAG laser guiding fiber. Black regions represents the areas forbidden to propagation of light. The diagrams might seem same however it is important to note that bilayer thickness (a) is different for each fiber design.

The projected band diagram is a complicated way to explain the omnidirectional reflectivity inside transmission bragg fibers. In order to clarify the picture we prefer to use an angle dependent spectral intensity model. This model presents the reflectivity performance of a fiber related to angle of incidence, wavelength and reflected intensity of incident light. This three dimensional model presents the omnidirectional reflection from dielectric layers placed inside fibers more explicit than projected band diagram which requires serious knowledge about photonic crystal structures. This model is applied for each transmission bragg fiber design on this thesis and the results are presented at Figure 5.4.

The transmission performance of fabricated fiber bundles are tested through coupling these fibers into Bruker Tensor 37 FTIR and measure the output intensity of HO:YAG laser guiding fiber and CO_2 laser guiding fiber. The coupling is made through a parabolic ZnSe mirror which is highly transparent between wavelengths 2 μm and 16 μm. However, there are important consequences incident in this measurement setup. First one is the absorption of materials which

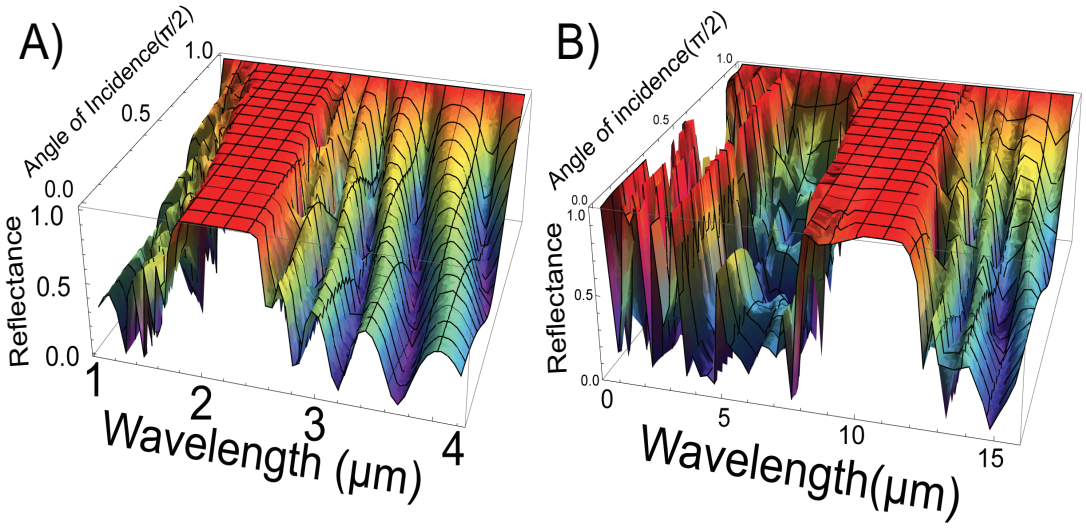

Figure 5.4: Angle dependent spectral intensity model for (A) HO:YAG laser guiding fiber and (B) CO_2 laser guiding fiber.

are incident at air such as gases like CO_2 which tends to absorb heavily at Mid-IR regime of the spectrum. Second, the minimum area which the lens can focus light, which is important because we are dealing with fibers with core diameters 500 μm at maximum. The effect of decreasing core diameter can be observed from Figure 5.5(A) which presents the performance of three transmission bragg fibers working around 10.6 μm. Higher wavelengths correspond to higher fiber dimensions which is a prerequisite of fabrication method. As it can be seen from the figure higher working wavelengths corresponds to higher the transmission intensity due to increased light coupling from source to fiber.

During Chapter 4 the effect of preform mold materials to the fiber has been discussed and it is decided that the PTFE can be used as mold material instead of glass. But, the optical performance measurements (Figure 5.5(B)) indicate the severe effect of scattering which corresponds to lower transmission intensity. According to optical measurements it is possible to state that the transmission bragg fibers which are built to guide CO_2 lasers works efficiently. Moreover we have demonstrated that these fibers are capable to guide high energy laser beams. A pulsed CO_2 laser with 15 watt peak power is sent inside these fibers without any consequence.

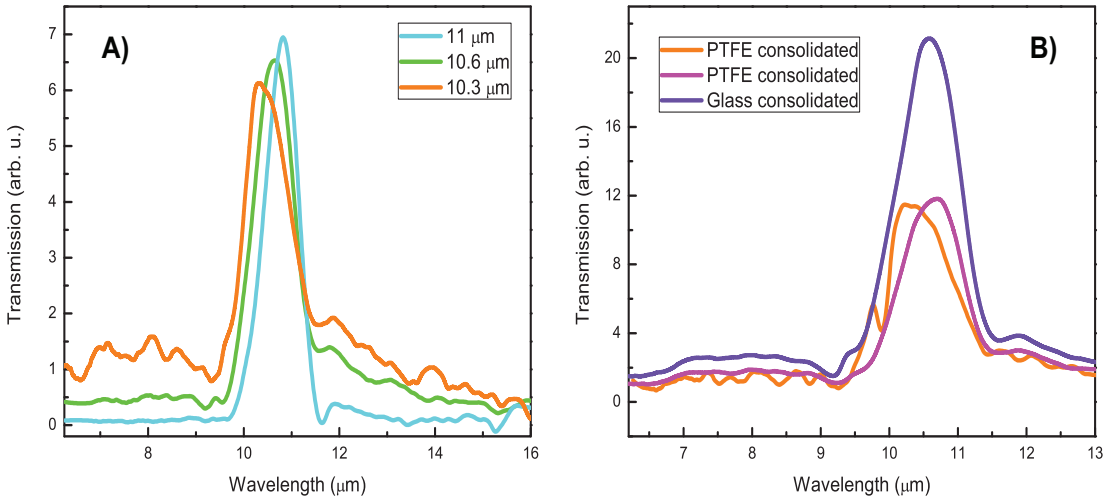

Figure 5.5: Optical performance of transmission bragg fibers for CO_2 laser guiding. (A) Effect of fiber dimensions to coupling of light inside fiber and (B) Influence of preform mold materials to optical performance is presented.

Due to propagation of light inside a hollow core, these fibers omit the losses coming from the media of propagation except the losses coming from the gases incident inside air. But it is useful to state that these fibers have their own loss mechanisms [55]. Therefore we have made a loss analysis specifically for CO_2 laser guiding fibers. The most common loss mechanism for optical fibers is bending loss. The bending loss is also incident for bragg fiber designs. The bending loss performance of transmission bragg fiber that we have fabricated for CO_2 laser guiding is presented at Figure 5.6.

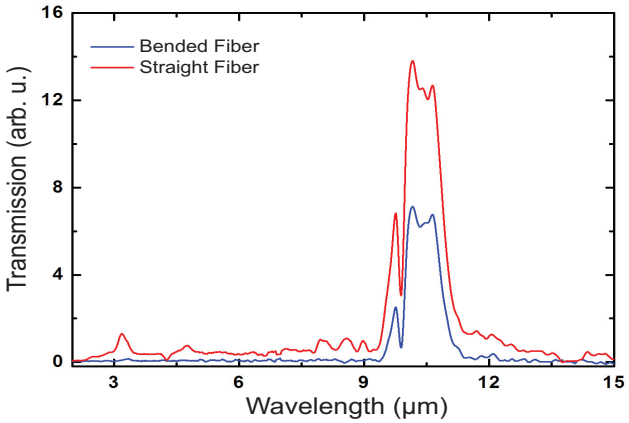

Figure 5.6: Bending loss of a CO_2 laser guiding fiber. The fiber is bent 90° with a 30 cm radius of curvature.

Another loss mechanism is the propagation length of the light inside fiber. This loss is inevitable for every conventional optical fiber design. Unfortunately this loss mechanism is valid for bragg fiber designs which the losses are highly dependent to material dispersion. In case of our bragg fiber the losses are generally coming from propagation of light inside polymer which tends to absorb more than glassy materials at infrared region of the spectrum. The propagation losses inside transmission bragg fibers for CO_2 laser guiding is presented at Figure 5.7.

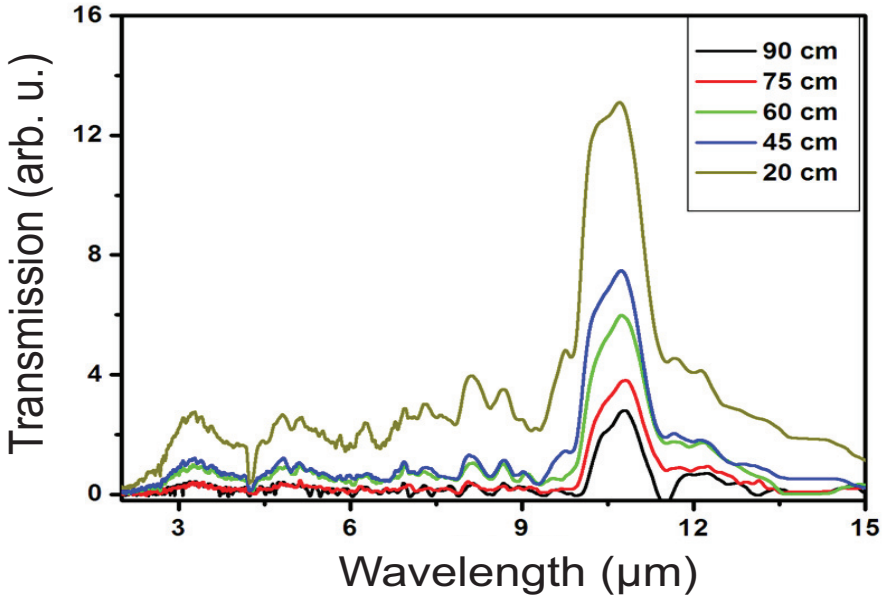

Figure 5.7: Propagation losses inside a CO_2 laser guiding fiber.

In general the propagation losses are expressed through using Eq.5.1. I_{in} corresponds to the intensity introduced into fiber and I_{out} corresponds to the intensity measured at the end of the fiber. The loss of CO_2 laser guiding fiber can be calculated from the information acquired from Figure 5.7. In order to clarify the picture Figure 5.8 which explains all fibers logarithmic intensity with respect to its length is introduced. Simply by multiplying the slope of this graph with ten will provide us the loss of CO_2 laser guiding fibers [79].

$$Loss(dB) = 10Log\left(\frac{I_{in}}{I_{out}}\right) \tag{5.1}$$

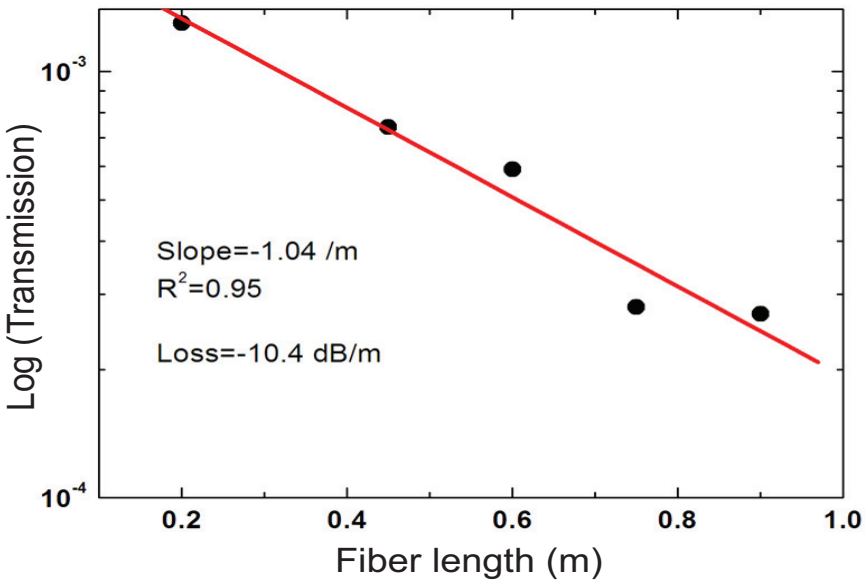

Figure 5.8: Logarithmic transmission intensity of CO_2 laser guiding fiber with respect to its length. Propagation loss for this fiber is found to be -10.4 dB/m.

Additional to CO_2 laser guiding bragg fibers this thesis also includes the design and fabrication of HO:YAG laser guiding fibers. HO:YAG laser is known as one of the most utilized laser system for medical applications. It is used for many different medical procedures at orthopedics, cardiovascular system surgeries, urology and otolaryngology [9]. The laser delivery of such mechanisms is bound to silica fibers which are not flexible enough due to bending loss issues. Rather than using silica wave guiding we have built a transmission bragg fiber for HO:YAG laser wavelength instead of CO_2 laser wavelength. The optical performance analysis of such fibers requires more effort and versatility than CO_2laser guiding fibers. Different from CO_2 laser guiding fibers these fibers are made at smaller dimensions which will correspond to more serious coupling problems during optical performance analysis. Because of this the measured intensities for several fibers are normalized. The optical performance of several transmission bragg fiber including the HO:YAG laser guiding fiber is presented with transmission data acquired from Bruker Tensor 37 FTIR system at Figure 5.9.

The samples presented at Figure 5.9 are obtained from the same drawing procedure which means the working wavelength of the fibers can be modified

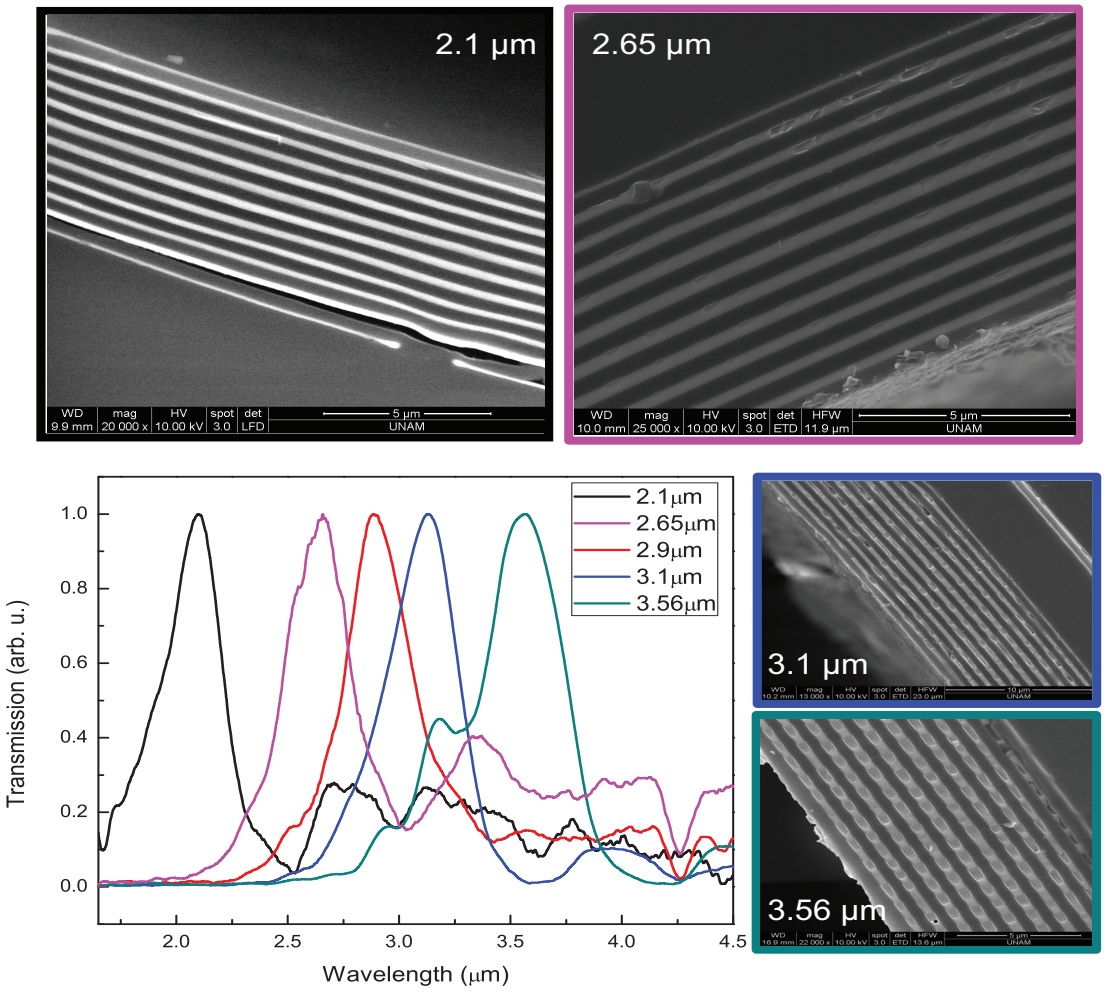

Figure 5.9: Normalized transmission results for wavelength scalable transmission bragg fibers with cross-section SEM images of reflective layers.

during fabrication. Other than HO:YAG laser guiding fiber we have the chance to built many fibers working at different frequencies. However, one of the problems stated before has comes into play while manipulating the working frequency of the fibers. There are many gases incident inside air however the most heavily absorbing gas at our working frequency regime is CO_2. CO_2 gas absorbs heavily at a wavelength of 4.2 μm which disturbs the transmission performance of a bragg fiber designed to guide light at 4.2 μm. Even though this event disturbs the performance of a transmission bragg fiber it encourages other applications such as CO_2 sensing. It is possible to confirm an increase or decrease at the concentration of CO_2 through the modulation of absorption effect at 4.2 μm.

The corresponding idea can be seen through transmission spectrum of the sensing fiber acquired from Bruker Tensor 37 FTIR at Figure 5.10.

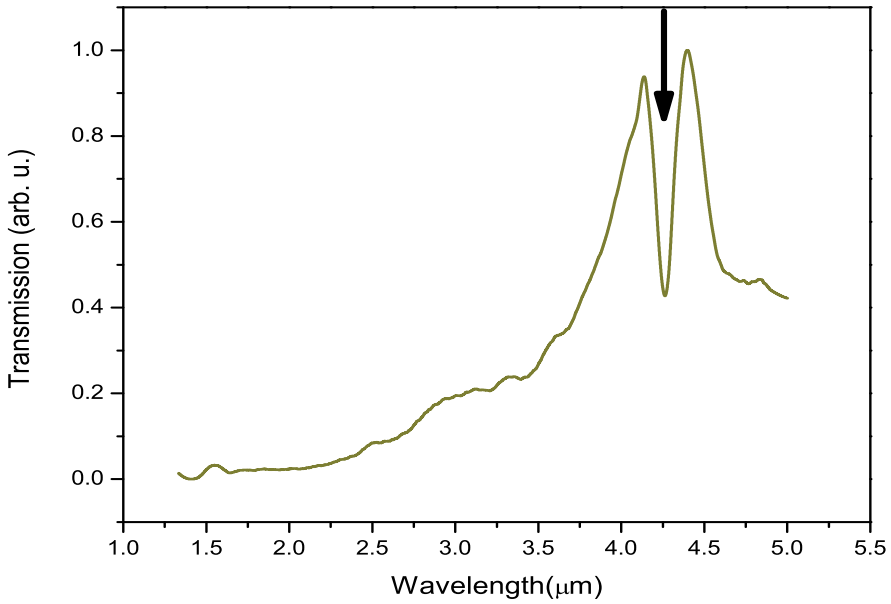

Figure 5.10: Normalized transmission performance of a transmission bragg fiber at 4.2 μm. The arrow points the absorption of CO_2 at 4.2 μm.

The optical performance results of transmission bragg fibers which are designed for medical applications have been presented during this section. Additional to wave guiding another common application of hollow core waveguides have been observed along this work which is sensing. Generally focusing on the main idea of wave guiding this interesting option is merely presented at this section. The next section will mainly focus on optical performance of external reflector fibers which are not related with medical applications. However, due to their unique properties these fibers have been fabricated and their optical performance has been analyzed inside this thesis.

5.2 Dielectric Bragg Fibers as External Reflectors

The primal bragg fiber designs exhibit a mirror structure at the inner surface of the fiber however this case is only useful to use such structures as waveguides. Instead of placing these reflective layers inside of the fiber, it is possible to place these layers at the outer surface of the fiber. The fabrication of such structures has been explained briefly at Chapter 4. The resulting external reflector bragg fibers are used to reflect a certain frequency of light which can be different for each fiber depending on the band gap structure. So, theoretically we are expecting a perfect mirror structure for a defined frequency range from these fibers. Even though we have demonstrated that the reflection from these fibers is omnidirectional, we have analyzed the reflection performance of these fibers at normal incidence with an FTIR spectrometer which has a focusing microscope unit. The reflection performance of a single external reflector fiber is presented with reflection data acquired from Bruker Vertex 70 FTIR with Hyperion Scanning Microscope at Figure 5.11.

It can be inferred from the previous figure that a single reflector fiber can reflect a long frequency range through using different band gap structures along its length. This will correspond to a position dependent reflector mechanism. It is possible to build a weave from these fibers which will add another dimension dependence to this reflector mechanism. The resultant garment is a position dependent mirror which can be used to express a brand or quality. Unfortunately, we cannot observe the reflectance performance after 1.3 μm which mainly corresponds to second order band gaps of external reflector fibers. The FTIR spectrometer fails to measure at near infrared regime with focusing microscope and other optical measurement devices such as ellipsometer fails to focus the source into a narrow point which is important to prevent ambiguous reflection

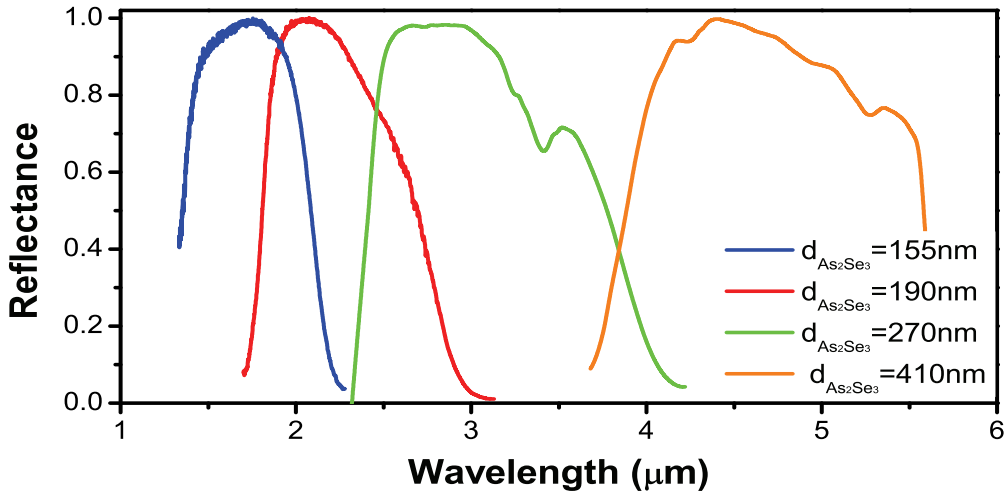

Figure 5.11: Reflection performance of a single external reflector fiber. Each measurement corresponds to a different layer thickness and band gap

from cylindrical surface of the fiber. So, we try to compensate the absence of these measurements with visual confirmation. Theoretically anticipated thickness results and visual images of fibers will be taken as the key confirmation point for success of structures. Besides visible regime, the missing first order band gap measurement at 1 μm and second order band gap around ultraviolet will be confirmed through cross section SEM image of the structure. The missing points through optical characterization of external reflector fibers have presented through optical photography and SEM images acquired from FEI Quanta 200 FEG at Figure 5.12.

With the visual confirmation of missing parts whole frequency picture is complete. In conclusion, optical performance of the external reflector fibers and visual images of fabricated fiber samples have been presented. It is confirmed from the results that the fibers are working according to their design. Also it's possible to state that we have built a frequency varying fiber reflector between ultraviolet and Mid-IR region of the electromagnetic spectrum.

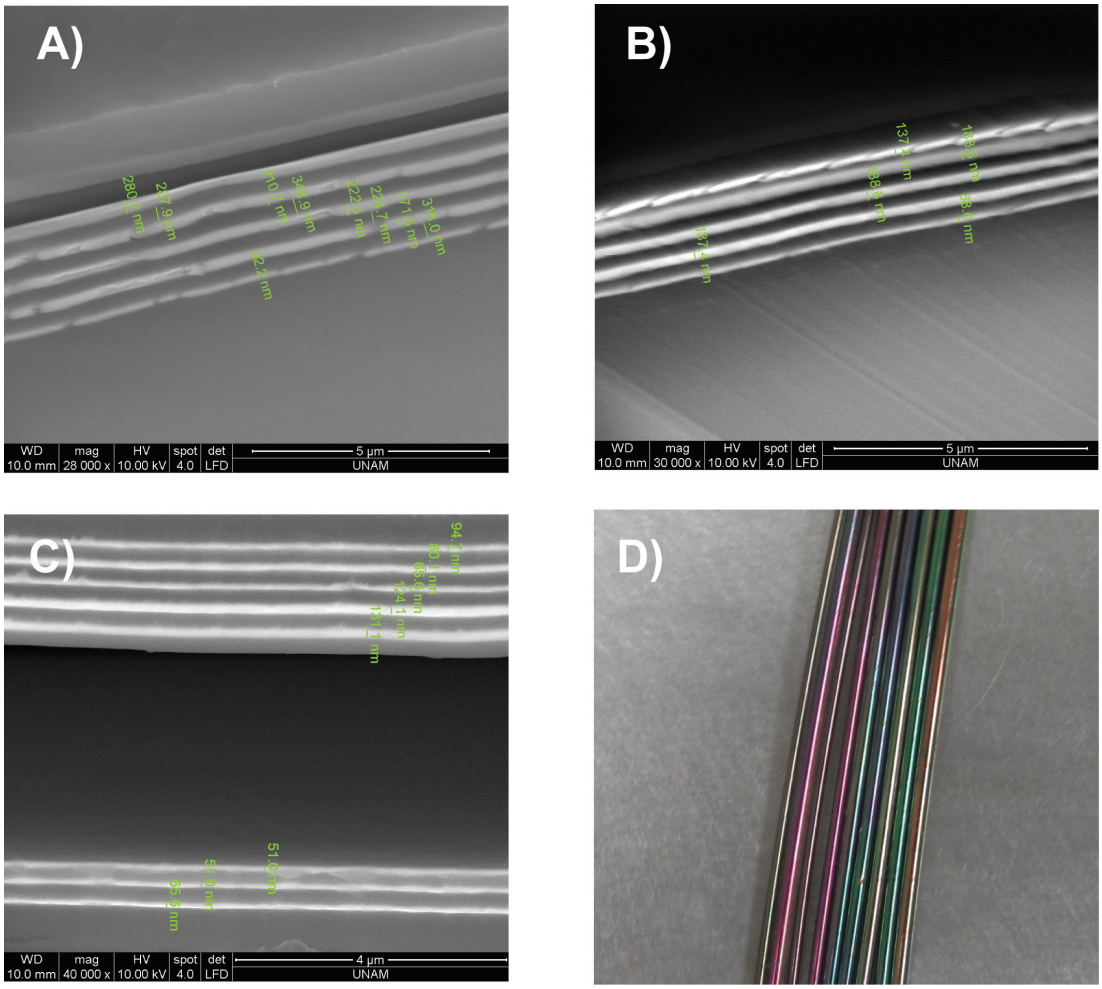

Figure 5.12: Visual presentation of external reflector fibers.(A) Layers of an external reflector fiber with a first order band gap at 3 μm and second order at 1 μm, (B) Layers of an external reflector fiber with a first order band gap at 2.1 μm and second order at 600 nm, (C) Layers of an external reflector fiber with a first order band gap at 1 μm and second order at 210 nm, (D) Visual image of resultant fibers which represents the visible regime performance.

Along this chapter the optical characterization of various bragg fiber designs are made according to their purpose and working frequency. The fibers are found to be working as it was anticipated during Chapter 4. As the major purpose of this thesis, designed and fabricated flexible transmission bragg fibers for utilized medical lasers are found to be working efficiently along with several other transmission bragg fibers which have been designed to work at different frequency regimes. Additional to medical applications, possible sensing application of a transmission bragg fiber have been shown. Other than transmission bragg fiber

designs, external reflector bragg fiber design is also tested along this section and it is found to work according to design predictions.

Chapter 6

CONCLUSIONS AND FUTURE WORKS

During the course of this thesis, we have started with a brief explanation of our motivations. In the next step we have investigated the theoretical calculations relating to dielectric mirrors and continue with PCFs. Theoretical performance analysis forms a basis with material characterization for PCF's fabrication. Design of PCF's is made according to this basis as the first step of fabrication. The second and last step of fabrication involves coating of reflective layers, preform formation and thermal drawing of this preform for a given PCF design. We have succeeded to fabricate all designs and described the challenges observed during fabrication. Finally, we have presented the optical performance of resultant fibers according to their purposes. The main objective of this thesis can be summarized as the design and fabrication of flexible transmission bragg fibers, which will work as a delivery system for important medical lasers. The optical performance results indicate that main objective is succeeded with many other collateral objectives such as external reflector fibers and transmission bragg fibers for gas sensing.

Even though we have demonstrated several qualities through bragg fiber technology, every fabricated design of this thesis can be stated as a primal prototype. The loss values of transmission fibers still require improvement which can be done by optimization of GAST coatings. Moreover, HO:YAG laser guiding fibers coupling problem, which can be easily solved through design and fabrication of a special fiber coupler remains untouched. Also due to coupling problem of HO:YAG laser guiding fibers, the loss values of these fibers are still unknown. The surface roughness values for each transmission fiber demands improvement in order to minimize scattering losses. Moreover, it has been demonstrated that it is possible to monitor the losses inside these fibers through building them with an additional semiconductor layer and contacts [80]. So, we need to build our fibers with that formation in order to analyze the performance of them easily. Besides the issues relating main objective of this thesis, the problems relating collateral objectives also demand improvement. The analysis of reflectance performance for external reflector fibers at near infrared and visible regimes requires a custom built measurement system. Another measurement system must be designed for transmission bragg fibers to analyze gas sensing capabilities.

Other than missing part of this thesis, it is possible to mention about some new research options which become available with the background obtained from this work, in brief possible future works. First idea is to insert a tunable cavity inside the band gap of these fibers through introducing a defect between photonic crystal lattices. The tuning of such structures with a different material is already made through use of light [6]. However, the tuning mechanism which is oriented from refractive index change of GAST glass with respect to temperature haven't been investigated. The manipulation of refractive index will give a shift to the spectral position of the cavity inside band gap. The experimental data for refractive index change of GAST glass with respect to temperature is acquired from a J.A. Woolam Ellipsometer. The results are presented at Figure 6.1.

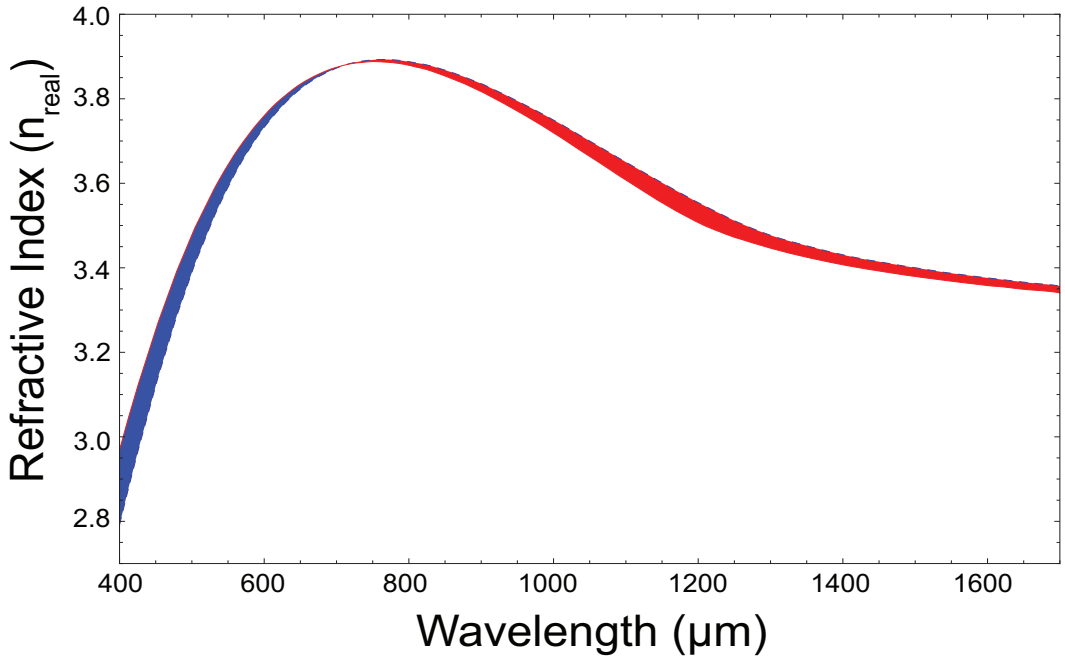

Figure 6.1: The temperature response of dispersion relation for GAST glass is presented. Blue shift corresponds to decrease and red corresponds to increase in refractive index with increasing temperature. The measurements are made between 25 °C and 125 °C.

Theoretical explanation of this mechanism is made through introducing the experimental refractive index change data into band calculator program that we have developed at Mathematica software. Due to fabrication problems of GAST glass, only defect layer which forms the cavity is designed from this glass. The mirror layers are designed from consecutive PEI and As_2Se_3 layers. The simulation of the designed structure is performed under consideration of these fabrication problems. The theoretical spectral response of this design is presented at Figure 6.2.

It is possible to confirm theoretically that the temperature change from 25 °C to 125 °C will result in a 6 nm shift at cavity position which is 3 times higher than the reported shift at Benoit et al. [6]. This shift is only made through the effect of cavity GAST glass layer, it is logical to expect a better shift from a structure made from GAST glass and PEI. So there lies a great potential for bragg fibers which are designed as tunable cavity devices. If these structures

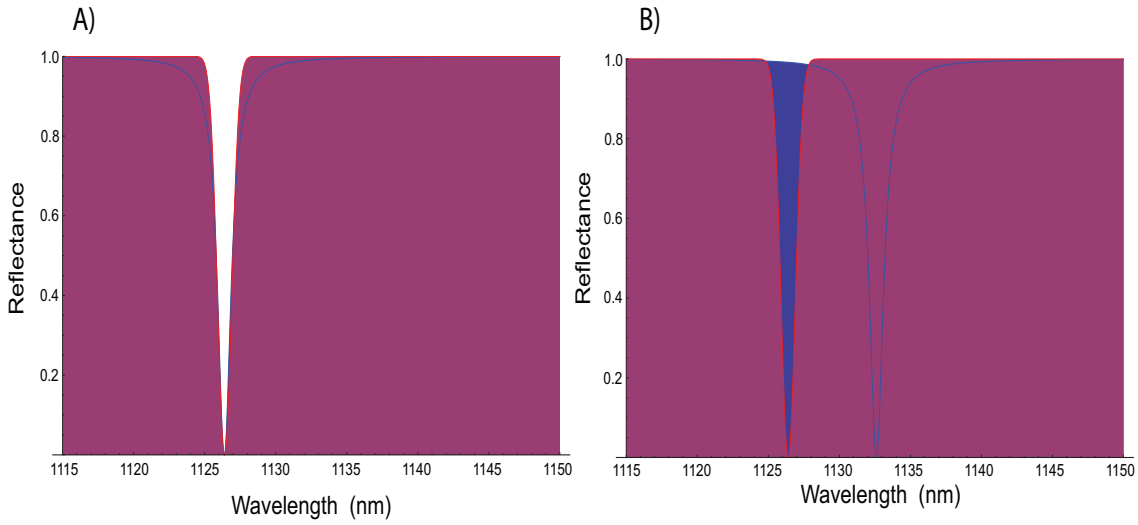

Figure 6.2: The shift of cavity inside the band gap with respect to temperature. (A) The cavity position at 25 °C, (B) the cavity position at 125 °C are presented.

can be fabricated it is possible to build an all fiber tunable cavity which can be used for several applications, namely photovoltaics, gas sensing, spectrometry and fiber lasers [81, 82].

Second idea is to build transmission fibers for near infrared and visible regime. Most of the medical lasers tend to operate between near infrared and visible regime unlike CO_2 and HO:YAG lasers. So, the idea is to build low loss hollow core transmission fibers for all of the medical laser systems. First obstacle to overcome for wave guiding at higher frequencies can be stated as coupling problem. The other problem is collapse of fiber core which is originated from thermo-mechanical fabrication procedure. The third and most important problem is absorption behavior of the materials mentioned during this thesis at near infrared and visible regimes. If we are able to avoid these problems we can build fibers to guide light from visible spectrum to mid-infrared without any problem. This development will result in fabrication of flexible low loss hollow core fibers for whole medical lasers. Different than these ideas there are also some interesting developments are made about this research field by other people. The most brilliant can be stated as the fiber camera idea which has been published by

Sorin et al. [83]. Another interesting work has been published about using these structures to form nano-scaled semiconductor filaments by Deng et al. [84].

As we have explained the summary of this thesis at the beginning of this chapter, we have mostly succeeded the primal objective of this thesis. We have introduced, designed, fabricated and analyzed hollow core photonic band gap fibers for medical applications. Additional to this primal objective we have successfully built other hollow core photonic band gap fibers for different applications. The background we have built during this thesis has helped us to suggest new designs and applications for photonic band gap fibers. At the end of this thesis here we are, improving our work and looking for some new aspects for such specialty fibers.

Bibliography

[1] J. N. Winn, Y. Fink, S. Fan, and J. D. Joannopoulos, "Omnidirectional reflection from a one-dimensional photonic crystal," *OSA Optics Letters*, vol. 23, no. 20, pp. 1573–1575, 1998.

[2] J. Knight, "Photonic crystal fibres," *Nature*, vol. 424, pp. 847–851, 2003.

[3] Y. Fink, D. J. Ripin, S. Fan, C. Chen, J. D. Joannopoulos, and E. L. Thomas, "Guiding optical light in air using an all-dielectric structure," *Journal of Lightwave Technology*, vol. 17, no. 11, pp. 2039–2041, 1999.

[4] B. Temelkuran, S. D. Hart, G. Benoit, J. D. Joannopoulos, and Y. Fink, "Wavelength-scalable hollow optical fibres with large photonic bandgaps for co_2 laser transmission," *Nature*, vol. 420, pp. 650–653, 2002.

[5] A. F. Abouraddy, M. Bayindir, G. Benoit, S. D. Hart, K. Kuriki, N. Orf, O. Shapira, F. Sorin, B. Temelkuran, and Y. Fink, "Towards multimaterial multifunctional fibres that see, hear, sense and communicate," *Nature Materials*, vol. 6, pp. 336–347, 2007.

[6] G. Benoit, K. Kuriki, J.-F. Viens, J. D. Joannopoulos, and Y. Fink, "Dynamic all-optical tuning of transverse resonant cavity modes in photonic bandgap fibers," *OSA Optics Letters*, vol. 30, no. 13, pp. 1620–1622, 2005.

[7] M. Bayindir, A. F. Abouraddy, J. Arnold, J. D. Joannopoulos, and Y. Fink*, "Thermal-sensing fiber devices by multimaterial codrawing," *Advanced Materials*, vol. 18, pp. 845–849, 2006.

[8] G. Kim, T. Cho, K. Hwang, K. Lee, K. S. Lee, Y.-G. Han, and S. B. Lee, "Strain and temperature sensitivities of an elliptical hollow-core photonic bandgap fiber based on sagnac interferometer," *OSA Optics Express*, vol. 17, no. 4, pp. 2481–2486, 2009.

[9] Q. Peng, A. Juzeniene, J. Chen, L. O. Svaasand, T. Warloe, K.-E. Giercksky, and J. Moan, "Lasers in medicine," *Rep. Prog. Phys.*, vol. 71, 2008.

[10] R. M. Verdaasdonkz and C. F. P. van Swol, "Laser light delivery systems for medical applications," *Phys. Med. Biol.*, vol. 42, pp. 869–894, 1997.

[11] M. S. Strong and G. J. Jako, "Laser surgery in larynx: Early clinical experience with continuous co_2-laser," *Ann. Oto. Rhinol. Laryn.*, vol. 81, pp. 791–798, 1972.

[12] S. M. Shapshay and J. F. Beamis, "Use of co_2-laser," *Chest*, vol. 95, pp. 449–456, 1989.

[13] A. K. Devaiah, S. M. Shapshay, U. Desai, G. Shapira, O. Weisberg, D. S. Torres, and Z. Wang, "Surgical utility of a new carbon dioxide laser fi ber: Functional and histological," *Laryngoscope*, vol. 115, pp. 1463–1468, 2005.

[14] A. S. Jacobson, P. Woo, and S. M. Shapshay, "Emerging technology: Flexible co_2 laser waveguide," *Otolaryn. Head Neck*, vol. 135, pp. 469–470, 2006.

[15] S. D. Hart, G. R. Maskaly, B. Temelkuran, P. H. Prideaux, J. D. Joannopoulos, and Y. Fink, "External reflection from omnidirectional dielectric mirror fibers," *Science*, vol. 296, pp. 510–513, 2002.

[16] J. W. Strutt, "On the maintenance of vibrations by forces of double frequency, and on the propagation of waves through a medium endowed with a periodic structure," *Philosophical Magazine*, vol. 24, no. 147, pp. 145–159, 1887.

[17] J. W. Strutt, "On the reflection of light from a regularly stratified medium," *Proceedings of Royal Society*, vol. 93, pp. 565–577, 1917.

[18] C. G. Darwin, "The theory of x-ray reflection, part ii," *Philosophical Magazine*, vol. 27, pp. 675–690, 1914.

[19] E. Yablanovitch and T. J. Gmitter, "Photonic band structure: The face-centered-cubic case," *Physical Review Letters*, vol. 63, no. 18, pp. 1950–1953, 1989.

[20] P. Yeh, A. Yariv, and C. S. Hong, "Electromagnetic propagation in periodic stratified media. i. general theory," *JOSA*, vol. 67, no. 4, pp. 423–438, 1977.

[21] Y. Fink, J. N. Winn, S. Fan, J. M. Chiping Chen, J. D. Joannopoulos, and E. L. Thomas, "A dielectric omnidirectional reflector," *Science*, vol. 282, pp. 1679–1682, 1998.

[22] D. Alsberg, J. Bankert, and P. Hutchison, "The wt4/wt4a millimeter wave transmission system," *Bell Syst. Tech. J.*, vol. 56, p. 1849, 1977.

[23] G. Benoit, S. D. Hart, B. Temelkuran, J. D. Joannopoulos, and Y. Fink, "Static and dynamic properties of optical microcavities in photonic bandgap yarns," *Advanced Materials*, vol. 15, no. 24, pp. 2053–2056, 2003.

[24] E. A. J. Marcatili and R. A. Schmetzer, "Hollow metallic and dielectric waveguides for long distance optical transmission and lasers.," *Bell Syst. Tech. J.*, vol. 43, p. 1783, 1964.

[25] M. Miyagi, A. Hongo, Y. Aizawa, and S. Kawakami, "Fabrication of germanium-coated nickel hollow waveguides for infrared transmission," *Applied Physics Letters*, vol. 43, p. 430, 1983.

[26] J. A. Harrington, "A review of ir transmitting, hollow waveguides," *Fiber Integrated Optics*, vol. 19, p. 211, 2000.

[27] R. Maurer and P. Schultz, *US Patent No. 3,659,915.* Corning Glass Works, 1972.

[28] P. S. J. Russell, "Photonic crystal fibers," *Science*, vol. 299, pp. 358–362, 2003.

[29] M. Ibanescu, Y. Fink, S. Fan, E. L. Thomas, and J. D. Joannopoulos, "An all-dielectric coaxial waveguide," *Science*, vol. 289, pp. 415–362, 2000.

[30] A. W. Snyder and J. D. Love, *Optical Waveguide Theory.* Chapman and Hall, N.Y., 1983.

[31] C. Yeh, *Handbook of Fiber Optics : Theory and Applications.* Academic Press Inc., 1990.

[32] A. Bornstein and N. Croitoru, "Experimental evaluation of a hollow glass-fiber," *Applied Optics*, vol. 25, p. 355, 1986.

[33] R. F. Cregan, B. J. Mangan, J. C. Knight, T. A. Birks, P. S. J. Russell, P. J. Roberts, and D. C. Allan, "Single-mode photonic band gap guidance of light in air," *Science*, vol. 285, pp. 1537–1539, 1999.

[34] J. A. Harrington and C. C. Gregory, "Hollow sapphire fibers for the delivery of co2 laser energy," *OSA, Optics Letters*, vol. 15, no. 10, pp. 541–543, 1990.

[35] *Fiber 101 Tutorial Selected Topics, Corning Incorporation,* ***2008.****, 15 June 2009, <http://media.corning.com/flash/opticalfiber/2008/fiber101/Fiber%20101%20select%20concepts.pdf>.*

[36] H. Taniyama, "Waveguide structures using one-dimensional photonic crystal," *JOURNAL OF APPLIED PHYSICS*, vol. 91, no. 6, pp. 3511–3515, 2002.

[37] A. Mekis, J. C. Chen, I. Kurland, S. Fan, P. R. Villeneuve, and J. D. Joannopoulos, "High transmission through sharp bends in photonic crystal waveguides," *Physical Review Letters*, vol. 77, no. 18, pp. 3787–3790, 1996.

[38] J. D. Joannopoulos, P. R. Villeneuve, and S. Fan, "Photonic crystals: puttin a new twist on light," *Nature*, vol. 386, pp. 143–149, 1997.

[39] E. Yablanovitch, T. J. Gmitter, and K. Leung, "Photonic band structure: The face-centered-cubic case employing non-spherical atoms," *Physical Review Letters*, vol. 67, no. 17, pp. 2295–2298, 1991.

[40] C. Cheng and A. Scherer, "Fabrication of photonic band-gap crystals," *Journal of Vacuum Science and Technology*, vol. 13, p. 2696, 1995.

[41] S. Fan, P. R. Villeneuve, R. D. Meade, and J. D. Joannopoulos, "Design of three-dimensional photonic crystals at submicron lengthscales," *Applied Physics Letters*, vol. 65, no. 11, pp. 1466–1468, 1994.

[42] S. N. A. Chutinan, "Design for waveguides in three-dimensional photonic crystals," *Japanese Journal of Applied Physics*, vol. 39, pp. 2353–2356, 2000.

[43] S. Leon-Saval, T. Birks, W. Wadsworth, P. S. J. Russell, and M. Mason, "Supercontinuum generation in submicron fibre waveguides," *OSA Optics Express*, vol. 12, pp. 2864–2869, 2004.

[44] L. Tong, R. R. Gattass, J. B. Ashcom, S. He, J. Lou, M. Shen, I. Maxwell, and E. Mazur, "Subwavelength-diameter silica wires for low-loss optical wave guiding," *Nature*, vol. 426, pp. 816–819, 2003.

[45] J. C. Knight, T. A. Birks, P. S. J. Russell, and D. M. Atkin, "All-silica single-mode optical fiber with photonic crystal cladding," *OSA Optics Letters*, vol. 21, no. 19, pp. 1547–1549, 1996.

[46] N. Venkataraman, M. T. Gallagher, C. M. Smith, D. Müller, J. A. West, K. W. Koch, and J. C. Fajardo, "Low loss (13 db/km) air core photonic band-gap fiber," *Proc. 28th Eur.Conf. Opt. Commun.*, 2002.

[47] T. A. Birks, P. J. Roberts, P. S. J. Russell, D. M. Atkin, and T. J. Shepherd, "Full 2-d photonic band gaps in silicdair structures," *Electron. Lett.*, vol. 31, p. 1941, 1995.

[48] D. C. Allan, *Photonic Crystals and Light Localization in the 21st Century (edited by C. M. Soukoulis).* Kluwer Academic Publishers, Netherlands, 2001.

[49] J. B. Jensen, L. H. Pedersen, P. E. Hoiby, L. B. Nielsen, T. P. Hansen, J. R. Folkenberg, J. Riishede, D. Noordegraaf, K. Nielsen, A. Carlsen, and A. Bjarklev, "Photonic crystal fiber based evanescent-wave sensor for detection of biomolecules in aqueous solutions," *OSA Optics Letters*, vol. 29, no. 17, pp. 1974–1976, 2004.

[50] J. Limpert, T. Schreiber, S. Nolte, H. Zellmer, A. Tünnermann, R. Iliew, F. Lederer, J. Broeng, G. Vienne, A. Petersson, and C. Jakobsen, "High-power air-clad large-mode-area photonic crystal fiber laser," *OSA Optics Express*, vol. 11, no. 7, pp. 818–823, 2003.

[51] F. C. Holsinger, C. N. Prichard, G. Shapira, O. Weisberg, D. S. Torres, C. Anastassiou, E. Harel, Y. Fink, and R. S. Weber, "Use of the photonic band gap fiber assembly co_2 laser system in head and neck surgical oncology," *Laryngoscope*, vol. 116, no. 7, 2006.

[52] S. G. Johnson, M. Ibanescu, M. Skorobogatiy, O. Weisberg, T. D. Engeness, M. Soljacic, S. A. Jacobs, J. D. Joannopoulos, and Y. Fink, "Low-loss asymptotically single-mode propagation in large-core omniguide fibers," *OSA Optics Letters*, vol. 9, no. 13, pp. 748–779, 2001.

[53] M. Ibanescu, S. G. Johnson, M. Soljacic, J. D. Joannopoulos, and Y. Fink, "Analysis of mode structure in hollow dielectric waveguide fibers," *Physical Review E*, vol. 67, 2003.

[54] P. Yeh, A. Yariv, and E. Marom, "Theory of bragg fiber," *JOSA*, vol. 68, no. 9, pp. 1196–1201, 1978.

[55] J. D. Joannopoulos, S. G. Johnson, J. N. Winn, and R. D. Meade, *Photonic Crystals: Molding the flow of light (Second ed.)*. Princeton University Press, N.J., 2006.

[56] F. P. Kapron, D. B. Keck, and R. D. Maurer, "Radiation losses in glass optical waveguides," *Applied Physics Letters*, vol. 17, pp. 423–425, 1970.

[57] R. O. Ebewele, *Polymer Science and Technology*. CRC Press, N.Y., 2000.

[58] A. K. Varshneya, *Fundamentals of Inorganic Glasses*. Academic Press, N.Y., 1994.

[59] J. D. Verhoeven, *Fundamentals of Physcical Metallurgy*. John Wiley and Sons, N.Y., 1975.

[60] Z. U. Borisova, *Glassy Semiconductors*. Plenum Press, N.Y., 1981.

[61] P. G. Debenedetti and F. H. Stillinger, "Supercooled liquids and the glass transition," *Nature*, vol. 410, pp. 259–267, 2001.

[62] A. K. Varshneya, "Some comments on physical properties of chalcogenide glasses," *Journal of Non-crystalline Solids*, vol. 273, pp. 1–7, 2000.

[63] J. S. Sanghera and I. D. Aggarwal, "Active and passive chalcogenide glass optical fibers for ir applications: a review," *Journal of Non-crystalline Solids*, vol. 257, p. 6, 1999.

[64] A. R. Hilton, "Optical properties of chalcogenide glasses," *Journal of Non-crystalline Solids*, vol. 2, p. 28, 1970.

[65] D. W. V. Krevelen, *Properties of Polymers*. Elsevier Scientific, N.Y., 1990.

[66] W. D. J. Callister, *Materials Science and Engineering: An Introduction*. John Wiley and Sons, N.Y., 2007.

[67] A. Zakery and S. Elliott, "Optical properties and applications of chalcogenide glasses: a review," *Journal of Non-Crystalline Solids*, vol. 330, pp. 1–12, 2003.

[68] X. Zhang, H. Ma, and J. Lucas, "Applications of chalcogenide glass bulks and fibres," *Journal of Optoelectronics and Advanced Materials*, vol. 5, no. 5, pp. 1327–1333, 2003.

[69] J. S. Sanghera, V. Q. Nguyen, P. C. Pureza, F. H. Kung, R. Miklos, and I. D. Aggarwal, "Applications of chalcogenide glass bulks and fibres," *JOURNAL OF LIGHTWAVE TECHNOLOGY*, vol. 12, no. 5, pp. 737–741, 1994.

[70] N. F. Mott *Philosophical Magazine*, vol. 19, p. 835, 1969.

[71] K. D. Tsendin, "Superconductivity in chalcogenide glassy semiconductors," *Journal of Optoelectronics and Advanced Materials*, vol. 4, no. 3, pp. 763–772, 2002.

[72] A. S. Tverjanovich, "Temperature dependence of the viscosity of chalcogenide glass-forming melts," *Glass Physics and Chemistry*, vol. 29, p. 532, 2003.

[73] C. J. Seeton, "Viscosity-temperature correlation for liquids," *Tribology Letters*, vol. 22, no. 1, pp. 67–78, 2006.

[74] F. T. Trouton, "On the coefficient of viscous traction and its relation to that of viscosity," *Proc. Roy. Soc. London*, vol. A 77, pp. 426–440, 1906.

[75] D. W. V. Krevelen, *Properties of Polymers, Their Estimation and Correlation with Chemical Structure (2nd edition)*. Elsevier Press, Amsterdam, 1976.

[76] L. A. Cauchy *Bull. des. sc. math*, vol. 14, p. 9, 1830.

[77] Y. Matsuura, R. Kasahara, T. Katagiri, and M. Miyagi, "Hollow infrared fibers fabricated by glass-drawing technique," *OSA Optics Express*, vol. 10, no. 12, pp. 488–492, 2002.

[78] K. Lyytikainen, J. Zagari, G. Barton, and J. Canning, "Heat transfer within a microstructured polymer optical fibre preform," *Modelling Simul. Mater. Sci. Eng.*, vol. 12, pp. 255–265, 2004.

[79] S. Ungar, *Fibre Optics: Theory and Applications*. John Wiley and Sons, New York, 1990.

[80] M. Bayindir, O. Shapira, D. Saygin-Hinczewski, J. Viens, A. F. Abouraddy, J. D. Joannopoulos, and Y. Fink, "Integrated fibres for self-monitored optical transport," *Nature Materials*, vol. 4, no. 12, pp. 820–825, 2005.

[81] O. Shapira, K. Kuriki, N. D. Orf, A. F. Abouraddy, G. Benoit, J. F. Viens, A. Rodriguez, M. Ibanescu, J. D. Joannopoulos, and Y. Fink, "Surface-emitting fiber lasers," *OSA Optics Express*, vol. 14, no. 9, pp. 3923–3935, 2006.

[82] H. E. Kondakci, M. Yaman, O. Koylu, A. Dana, and M. Bayindir, "All-chalcogenide glass omnidirectional photonic band gap variable infrared filters," *Applied Physics Letters*, vol. 94, p. 111110, 2009.

[83] F. Sorin, O. Shapira, A. F. Abouraddy, M. Spencer, N. D. Orf, J. D. Joannopoulos, and Y. Fink, "Exploiting collective effects of multiple optoelectronic devices integrated in a single fiber," *Nano Letters*, vol. 9, no. 7, pp. 2630–2635, 2009.

[84] D. S. Deng, N. D. Orf, A. F. Abouraddy, A. M. Stolyarov, J. D. Joannopoulos, H. A. Stone, and Y. Fink, "In-fiber semiconductor filament arrays," *Nano Letters*, vol. 8, no. 12, pp. 4265–4269, 2008.